Government of Canada
Fisheries and Oceans

Gouvernement du Canada
Pêches et Océans

MANUSCRIPT REPORT SERIES NO. 9

INTERNAL TIDES IN A PARTIALLY MIXED ESTUARY

L.R. MUIR

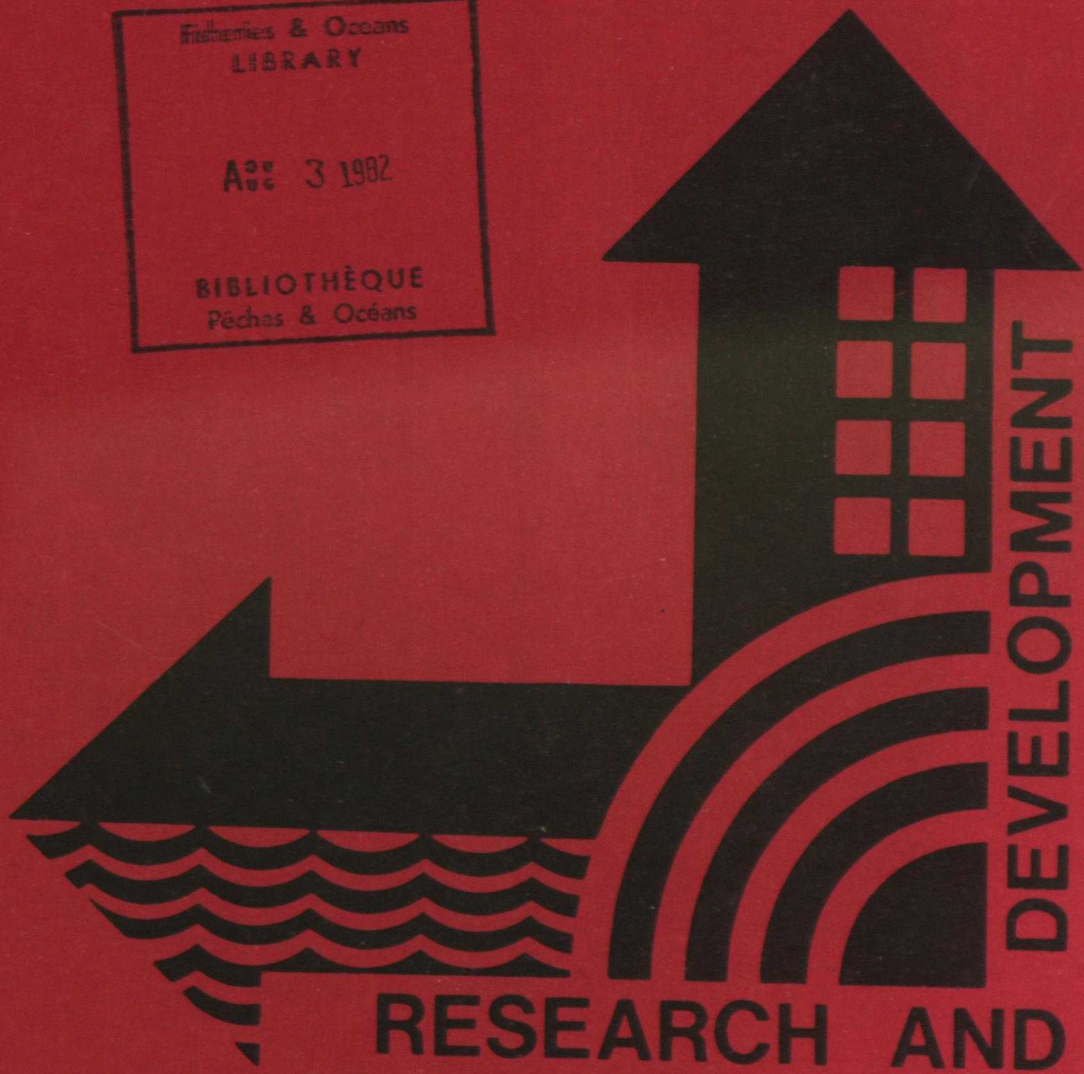

OCEAN SCIENCE AND SURVEYS
CENTRAL REGION
CANADA CENTRE FOR INLAND WATERS
BURLINGTON, ONTARIO

INTERNAL TIDES IN A PARTIALLY-MIXED ESTUARY

by

Langley Russell Muir

This is an internal technical report which has received only limited circulation. On citing this report, the reference should be followed by the words "UNPUBLISHED MANUSCRIPT."

The text of this report is, with minor editorial corrections, identical to a thesis submitted in partial fulfillment of the requirements for a PhD at the Department of Oceanography, University of Southampton.

P.O. Box 5050
Burlington, Ontario
L7R 4A6

Acknowledgements

The research for this report was done while the author was on educational leave from the Research and Development Division, Ocean Science and Surveys, Central Region, Department of Fisheries and Oceans, Government of Canada. The author is grateful to the Government of Canada for financial support during this leave.

I would like to thank all of those individuals who have helped with the data gathering, reduction and analysis. In particular, I would like to thank Mr. Paul Budgell, Dr. Gabriel Godin and Dr. Ian Robinson for their help and very valuable discussions.

CONTENTS

LIST OF TABLES

LIST OF FIGURES

cont'd...

LIST OF FIGURES (continued)

CHAPTER 1

Introduction

1.0 History and Objectives

In late 1972, the author was asked to undertake a tidal current survey of the Middle Estuary of the St. Lawrence River in order to supplement the recharting of the whole St. Lawrence by the Canadian Hydrographic Service. At that time, it was envisaged that the results of these current surveys, which were to be of limited extent, would be used to update the 1939 Tidal Current Atlas, and would be of some use in verifying the numerical and physical models of the St. Lawrence that had been produced by the National Research Council. In early 1973, Acres Consulting Services Limited requested help in carrying out a small survey on the currents and water properties in the Kamouraska area, across the River from Pointe au Pic, so that they could complete a feasibility study for a proposed deep-water terminal for oil tankers.

The survey in conjunction with Acres Consulting Services was carried out in the Spring of 1973, and a small pilot survey in the Ile d'Orleans region was conducted from the C.C.G.V. Porte Dauphin in July and August 1973 by the author. The data from these two surveys is given in the 1973 St. Lawrence Current Survey: Data Report (Muir and Budgell, 1975).

The surveys in 1973 were reasonably successful, and with the reorganization of Ocean and Aquatic Sciences, further surveys were planned. In addition to the very limited objectives of a tidal current atlas, it was decided that the surveys on the St. Lawrence should

encompass the range of physical oceanography and that it was necessary to determine, and quantify if possible, all of the physical processes that were dominant in the Estuary. At this time it was believed that the Middle Estuary of the St. Lawrence was a fairly simple and typical, partially mixed estuary.

In 1974, a survey was conducted from the C.S.S. Bayfield using the C.C.G.V. Simon Frazer to lay and recover moorings. This survey recovered 9 current meter records of sufficient quality to be subjected to a tidal analysis and occupied 30 profiling stations for a minimum of 13 hours each. At the profiling stations current speed and direction and the water temperature and salinity were recorded at approximately 10 depths every 45 minutes. The 1975 survey marked the beginning of the proper oceanographic surveys of the Middle Estuary. A series of 12 stations was chosen, and some of them were revisited as many as three times, at various stages of the Spring-Neap cycle. The survey was conducted from the C.S.S. Bayfield, and the C.S.S. Limnos was used to lay and recover the moorings. The data from these two surveys are reported in Budgell and Muir (1975) and in Muir (1978) respectively.

The 1977 St. Lawrence current survey concentrated the profiling efforts in the Hare Island area of the Middle Estuary and was conducted from the C.S.S. Limnos. It was the most extensive of the surveys and the data are reported in Muir (1979a).

Due to the extensive amount of work that had to be done in developing computer programs to transcribe, edit and display the data, in devising data bases in which to hold the data and analysis programs to utilize the data, as well as the logistics involved in developing instrumentation to collect the data, no real analysis was done on the

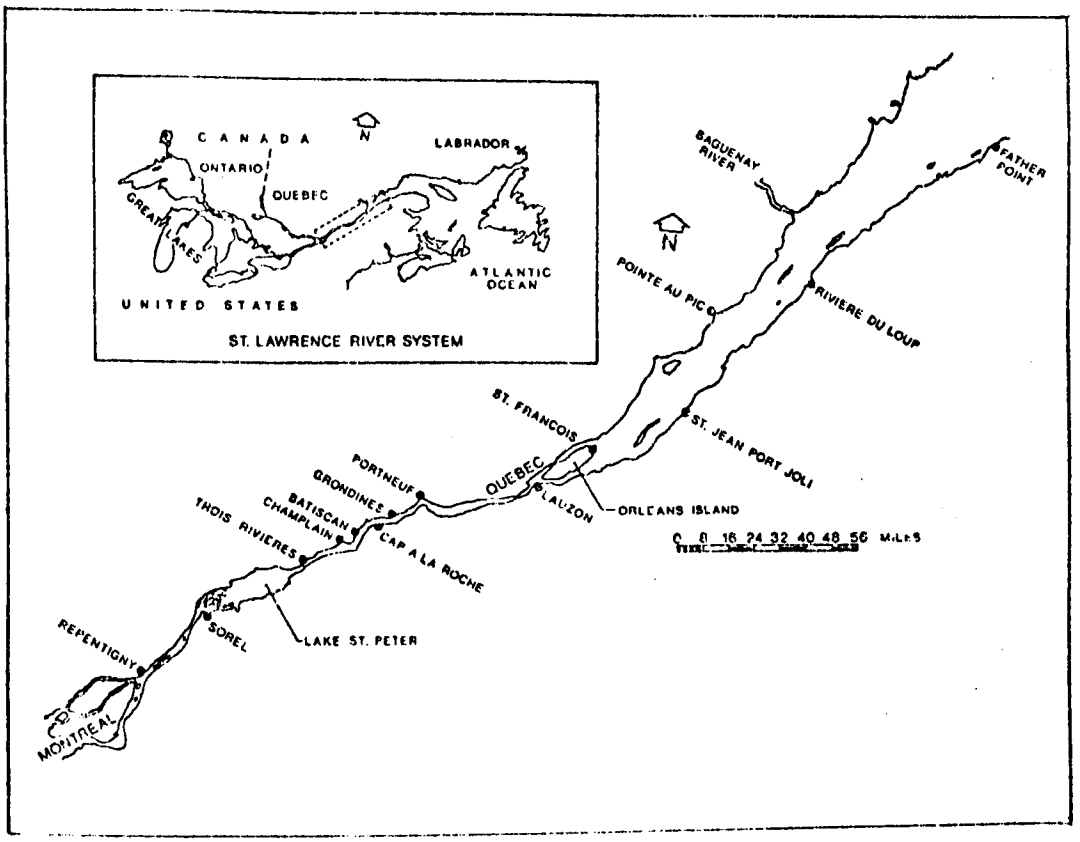

Figure 1.1.1 The St. Lawrence River System.

collected data until after the production of the 1975 Data Report. By the time of the 1977 Survey, it had become obvious that the St. Lawrence Middle Estuary was not a simple partially-mixed Estuary driven solely by the barotropic tide. This report is an attempt to describe the major physical processes controlling the instantaneous circulation and water properties of the Middle Estuary. It is primarily concerned with time scales which range from the semi-diurnal tidal period to one or two hours and space scales which are on the order of kilometres. The tidal records show that almost all of the energy in the currents is confined to the tidal frequencies and so it is this scale of motion that is considered here. Throughout the report processes outside these scales are mentioned only briefly, inasmuch as they modify the tidal processes.

In Chapter 2 the instantaneous temperature-salinity relationships and the tidally-averaged depth-density relationships are examined. In Chapter 3, the tidal current records are analysed in some detail, and it is shown that a simple theory of barotropic motion cannot account for the features that are found on the St. Lawrence, but qualitative arguments are given which show that baroclinic motions can explain some of these anomalous features.

Chapter 4 reviews the linear theory of internal tides and examines the vertical structures that could be found on the St. Lawrence in the light of the tidally-averaged depth-density relationships that are discussed in Chapter 2. In Chapter 5 the horizontal propagation of the internal tides is discussed both for the case of no horizontal density gradients and for the case of arbitrary horizontal density gradients. It is shown that the horizontal advection of the tidally-averaged density gradients is very important in interpreting the measurements that are made by fixed measuring instruments.

In Chapter 6, two problems are considered. The first is the direct problem of predicting the measurements that would be made by a fixed instrument in an estuary, given the density and wave fields. It is shown that the patterns that emerge are very similar to those observed in partially-mixed estuaries. The second problem that is discussed is the inverse problem which is, given the measurements, to determine the wave field which caused these measurements. It is shown that the solution to this problem is not unique.

Chapter 7 is an attempt to widen the field of discussion and to indicate all of the physical processes that go on in the Middle Estuary of the St. Lawrence and to show how these processes interact with one another. The final Chapter is a brief summary of the conclusions of all of the previous chapters along with some recommendations for further research.

1.1 Geography of the St. Lawrence

The drainage basin of the St. Lawrence system encompasses an area of 1.5×10^6 km^2 and a population of about 30 million people (Neu, 1975). It contains the Great Lakes, the St. Lawrence River proper which extends from the outflow of Lake Ontario to Quebec City, the Upper Estuary which extends from Quebec City to Ile aux Coudres, the Middle Estuary which extends from Ile aux Coudres to the Saguenay River, the Lower Estuary which extends from the Saguenay to about Pointe des Monts and the Gulf of St. Lawrence. The tide penetrates as far up the River as the St. Lambert locks in Montreal, while salt penetrates up to the Ile d'Orleans which is just downstream of Quebec City. Figure 1.1.1 gives a location chart which shows the features of interest in the whole system.

The Estuary of the St. Lawrence River and the Gulf of St. Lawrence form a closely-coupled system which is of indisputable importance to Canada and M. Dunbar has written of its importance in Steven (1974). Approximately 65% of all Canadian shipping traverses the system, and it provides access to about 60% of the Canadian population. The St. Lawrence River provides 50% of the fresh water input to the Gulf, and since a large population lives upstream of the Middle Estuary, it is an open sewer carrying the effluent of a large portion of the Canadian and U.S. population. The Gulf has been declared an exclusive Canadian fishing zone and about 40% by weight of all the Canadian sea fish catch comes from the Gulf.

Topographically, the Middle Estuary, the Lower Estuary and the Saguenay River form three distinct areas. The Lower Estuary is dominated by the Laurentian Trough which is a 1000 km long glaciated valley which crosses the Gulf of St. Lawrence and reaches the continental shelf. The depths in the Laurentian Trough reach 350 m and it provides a passage for the intrusion of shelf waters into the Lower Estuary. At the upstream end of the Laurentian Trough is a sill, separating the Lower and Middle Estuaries, which has a depth of only 50 m. The Saguenay River is really a fjord and is very long (about 92 km) and narrow (about 1-6 km) with high rock walls and deep basins which reach depths of about 250 m. The Saguenay is divided by two sills, the shallowest of which is at the entrance to the fjord and is only 20 m deep.

The topography of the Middle Estuary is shown in Figure 1.1.2. At the downstream end, the Middle Estuary is split into two distinct channels by Ile aux Lievres (Hare Island). The South Channel is a broad shallow region, while the North Channel is much deeper with depths reaching 180 m. just off Cap au Saumon. The two channels converge at the

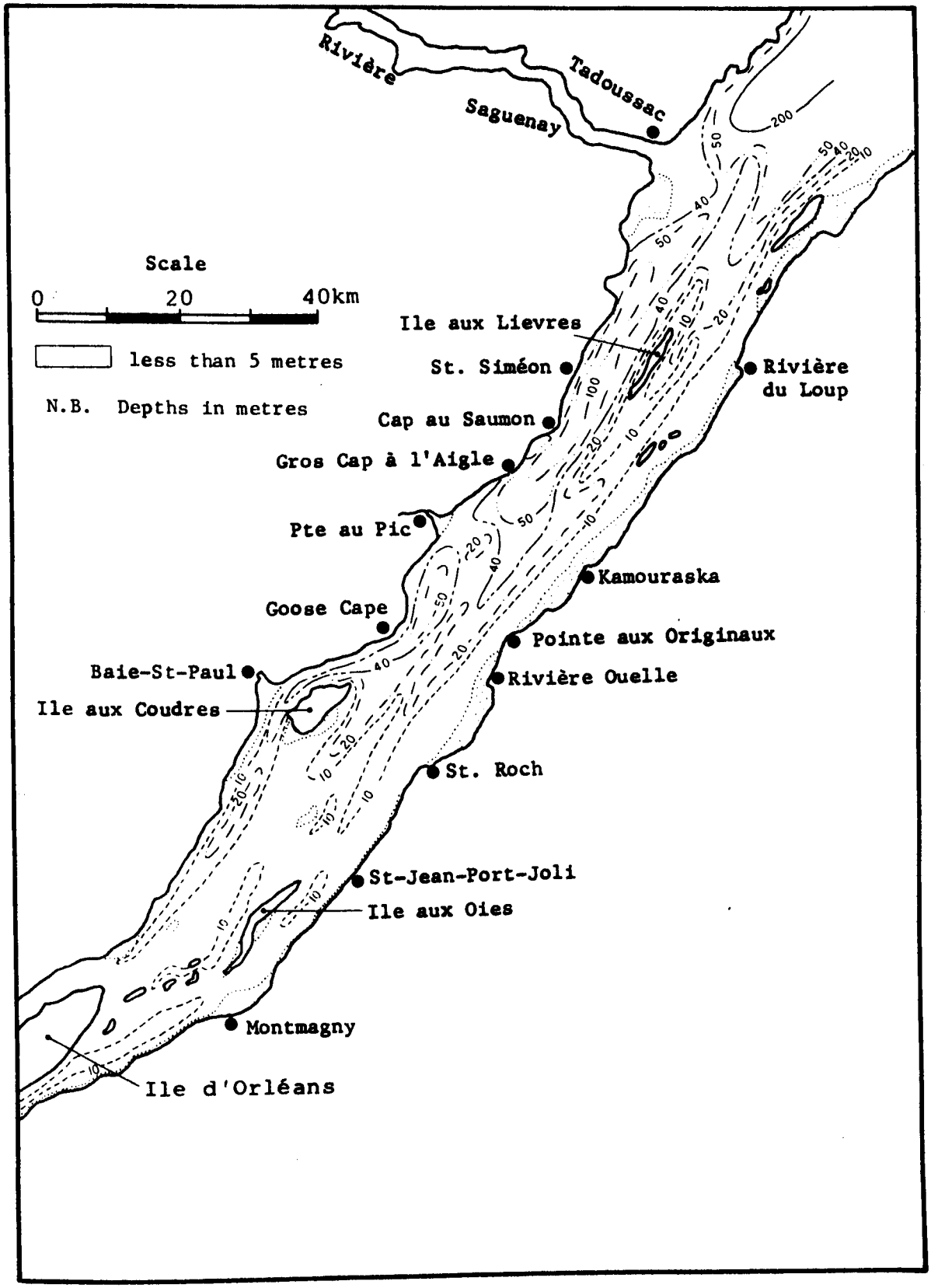

Figure 1.1.2 Topography of the Middle Estuary

upstream end of Ile aux Lievres, but the Estuary is partially blocked near Pte au Pic by a feature that has no official name but will be called the Morin Bank. The maximum depth of water over this bank is about 36 m and upstream of the bank the water deepens to about 85 m near Goose Cape. The main channel takes a distinct bend in passing north of Ile aux Coudres and upstream of Ile aux Coudres the Upper Estuary begins. It will be shown that the topography of the Middle Estuary is a very important factor in the circulation processes.

1.2 Data Base

Although a very large part of the resources of McGill University, Laval University, The University of Quebec at Rimouski, and GIROQU have been concentrated in the Gulf and Lower Estuary of the St. Lawrence, very little physical oceanographic work has been done in the Middle Estuary. The bibliography by El-Sabh, et al. (1969) lists about 230 publications dealing with the physical oceanography of the Gulf and Estuary, but a very small number of them deal with the Middle Estuary, although a large number of them acknowledge the contribution of the Middle Estuary in determining the overall physics of the Gulf.

The data from the field surveys of 1974, 1975 and 1977 form almost the total data base for the Middle Estuary which has been collected on a systematic basis and is available in computer compatible format for easy analysis. Tabular listings of the data obtained are available in the Data Reports, and complete descriptions of the field work are available in the Final Field Reports issued by the technical officers in charge of the field logistics. All of the data is available in computer compatible format to anyone who asks for it.

Since the data is freely available, no attempt will be made here to exhaustively discuss the data collected or the details of the collection systems.

The locations of the stations occupied during each of the surveys are given in Figures 1.2.1 to 1.2.3 and a brief summary of the relevant details of each of the profiling stations is given in Tables 1.2.1 and 1.2.2. The identification number for a current meter record consists of 13 characters of the form

yy-ssC-mmZddd

where yy represents the year of the survey, ss represents the survey location, mm is the mooring number and ddd is the depth of the meter below chart datum in metres. For example, 74-12C-01Z005 specifies the record taken from a current meter that was deployed in 1974, in the Middle Estuary of the St. Lawrence (location 12), on mooring string number 1 at a depth of 5 metres below chart datum. The identification number for a profiling station consists of 7 characters of the form

yy-mmmr

where yy represents the year of the survey, mmm is the station number, and r is the repetition letter. For example, 74-001B specifies a station occupied in 1974, at location 001 and is the second set of data collected at that location.

In Tables 1.2.1 and 1.2.2 the column heading abbreviations are: ND/NT, number of depths and number of times sampled; THW, time of high water; RB/RA, tide ranges during station occupation.

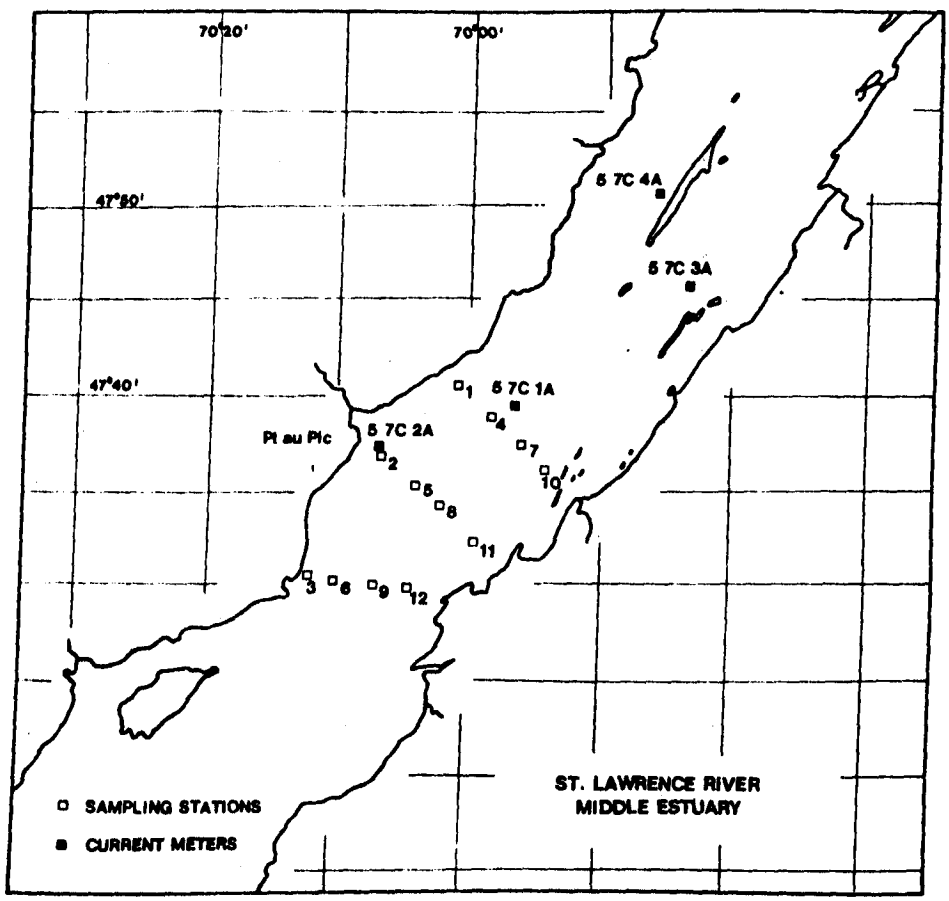

Figure 1.2.1 Locations for the 1974 St. Lawrence Current Survey (from Budgell and Muir, 1975)

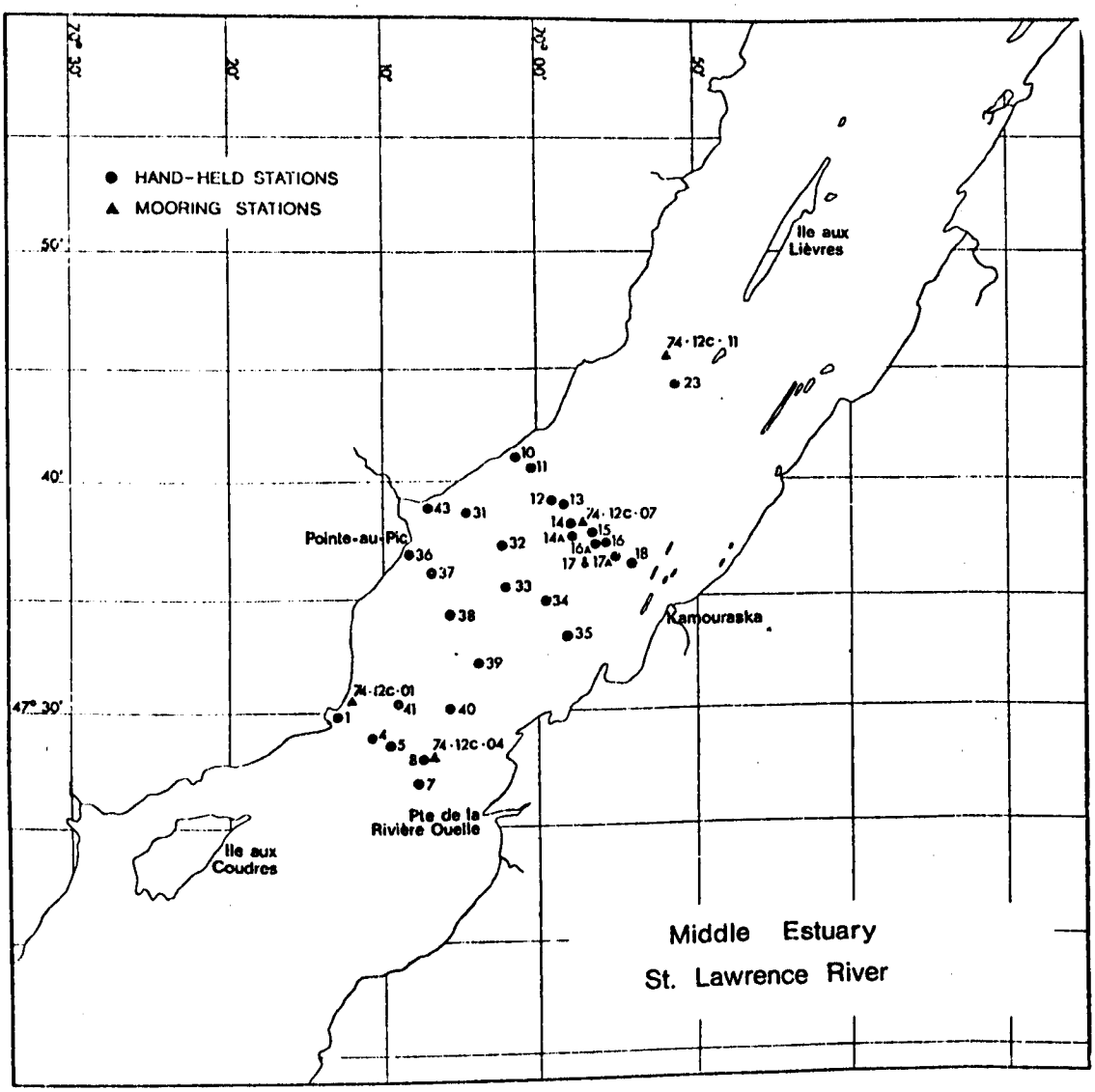

LOCATIONS OF CURRENT MEASURING STATIONS

Figure 1.2.2 Locations for the 1975 St. Lawrence Current Survey (from Muir, 1978).

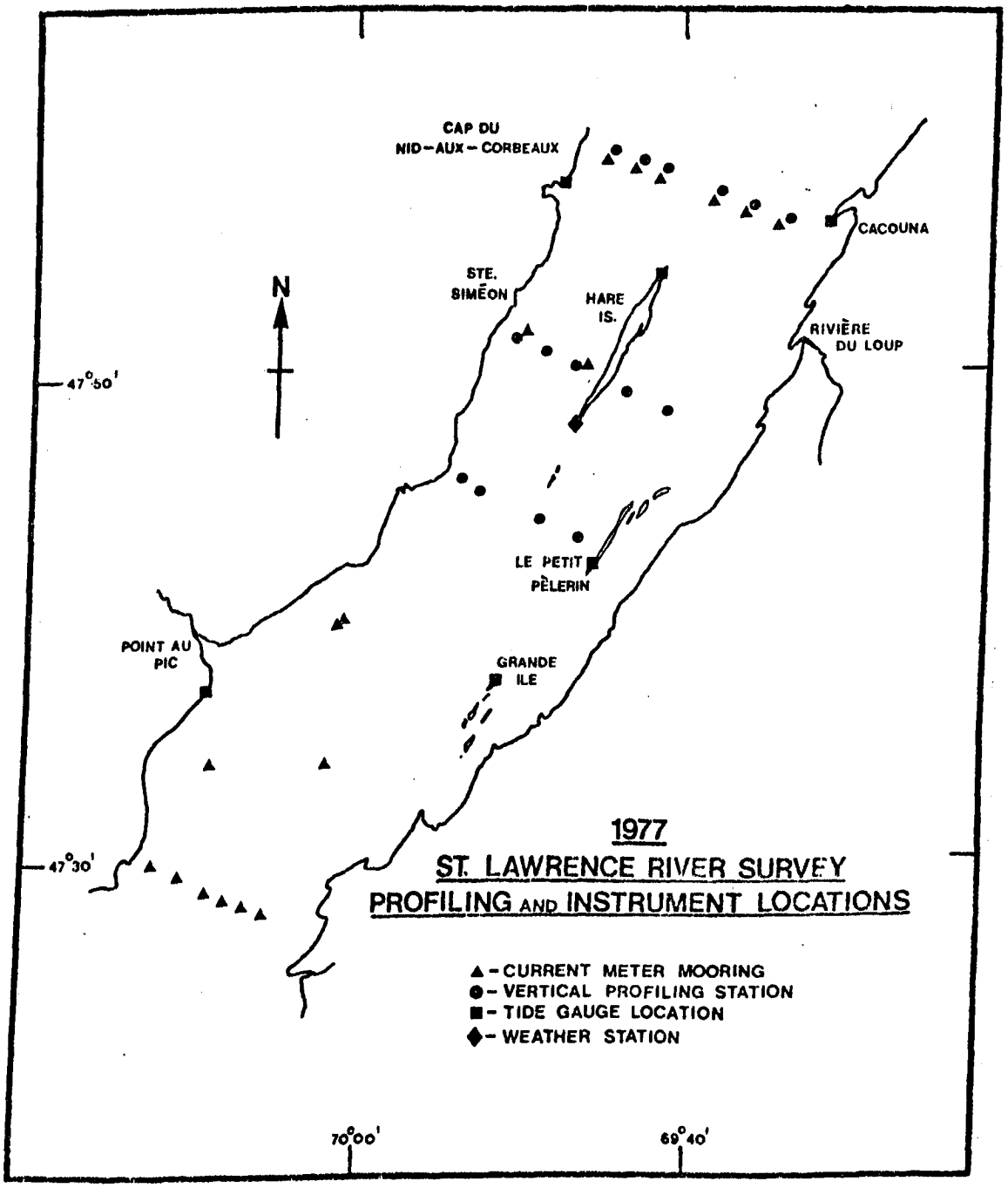

Figure 1.2.3 Locations for the 1977 St. Lawrence Current Survey (from Muir, 1979a).

TABLE 1.2.1. STATION SUMMARY

Station Number	Date	ND/NT	Start Time	Stop Time	TEW	RB/RA	Sounding	Freshwater Discharge (Montreal)
75-001A	17.5.75	11/27	11:27	00:20	23:45	2.3/2.0	69.0	15810
75-001B	23.5.75	12/27	10:46	23:55	17:45	3.1/2.7	56.0	14630
75-001C	5.6.75	11/27	16:20	5:25	04:25	2.2/2.3	52.0	14150
75-002A	18.5.75	11/27	11:15	00:28	12:00	2.5/2.8/2.3	34.0	15630
75-002B	24.5.75	12/27	11:47	00:54	18:35	3.3/2.9	36.0	14440
75-002C	10.6.75	11/27	10:21	23:22	19:35	2.9/2.6	32.3	15960
75-003A	19.5.75	11/26	02:41	15:55	13:25	2.3/2.6	53.0	15290
75-003B	25.5.75	11/14	11:17	18:28			52.5	14290
75-004B	30.5.75	12/27	11:02	00:08	19:20	3.4/2.9	56.0	14030
75-004B	6.6.75	12/24	21:16	08:52	05:05	2.5/2.7	57.0	14630
75-005A	31.5.75	10/27	10:01	23:07	11:05	2.3/2.5/2.0	21.5	14400
75-005B	11.6.75	11/27	14:51	03:50	20:10	3.0/2.8	19.0	15810
75-006A	1.6.75	11/27	00:30	13:38	11:45	1.6/1.8/2.0	36.9	14440
75-007A	2.6.75	12/27	19:00	08:07	01:40	1.6/1.4	45.0	14550
75-008A	3.6.75	12/27	14:00	03:08	02:35	1.3/1.7/1.6	35.0	14330
75-008B	11.6.75	11/27	00:53	13:54	07:40	3.6/3.9	30.0	15810
75-009A	4.6.75	11/27	10:04	23:05	14:55	1.3/1.4	18.7	14220
75-010A	22.5.75	12/27	11:32	00:40	16:55	2.9/2.7	31.0	14550
75-010B	27.5.75	11/27	21:04	10:08	08:45	2.7/3.5/3.8	28.5	14590
75-010C	6.6.75	11/27	07:04	20:09	16:55	2.7/2.7	32.0	14630
75-011A	20.5.75	10/27	07:48	20:54	14:40	2.3/2.5	20.0	14960
75-011B	28.5.75	8/27	11:30	00:36	21:25	3.5/2.9/2.5	19.5	14590
75-011C	9.6.75	10/27	03:47	16:51	06:30	3.2/3.4	18.0	15850
75-012A	19.5.75	11/27	17:17	06:23	02:10	2.4/2.2	18.0	15290
75-012B	29.5.75	9/27	08:01	21:05	09:40	3.2/3.4	17.3	14110
UNITS			GMT	GMT			M.	m^3/sec.

TABLE 1.2.2

1977

STATION SUMMARY

Station Number	Date	ND/NT	Start Time	Stop Time	TEW	RB/RA	Sounding	Freshwater Discharge (Montreal)
77-001A	8.5.77	11/27	15:00	04:11	23:10	2.9/2.5	74.7	
77-001B	13.6.77	11/27	00:30	13:40	04:45	2.2/2.4		
77-002A	6.5.77	12/27	19:00	08:12	21:15	3.7/3.4	61.0	
77-002B	29.5.77	9/51	06:00	07:08	15:50/04:15	2.3/2.5/3.1/3.2		
77-002C	11.6.77	9/27	20:30	09:30	03:50	2.1/2.2		
77-002D	28.6.77	11/51	02:30	03:40	03:55	3.0/3.2		
77-003A	4.5.77	9/10	18:30	23:05	19:35	4.1/3.8	29.5	
77-003B	5.5.77	9/26	16:00	05:35	20:20	4.0/3.6		
77-003C	28.5.77	8/47	03:30	04:38	14:55/03:25	2.0/2.2/2.5/2.5		
77-003D	11.6.77	9/27	06:00	19:08	15:15	1.6/1.6		
77-004A	4.5.77	8/27	04:00	17:04	07:00	4.5/4.8	28.0	
77-004B	10.6.77	9/27	15:30	04:39	03:00	1.8/2.1/2.0		
77-004C	29.6.77	9/51	05:30	06:37	17:35/05:55	2.9/2.7/3.7/4.1		
77-005A	3.5.77	9/27	13:30	02:39	18:50	3.8/3.7	28.0	
77-005B	9.6.77	9/51	13:30	14:38	13:05	2.0/2.2/2.2		
77-006A	2.5.77	10/27	22:50	12:18	06:20	4.0/4.3	25.0	
77-006B	8.6.77	10/27	23:31	12:39	00:50	2.4/2.1		
77-007A	11.5.77	12/27	05:30	18:45	13:50	2.1/2.2	80.4	
77-007B	21.5.77	12/27	08:00	21:10	08:45	3.0/3.2/2.4		
77-007C	25.6.77	11/51	11:30	12:43	13:05/01:55	2.3/2.5/2.3/1.9		
77-008A	11.5.77	11/27	20:00	09:10	02:40	2.1/1.9	63.5	
77.008B	21.5.77	11/27	22:30	11:40	09:25	2.1/2.9/3.1		
77-008C	24.6.77	10/51	09:30	10:38	12:00/00:50	2.1/2.4/2.3/2.0		
77-009A	12.5.77	9/27	10:30	23:38	15:00	1.9/2.1	48.2	
77-009B	22.5.77	9/27	15:00	04:11	21:55	2.2/1.8		
77-009C	23.6.77	9/51	05:31	06:38	11:10	2.4/2.6/2.3/2.0		

continued.....

continued.....

1977

TABLE 1.2.2 (con't)

STATION SUMMARY

Station Number	Date	ND/NT	Start Time	Stop Time	THW	RB/RA	Sounding	Freshwater Discharge (Montreal)
77-010A	13.5.77	10/27	01:30	14:39	03:35	2.2/2.1/2.0	24.8	
77-010B	20/5/77	10/27	16:59	06:11	20:45	2.2/2.3		
77-010C	22.6.77	9/51	02:30	03:40	10:25	2.6/2.8/2.7/2.1		
77-011A	13.5.77	8/27	15:30	04:30	16:05	2.0/2.1/2.3	17.0	
77-011B	20.5.77	7/27	03:00	16:07	08:05	3.2/3.4		
77-011C	21.6.77	8/51	00:30	01:37	09:35	2.8/3.0/2.4/2.2		
77-012A	14.5.77	12/27	10:00	23:14	16:50	2.1/2.2	129.8	
77-012B	18.6.77	13/51	10:01	11:14	20:30	3.3/2.5/2.3/3.0		
77-013A	16.5.77	13/27	04:30	17:49	07:45	4.6/4.9	114.7	
77-013B	17.6.77	12/51	08:00	09:11	19:55	3.3/2.2/2.3/3.1		
77-014A	18.5.77	7/51	10:30	11:35	19:40	2.8/2.5/3.2/3.5	15.4	
77-014B	16.6.77	8/51	04:30	05:37	06:40	2.8/3.2/2.6/2.3		
77-015A	15.5.77	8/51	01:30	02:36	05:20	2.6/2.7/2.4/2.3	16.3	
77-015B	14.6.77	8/4	14:30	16:06				
77-015C	14.6.77	8/51	18:01	03:38	17:55	1.9/2.6/3.0/2.4		

CHAPTER 2

The Physical Environment

2.0 Introduction

The Middle Estuary of the St. Lawrence River is characterized by its horizontal and vertical variations in temperature and salinity. Since temperature and salinity are the two major components of density, their variability gives rise to the variability in density throughout the Middle Estuary. It will be shown later that the tidally-averaged density structure is one of the major controlling factors in the circulation of the Estuary. In this Chapter, attempts will be made to elucidate the variability, in both space and time, of the temperature and salinity and of the tidally-averaged density. The approach, due to a lack of physical theories of mixing, will be primarily statistical.

2.1 Temperature-Salinity Relationships

At the extreme upstream end of the Estuary, the source of fresh water is the St. Lawrence River which drains the Great Lakes basin. The salinity of this water is essentially zero, since salt water penetrates only as far as the Ile D'Orleans (Muir, 1975). The lowest temperature, which is $1^{o}C$ occurs in the spring and rises more or less monotonically throughout the year to a maximum in the autumn. In the course of the water's passage through the upper parts of the river, and particularly such very shallow sections as Lake St. Peter, its temperature is modified from that found in the outflow from Lake Ontario.

In the warm, sunny days of the spring, the water temperature is raised considerably, while in the autumn its temperature is lowered.

The City of Quebec Waterworks Board has occasionally measured the water temperature at the entrance to their filtration factory which is approximately 2.5 km from the river. The intake is located some 5 km upstream of the Pont du Quebec, is 3 m below chart datum, and the water takes approximately 56 minutes to get from the river to the filtration factory (Roy, personal communication). Figure 2.1.1 shows that in 1977 the water temperature had a general trend upwards over the summer, but that there was a fairly large noise level attached to the general trend. Since the intake pipe is buried a minimum of 3 m in the ground, the temperatures at the filtration factory should fairly accurately reflect the water temperature in the river.

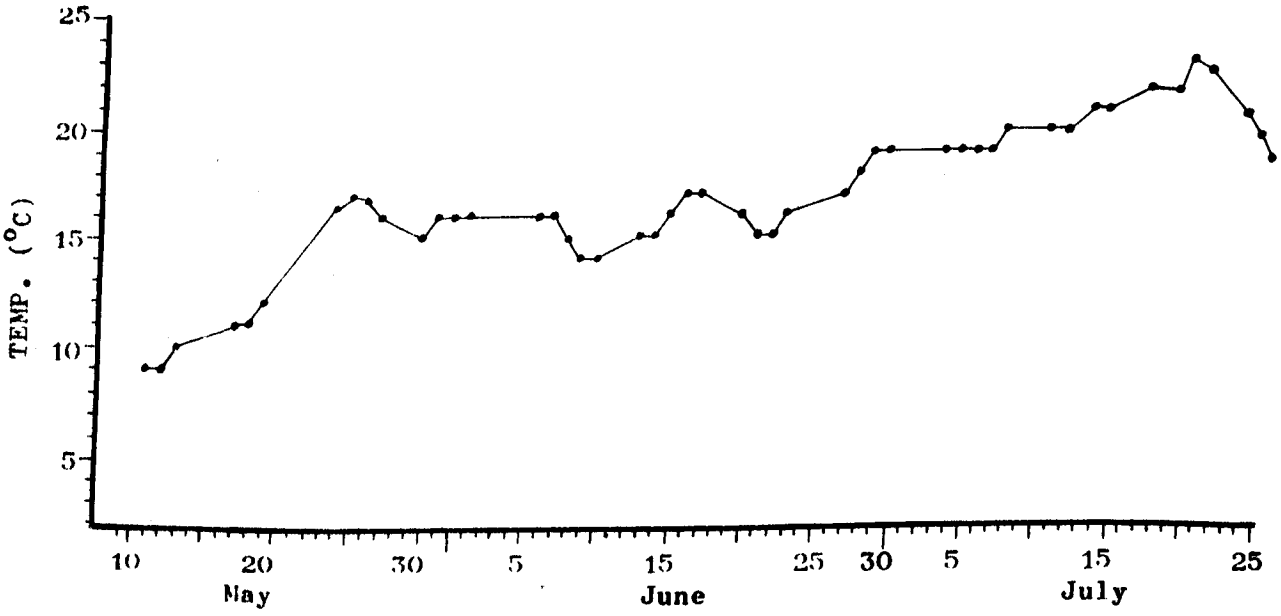

Figure 2.1.1 Water temperature at Quebec City, 1977.

At the opposite end of the Middle Estuary is the Lower Estuary whose characteristics have been known for a number of years. The most recent descriptions may be found in El-Sabh (1979), Koutitonsky (1979) and Ingram (1979). There is a three-layer circulation pattern where the bottom of the intermediate layer is approximately 100 m deep. The intermediate layer is formed by advection from the Gulf and is mixed with the surface layer by means of breaking internal waves and vertical diffusion. The minimum seasonal temperature occurs in April and there is usually a temperature minimum at about 60 m depth. The water in the bottom layer is of little interest here since it cannot penetrate the 50 m deep sill at the top of the Laurentian Trough. There is a substantial input of fresh water into the surface layer from the Saguenay River.

There is no substantial input of fresh water into the Middle Estuary between Quebec City and the Saguenay River and so it would be expected that a T-S diagram would show conservative mixing. This is true if a T-S diagram is plotted for an individual station. The magnitude of the correlation coefficient for each one of the 66 stations is seldom below -0.99 and the plots are remarkably linear. However, if a single T-S diagram is drawn for the Middle Estuary as a whole, the effects of the variability in the end members are immediately apparent.

For the 5566 temperature-salinity pairs measured on the 1975 survey, which was concentrated around Pointe Au Pic, the correlation coefficient is -0.946 and the equation of the T-S line is

$$S = -1.8601T + 30.4991$$

For the 9801 temperature-salinity pairs measured in the 1977 survey,

which was further downstream than the 1975 survey and which covered a longer length of the Estuary, the correlation coefficient drops to -0.7835 and the equation of the T-S line is

$$S = -1.3933T + 30.7696$$

The standard errors of estimate for the slopes of the two lines are 0.00856 and 0.0112 respectively.

It is, therefore, impossible to relate density to either temperature or salinity alone over the whole Middle Estuary at all times. This is in spite of the fact that the T-S diagram for a single station is linear, and that there is conservative mixing over the Estuary as a whole. The properties of the end members change sufficiently rapidly that there is no generally applicable T-S relationship that could be used, even over the one- or two-month period of a particular survey.

There is virtually no correlation between the slope of the individual regression lines and the distance upstream, the distance cross-stream, the depth of the water, the tide height, the square of the tide height (energy) or the upstream water temperature. There is a weak correlation between the slope of the T-S lines and the date, but the correlation coefficient is not high and only 50% of the variance is explained. Stepwise regressions on various linear combinations of the above parameters do not reveal anything useful. Hence, it would not be possible to monitor the density structure in the Middle Estuary by simple means, such as recording the upstream water temperature for example.

2.2 Depth-Density Relationships

If it were possible to find a linear T-S relationship for the whole Middle Estuary, then it could be argued that density was related to salinity alone and then the conservation equations which are known to hold for salinity would also hold for density. This argument cannot be used on the St. Lawrence. Since there is no easily discernible relationship between temperature and salinity, there will be no simple relationship between salinity alone and density.

One of the most important assumptions in any model of estuarine circulation is that of the relationship between the depth and the tidally-averaged density. Two assumptions are typically made. The first, and most critical, is that the depth-density relationship is of the form

$$\bar{\rho}(x,y,z) = \rho_o(x,y)D(z) \qquad (2.2.1)$$

That is, that the horizontal variation in the density is separable from the vertical variation. The second assumption concerns the mathematical form of the function $D(z)$.

In her book on internal waves, Roberts (1975) discusses a number of different forms for $D(z)$ that are usually used to represent the vertical structure, but most of these forms are concerned with the structures found in the open ocean and which are very unlike the tidally-averaged density structures found in partially-mixed estuaries such as the St. Lawrence. These vertical distributions may be ignored with impunity. There are two criteria which must be met by any usable vertical density distribution and these are: that the analytical form must correspond closely to the observed density distributions, and that the analytical

form and its first derivative (which enters into the Brunt-Vaisala frequency) must have mathematically tractable properties. In this section an attempt will be made to explore the applicability of the separability hypothesis and to find an appropriate form for the relationship between depth and the tidally-averaged density.

In the following three sections, three different models relating the tidally-averaged density and depth will be examined. The first model is a general exponential model of the form

$$\bar{\rho} = \rho_o(x,y)\exp\left(\sum_{i=1}^{I} a_i z^i\right) \qquad (2.2.2)$$

which has the advantage that the Brunt-Vaisala frequency is then given by a polynomial in z. One of the most common vertical forms chosen to represent vertical density structures is a simple exponential, and so this form seems to be a natural one to try. The second model is one that Forrester (1974) found appropriate for the tidally-averaged density structure of the Lower St. Lawrence Estuary. The form used is given by

$$\bar{\rho} = \rho_o(x,y)\exp(a_1/z+a_2) \qquad (2.2.3)$$

The third model to be tested is a generalization of that used by Magaard (1962) in his studies of the propagation of internal waves over topography. It is given by the form

$$\bar{\rho} = \rho_o(x,y)\left(1 + \sum_{i=1}^{I} a_i z^i\right)^{\frac{1}{2}} \qquad (2.2.4)$$

Each of these models will be used in a least-squares fit of the tidally-averaged density structure at each of the 65 stations in the Middle Estuary. If the computer programs are written in a

general form, such that the constants in the vertical part of the equation may be constrained to be constants over the whole estuary, then it is possible to test the separability hypothesis by examining the variation in these coefficients when they are allowed to vary with each individual station.

2.3 The Exponential Model

The appropriate order of the polynomial in the exponential model is not immediately obvious. Hence it is necessary to derive the equations for a very general case. The individual stations will be indexed by k, with the maximum number of stations being N and a particular station being K. At each individual station, the depths are indexed by j and the maximum number of depths at station k is M_k. The powers of the exponential function are indexed by i, and the order of the polynomial is I, with a particular power given by ℓ. The observed tidally-averaged density at station k and depth j is $\bar{\rho}_{k,j}$, while the computed density at the same location is $\bar{\rho}_{c,k,j}$ and the j^{th} depth at station k is $z_{k,j}$. Then, taking logarithms of both sides of (2.2.2) gives

$$\ell n(\bar{\rho}_{c,k,j}) = \ell n(\rho_{o,k}) + \sum_{i=1}^{I} a_i z_{k,j}^i$$

The least-squares equation at the station K is

$$\sum_{j=1}^{M_K} \left[\ell n(\bar{\rho}_{K,j}) - \ell n(\rho_{o,K}) - \sum_{i=1}^{I} a_i z^i_{K,j} \right]^2 = \text{minimum} \qquad (2.2.5)$$

and taking derivatives, with respect to $\ell n(\rho_{o,K})$ gives a set of N equations of the form

$$M_K \ell n(\rho_{o,K}) + \sum_{j=1}^{M_K} \left(\sum_{i=1}^{I} a_i z^i_{K,j} \right) = \sum_{j=1}^{M_K} \ell n(\rho_{K,j})$$

The least-squares equation for all N stations is formed by adding together the N equations of the form (2.2.5) and then, differentiating I times in succession with respect to a_ℓ gives the I normal equations of the form

$$\sum_{k=1}^{N} \sum_{j=1}^{M_k} z^\ell_{k,j} \ell n(\rho_{o,k}) + \sum_{k=1}^{N} \sum_{j=1}^{M_k} \sum_{i=1}^{I} a_i z^{i+\ell}_{k,j} = \sum_{k=1}^{N} \sum_{j=1}^{M_k} z^\ell_{k,j} \ell n(\rho_{k,j})$$

Since there are N+I unknowns, these two forms of equations may be added together into one matrix equation of the form

$$
\begin{pmatrix}
M_1 & 0 & \cdots & 0 & \sum_{j=1}^{M_1} z_{1,j} & \cdots & \sum_{j=1}^{M_1} z_{1,j}^{I} \\
0 & M_2 & & & & & \\
\vdots & \vdots & & & \vdots & & \vdots \\
0 & \cdots & \cdots & M_N & \sum z_{N,j} & \cdots & \sum z_{N,J}^{I} \\
\sum_{j=1}^{M_1} z_{1,j} & \sum_{j=1}^{M_2} z_{2,j} & \cdots & \sum_{j=1}^{M_N} z_{N,j} & \sum_{k=1}^{N} \sum_{j=1}^{M_k} z_{k,j}^{2} & \cdots & \sum_{k=1}^{N} \sum_{j=1}^{M_k} z_{k,j}^{I} \\
\sum_{j=1}^{M_1} z_{1,j}^{2} & \sum_{j=1}^{M_2} z_{2,j}^{2} & \cdots & \sum_{j=1}^{M_N} z_{N,j}^{2} & \sum_{k=1}^{N} \sum_{j=1}^{M_k} z_{k,J}^{3} & \cdots & \sum \sum z_{k,j}^{I+1} \\
\vdots & \vdots & & \vdots & \vdots & & \vdots \\
\sum_{j=1}^{M_1} z_{1,j}^{I} & \sum_{j=1}^{M_2} z_{2,j}^{I} & \cdots & \sum_{j=1}^{M_N} a_{N,j}^{I} & \sum_{k=1}^{N} \sum_{j=1}^{M_k} z_{k,j}^{I+1} & \cdots & \sum_{k=1}^{N} \sum_{j=1}^{M_k} z_{k,j}^{2I}
\end{pmatrix}
\begin{pmatrix}
\ln(\rho_{o,1}) \\
\ln(\rho_{o,2}) \\
\vdots \\
\ln(\rho_{o,N}) \\
a_1 \\
a_2 \\
\vdots \\
a_I
\end{pmatrix}
$$

$$
= \begin{pmatrix}
\sum_{j=1}^{M_1} \ln(\bar{\rho}_{1,j}) \\
\sum_{j=1}^{M_2} \ln(\bar{\rho}_{2,j}) \\
\vdots \\
\sum_{j=1}^{M_N} \ln(\bar{\rho}_{N,j}) \\
\sum_{k=1}^{N} \sum_{j=1}^{M_k} z_{k,j} \ln(\bar{\rho}_{k,j}) \\
\vdots \\
\sum_{k=1}^{N} \sum_{j=1}^{M_k} z_{k,j}^{I} \ln(\bar{\rho}_{k,j})
\end{pmatrix}
\qquad (2.2.6)
$$

This matrix equation is linear in the unknowns, and as a result, may be easily solved using any one of a number of proprietary routines. If $N = 1$, then the surface, tidally-averaged density and the constants a_1 to a_I are allowed to vary with each station, but if the whole equation is used and N is set equal to the number of stations, then $\rho_{o,k}$ is allowed to vary for each station, but the constants a_1 to a_I are fixed for all of the stations. The appropriate degree for the polynomial may be determined by a step-wise regression process.

Since the equations for the exponential model are linear, and therefore quick and easy to solve, a large number of computer runs were made with this model. Two types of test were done. First of all, five different forms of the polynomial were used; a simple monomial, quadratic, a cubic, a quartic, and a model used by Krauss (1966), the partial cubic, which is

$$\bar{\rho} = \rho_o \exp(a_1 z + a_3 z^3)$$

The second test was to group the stations into combinations in order to determine whether or not there were any significant differences in the various combinations. The combinations of stations were: all of the data as one group, the 1975 stations, the 1977 stations, the stations in the North Channel, and the stations in the South Channel. Table 2.3.1 lists the results of the tests of significance for the various combinations of models and station groupings. The various combinations may be compared by using an F test (Snedecor and Cochran, 1967) and the analysis of variance results are listed here in the standard format. The column headed 'Sum of Squares' gives the sum of the squares of the observed minus the computed density. The column headed 'Mean Square'

gives the mean of the deviations squared and the square root of this value is the standard error of estimate of the deviations in units of gm/ml.

For all of the station groupings, except for the South Channel, the reduction in the variance of the deviations is quite marked up to the cubic exponential. This is shown by the large F-values. The reduction in variance gained by adding the quartic is still significant for some of the groups at the .01 significance level, but this reduction in variance is not particularly significant in a practical sense. For example, for the All station grouping, the standard error of estimate is increased from 1.13 to 1.14 sigma-t units, while for the 1977 Stations the standard error of estimate is reduced from 0.836 to 0.826 sigma-t units. Since the limit of practical measurement of density is barely accurate to 0.01 sigma-t units, this error reduction can have no practical significance.

The South Channel is clearly different from the rest of the station groupings. In this area, there is no practical reason for preferring a polynomial of order more than one, and this agrees with the data, since the South Channel stations are very often, although not always, vertically homogeneous. Figures 2.3.1 through 2.3.5 give plots of depth versus density for the five groups of stations and also the curves derived from the exponential cubic model. The densities have been normalized by dividing through by the surface density derived from the exponential cubic model in order to remove the effects of the varying surface density. Figure 2.3.6 plots the surface densities from the exponential cubic model on a chart of the Middle Estuary and gives an indication of the variation that is in the Estuary. More will be made of this variation in the section on the separability hypothesis.

Table 2.3.1

TESTS OF SIGNIFICANCE FOR EXPONENTIAL MODELS

ANALYSIS OF VARIANCE

Source of Variance	Degrees of Freedom	Sum of Squares	Mean Square	F
1975 STATIONS				
Exponential	226	0.000600861		
Quadratic	225	0.000261755	0.000001163	
				291.6
Quadratic	225	0.000261755		
Cubic	224	0.000252302	0.000001126	
				8.4
Partial Cubic	225	0.000295437		
Cubic	224	0.000252302	0.000001126	
				38.3
Cubic	224	0.000252302		
Quartic	223	0.000250175	0.000001122	
				1.9
1977 STATIONS				
Exponential	333	0.000418612		
Quadratic	332	0.000230111	0.000000693	
				272.0
Quadratic	332	0.000230111		
Cubic	331	0.000230108	0.000000695	
				0.0
Partial Cubic	332	0.000239104		
Cubic	331	0.000230108	0.000000695	
				12.9
Cubic	331	0.000230108		
Quartic	330	0.000225070	0.000000682	
				7.4

Table 2.3.1 (continued)

Source of Variance	Degrees of Freedom	Sum of Squares	Mean Square	F
NORTH CHANNEL STATIONS				
Exponential	331	0.000762494		
Quadratic	330	0.000318194	0.000000964	
				460.9
Quadratic	330	0.000318194		
Cubic	329	0.000281951	0.000000857	
				42.3
Partial Cubic	330	0.000384897		
Cubic	329	0.000281951	0.000000857	
				120.1
Cubic	329	0.000281951		
Quartic	328	0.000281734	0.000000859	
				4.00
SOUTH CHANNEL STATIONS				
Exponential	228	0.000434806		
Quadratic	227	0.000431116	0.000001899	
				1.9
Quadratic	227	0.000431116		
Cubic	226	0.000430485	0.000001905	
				2.5
Partial Cubic	227	0.000431781		
Cubic	226	0.000430485	0.000001905	
				1.43
Cubic	226	0.000430485		
Quartic	225	0.000427053	0.000001898	
				1.8

Table 2.3.1 (continued)

Source of Variance	Degrees of Freedom	Sum of Squares	Mean Square	F
ALL STATIONS				
Exponential	560	0.001431251		
Quadratic	559	0.000761594	0.000001362	
				491.7
Quadratic	559	0.000761594		
Cubic	558	0.000723718	0.000001297	
				29.2
Partial Cubic	559	0.000857896		
Cubic	558	0.000723718	0.000001297	
				103.45
Cubic	558	0.000723718		
Quartic	557	0.000723457	0.000001297	
				5.0

Useful F-Values:

$F_{500,1,0.01} = 6.69$ $F_{200,1,0.01} = 6.76$

$F_{500,1,0.05} = 3.86$ $F_{200,1,0.05} = 3.89$

$F_{500,500,0.05} = 1.16$ $F_{200,200,0.05} = 1.26$

$F_{500,500,0.01} = 1.23$ $F_{200,200,0.01} = 1.39$

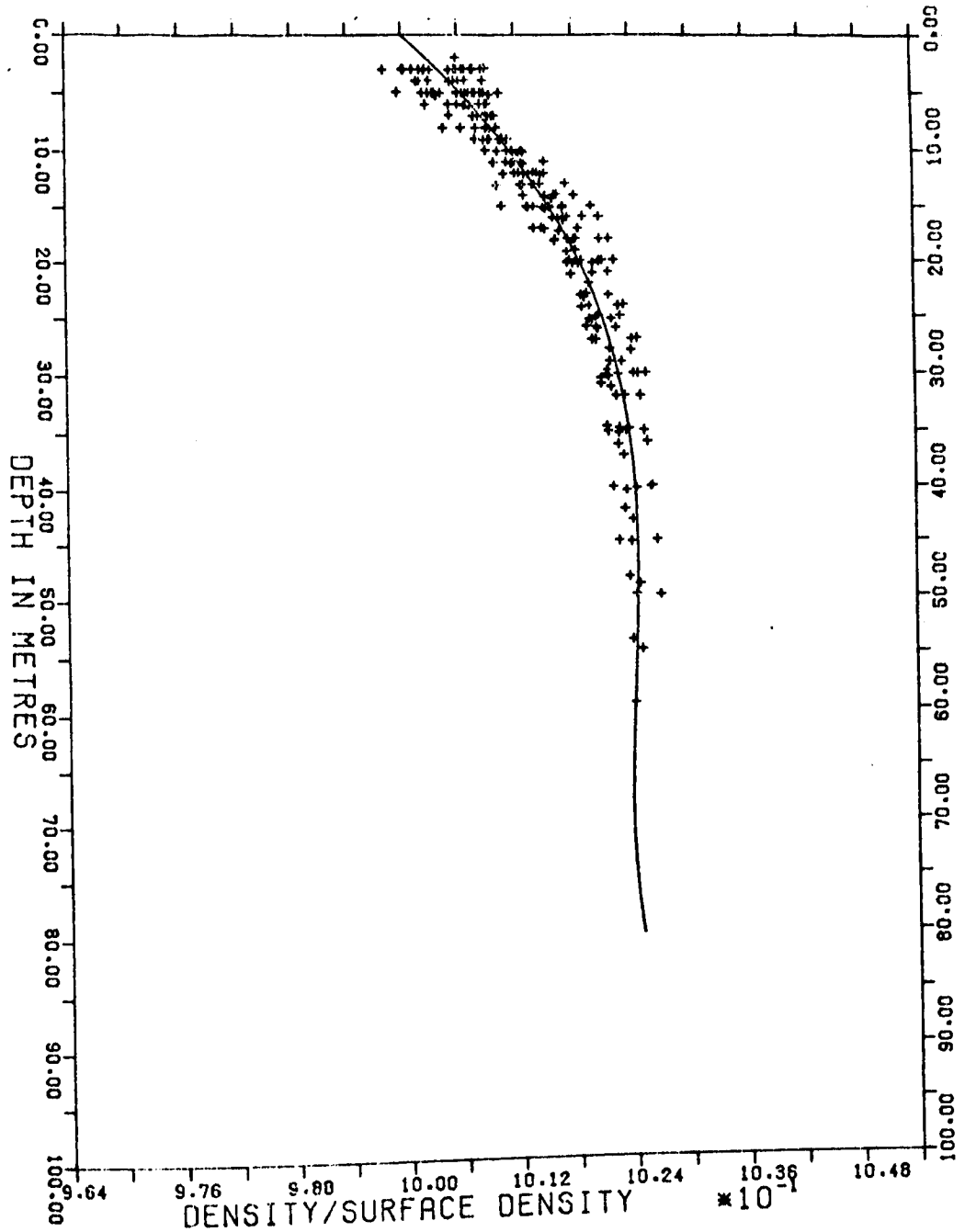

Figure 2.3.1 **Depth versus density for the 1975 Stations.**

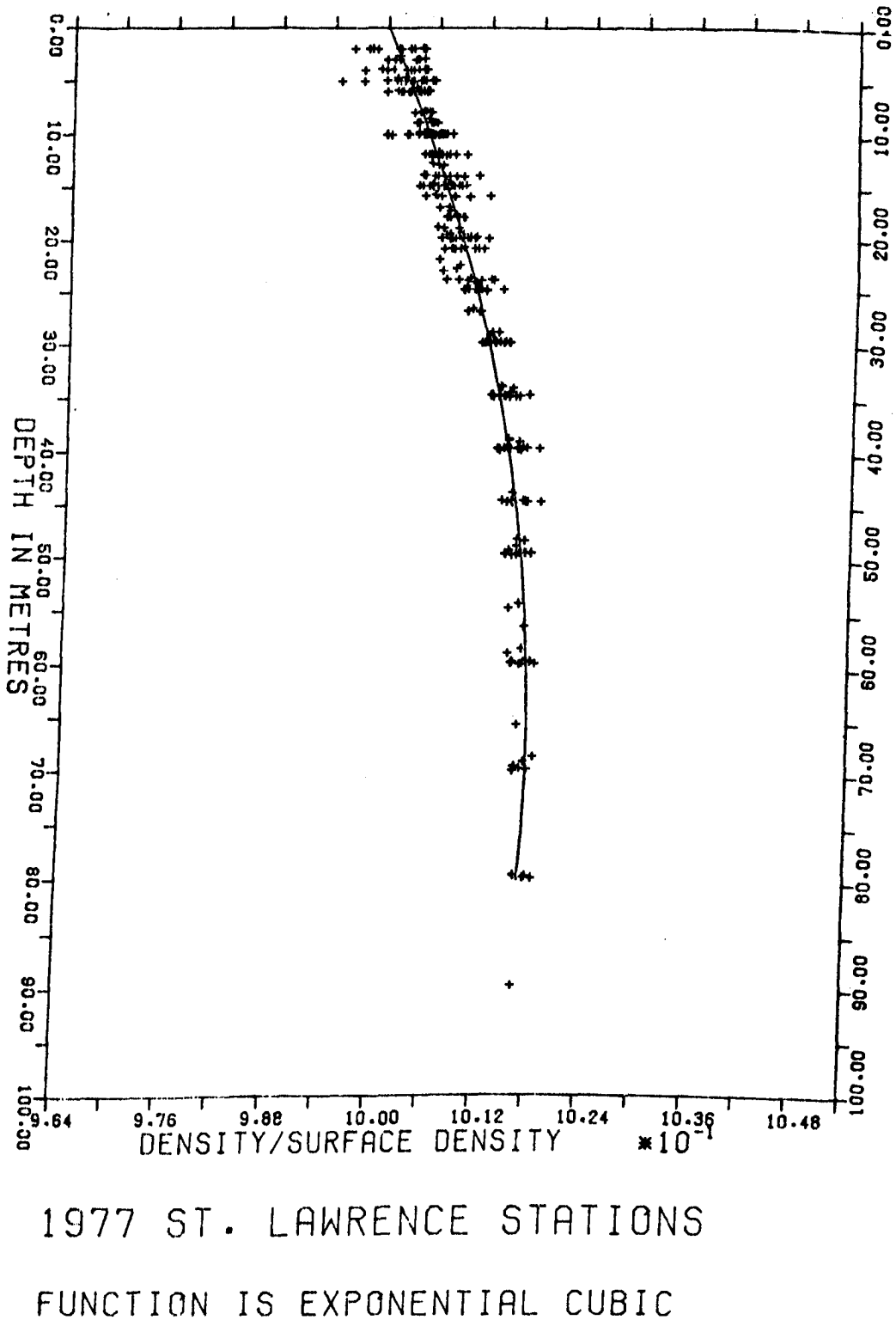

Figure 2.3.2 **Depth versus density for the 1977 Stations.**

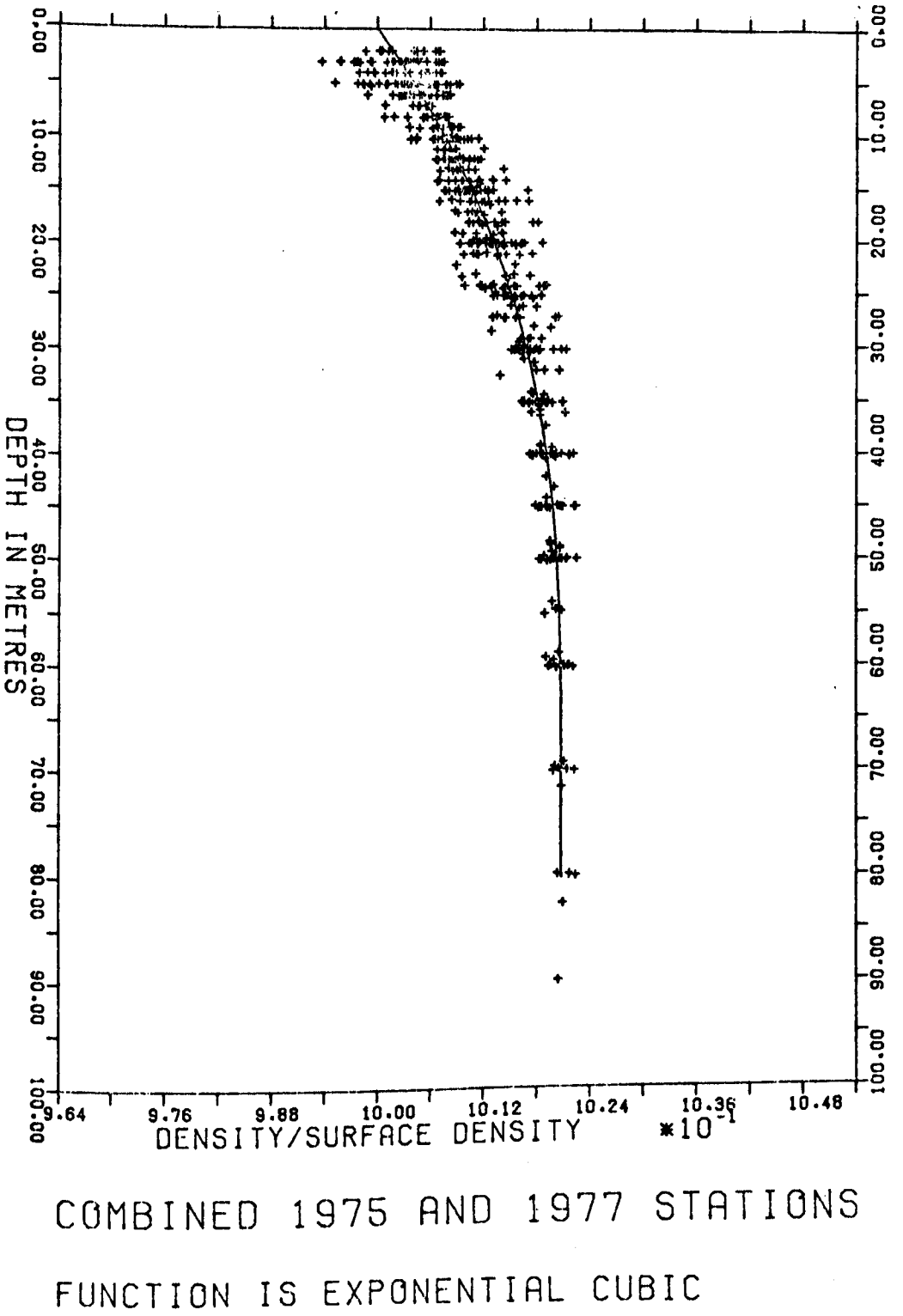

Figure 2.3.3 **Depth versus density for all of the Stations.**

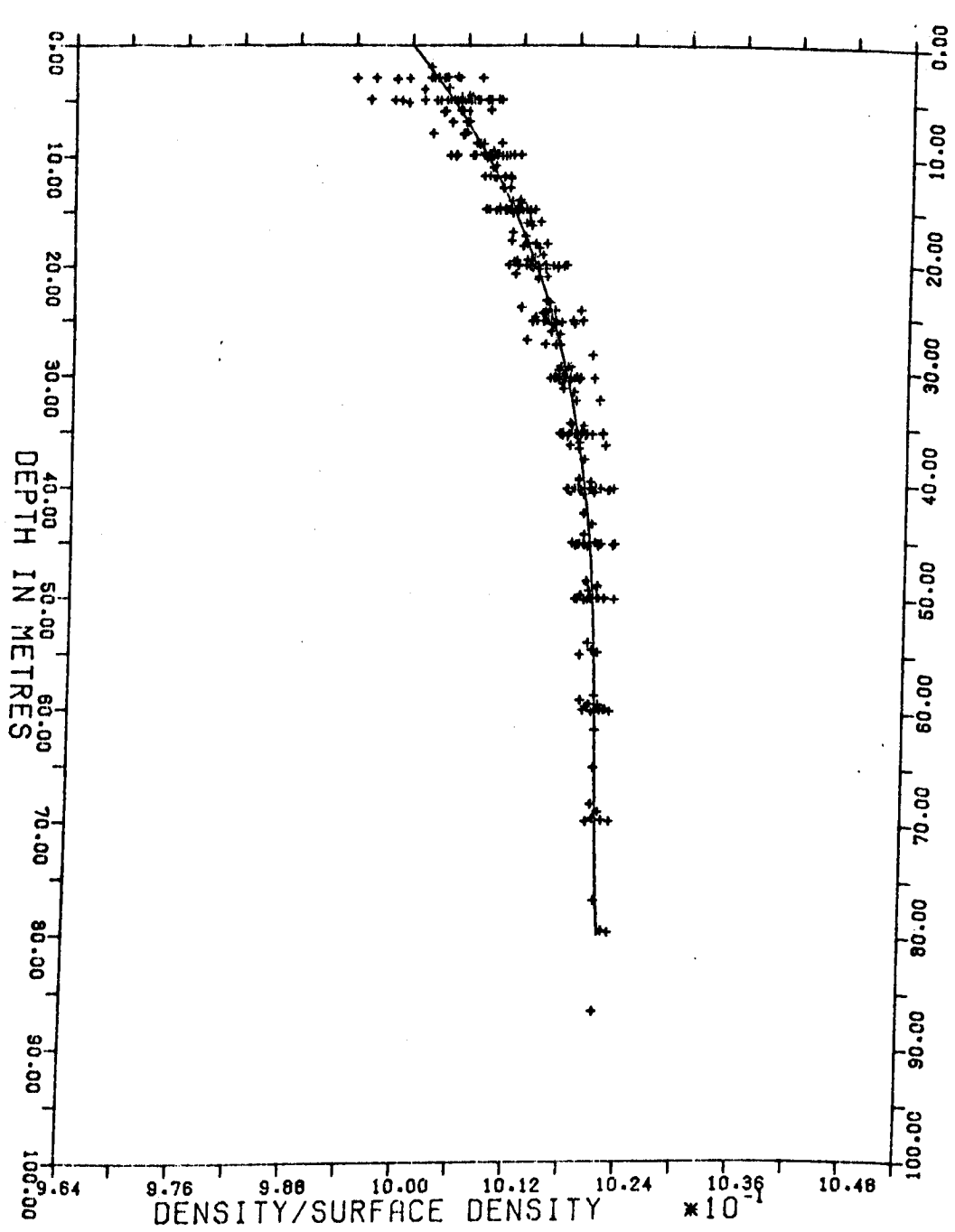

Figure 2.3.4 **Depth versus density for the North Channel Stations.**

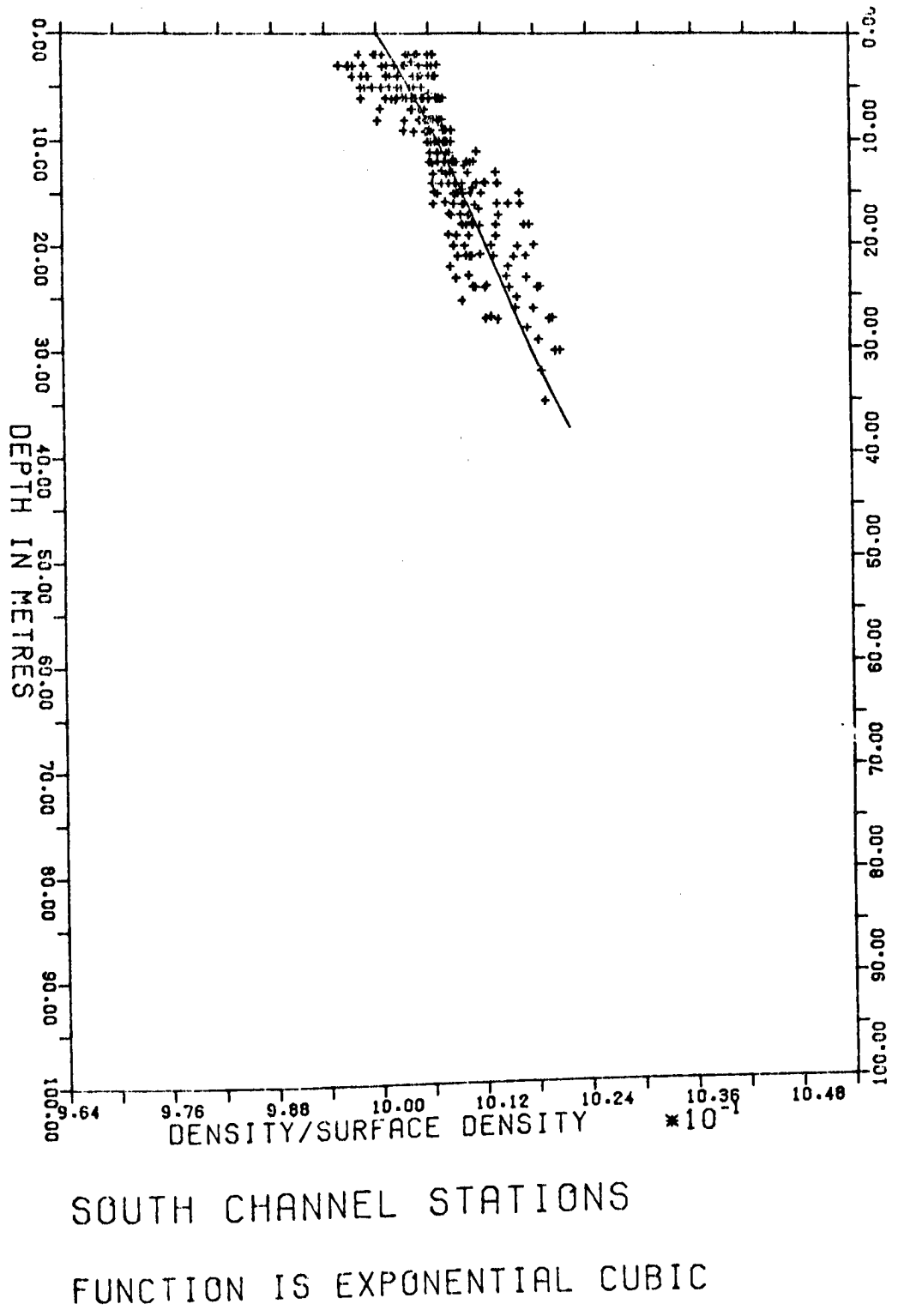

Figure 2.3.5 Depth versus density for the South Channel Stations.

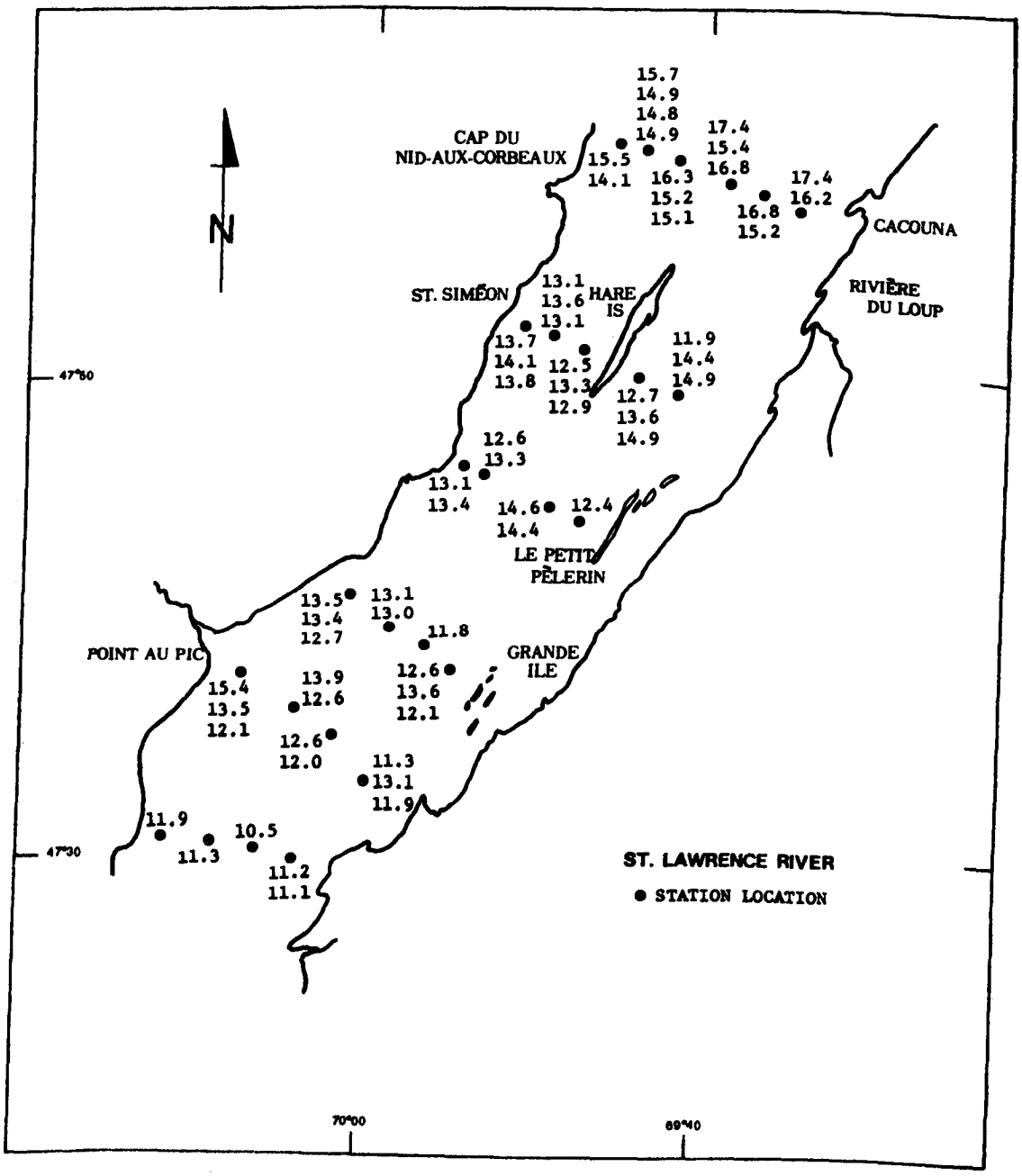

Figure 2.3.6 Surface σ_t values from all Station fit.

2.4 Forrester's Model

Forrester's tidally-averaged density structure is given by equation (2.2.3) and after taking logarithms of each side, the least-squares criterion is given by

$$\sum_{k=1}^{N} \sum_{j=1}^{M_k} \left[\ell n(\bar{\rho}_{k,j}) - \ell n(\rho_{o,k}) - a_1/z_{k,j} + a_2 \right]^2 = \text{minimum}$$

and so for each of the N variables, $\ell n(\rho_{o,K})$, the equation is

$$\sum_{j=1}^{M_K} \left(\ell n(\bar{\rho}_{K,j}) - \ell n(\rho_{o,K}) - a_1/z_{K,j} + a_2 \right) = 0$$

while the two remaining normal equations are

$$\sum_{k=1}^{N} \left[\sum_{j=1}^{M_k} \left(\ell n(\bar{\rho}_{k,j}) - \ell n(\rho_{o,k}) - a_1/z_{k,j} + a_2 \right) (1/z_{k,j} + a_2) \right] = 0$$

$$\sum_{k=1}^{N} \left[\sum_{j=1}^{M_k} \left(\ell n(\bar{\rho}_{k,j}) - \ell n(\rho_{o,k}) - a_1/z_{k,j} + a_2 \right) \left(a_1/(z_{k,j} + a_2)^2 \right) \right] = 0$$

where the notation is the same as in the last section. There are the correct number of equations, but they are nonlinear and so cannot be solved directly.

There are, however, a number of proprietary subroutines that allow systems of nonlinear equations to be solved. The algorithms all start from a guessed solution and then iterate until an answer is found within the error limits chosen. The difference between the various algorithms is in the method of iteration, and this difference can be significant both in terms of computer time and in how the algorithm handles multiple roots and singularities in the equations.

The technique chosen in this instance is a quasi-Newton's method due to Brown (1967,1969) which was converted to Fortran and described by Muir (1975). The technique has been extensively tested and is very quick for this type of equation, which has no pathological mathematical properties.

Rather surprisingly, when this model was run on all of the data, there were no significant statistical differences between Forrester's model and the exponential cubic model. It is surprising because when Forrester's model is expanded in a power series it looks very different from the exponential cubic. There are, however, practical differences. Forrester's model has the advantage of being monotonically increasing with increasing depth while the exponential cubic is not necessarily monotonically increasing, as can be seen from Figure 2.3.1, which plots the exponential cubic for the 1975 data. The same thing is shown in Figure 2.3.2 which plots the 1977 data. The result is that Forrester's model does not fit the deeper densities quite as well as the exponential cubic, but on the other hand it ensures that the Brunt-Vaisala frequency is never negative. This problem with the exponential cubic does not arise when all of the data is taken together, as is shown in Figure 2.3.3.

2.5 Magaard's Model

In his studies of the propagation of internal waves over topography, Magaard (1962) used a parabolic curve to fit the vertical tidally-averaged density structure. As in the exponential cubic model, it is possible to derive the equations in a general form and

then to determine statistically the appropriate degree for the polynomial by means of a step-wise regression. If the density structure is assumed to be that given by equation (2.2.4), then the normal equation for the K^{th} station is

$$\sum_{j=1}^{M_K}\left[\left(\bar{\rho}^2_{K,j} - \rho^2_{o,K}\left(1 + \sum_{i=1}^{I} a_i z^i_{K,j}\right)\right)\left(1 + \sum_{i=1}^{I} a_i z^i_{K,j}\right)\right] = 0$$

and the normal equation for the ℓ^{th} coefficient a_ℓ is given by

$$\sum_{k=1}^{N}\sum_{j=1}^{M_k}\left[\left(\bar{\rho}^2_{k,j} - \rho^2_{o,k}\left(1 + \sum_{i=1}^{I} a_i z^i_{k,j}\right)\right)\rho^2_{o,k}\left(\sum_{i\neq\ell}\left(a_i z^i_{k,j} + z^\ell_{k,j}\right)\right)\right] = 0$$

where the notation is as before and the equations are again nonlinear. The same algorithm may be used to solve these equations as was used for Forrester's model.

After carrying out a step-wise regression, it was found that the polynomial in the vertical structure should be of degree 2, ie. I = 2. This was using all of the data from the 1975 and 1977 surveys for the fit. Again, rather surprisingly, there was no significant difference between Magaard's model and the others, as can be seen in Table 2.5.1.

Model	Sum of Squares Deviations	Std.Error of Estimate	F-Values	
			Forrester	Magaard
Exp.Cubic	.000724	1.139	1.04	1.04
Forrester	.000749	1.158		1.00
Magaard's	.000751	1.159		

Table 2.5.1 Comparison of three models on all stations.

In the above table, the standard error of estimate is in terms

of sigma-t units, while the sum of the squares of the deviations are in terms of gm/ml and there are approximately 559 degrees of freedom in the estimates of the F-values. Hence there is no reason for preferring one of the models over another, even at the 0.01 level, on a statistical basis. On a practical basis, the difference of 0.02 sigma-t units in the standard error of estimate is too small to be of any significance.

2.6 The Separability Hypothesis

Since all three of the models above are statistically and practically indistinguishable, the exponential cubic was chosen as the model to use when testing the separability hypothesis because it is linear and requires much less computer time than either of the other two. The tests above have assumed the hypothesis in that they have allowed the horizontal variation, $\rho_o(x,y)$, to vary with each station, but have required that the a_i's be constant over the whole estuary. By setting $N = 1$ in the matrix equation (2.2.6) it is possible to run the model for each of the 65 profiling stations individually and hence to let the constants a_i vary with each station. Table 2.6.1 gives the analysis of variance for the individual fits.

Source of Variance	Degrees of Freedom	Sum of Squares	Mean square Deviation	F
Regression	260	.004311897	.000016584	
Deviations	378	.000016136	.000000427	
				267

Number of stations 65

Percent explained variance = 99.37

Maximum errors = -.656 to +.484 sigma-t units

Table 2.6.1 Analysis of Variance of the individual exponential cubic models.

The next table gives an analysis of variance for a comparison between the individual fits and the overall fit using the exponential cubic model.

Source of Variance	Degrees of Freedom	Sum of Squares	Mean Square Deviations	F
Individual	378	.000016136	.0000000427	
Overall	558	.000723718	.000001297	
				9.2

Table 2.6.2 Analysis of Variance comparing the overall to the individual exponential cubic models.

The two tables show that the separability hypothesis is untenable in both a statistical and a practical sense over the whole estuary. In the overall fit, the amount of the explained variance was 81.1% for the exponential cubic, but for the individual fits the explained variance goes up to 99.4%. In addition, the maximum errors for the individual fits are much less than the standard error of estimate for the overall fit. Figure 2.6.1 gives a plot of the various fitted curves and the observed curves for three different stations. Station 75-001B is a typical station, station 75-001C is at the same location but has the worst fit in that the maximum errors for the overall fit occur at this station. Station 77-011C is in the South Channel and has the worst fits in terms of percentage error. Figure 2.6.2 gives a plot of the surface densities from the individual exponential cubic fits on a chart of the St.Lawrence, and this figure may be compared with Figure 2.3.6.

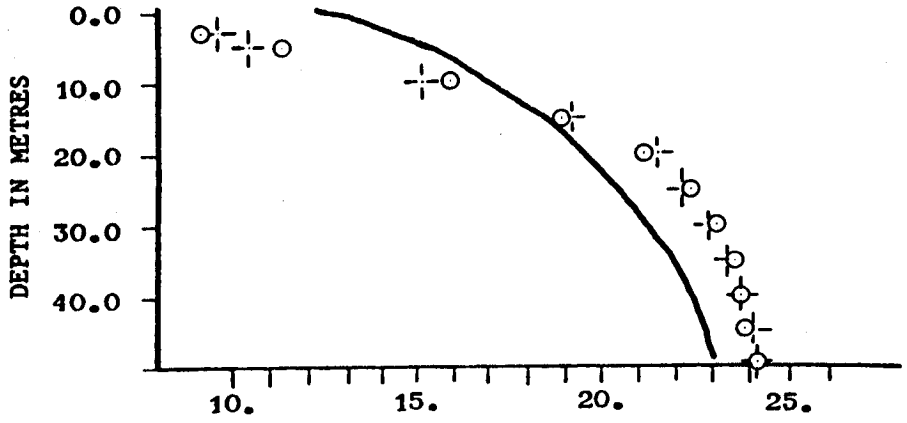

Sigma-t for 75-001C. Worst fit, Maximum errors.

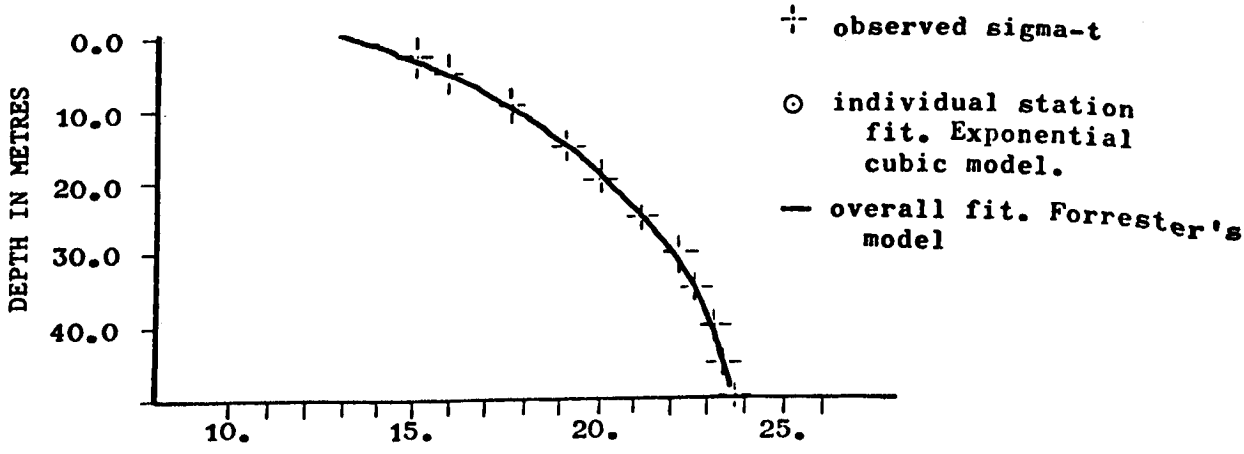

Sigma-t for 75-001B. Typical Station

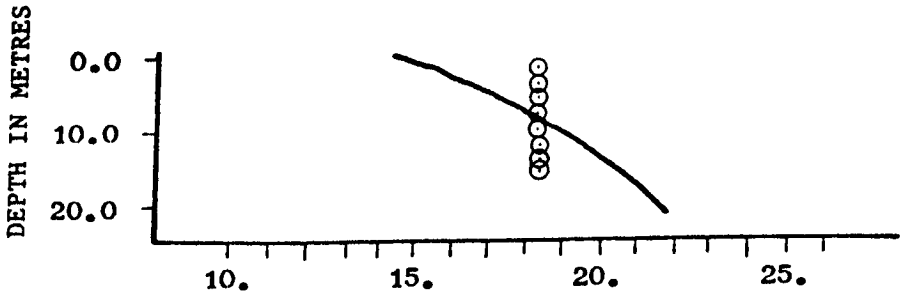

Sigma-t for 77-011C. Worst fit, % error.

Figure 2.6.1 Observed and predicted densities for three Stations.

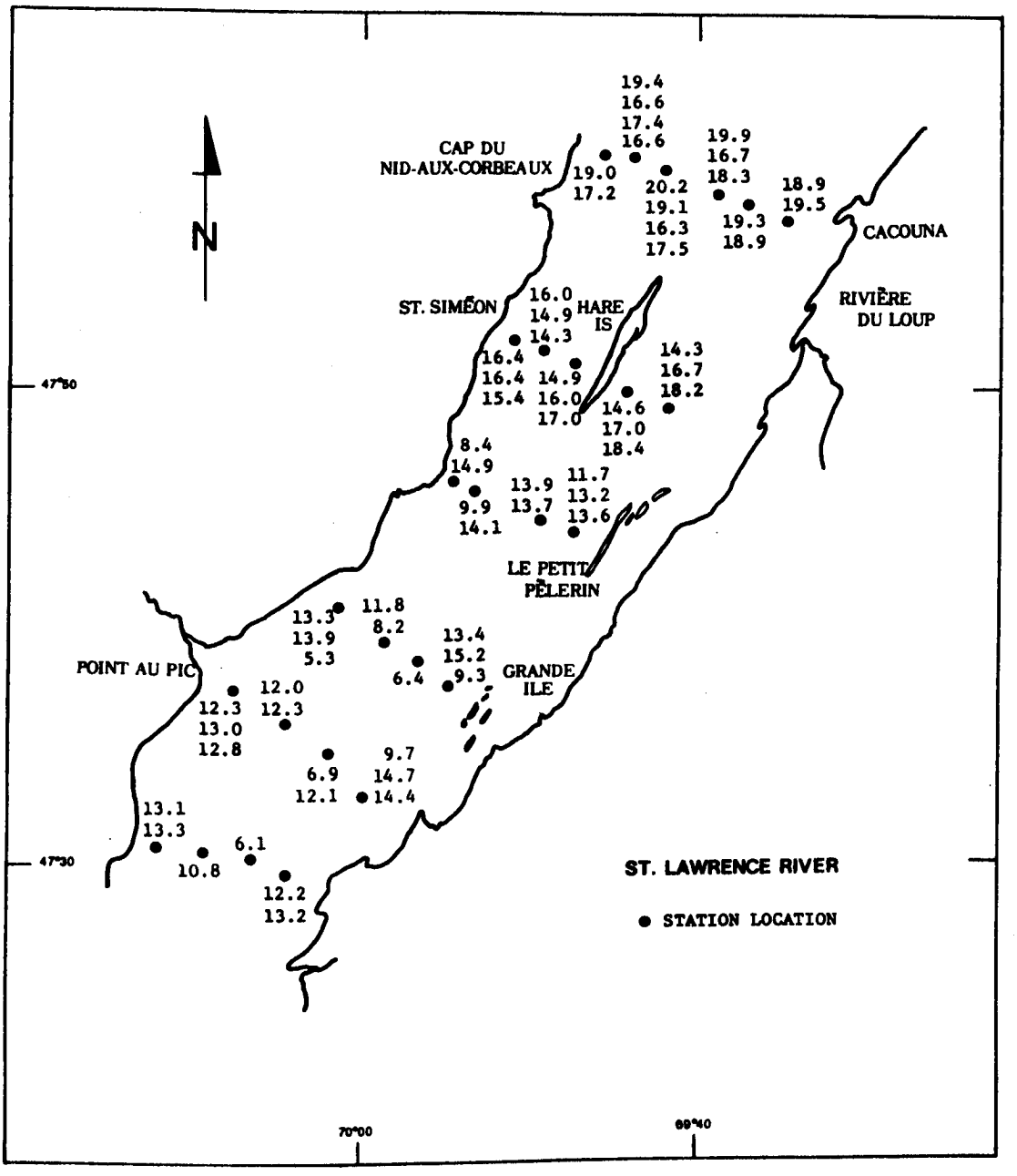

Figure 2.6.2 Surface σ_t values from individual Station fits.

2.7 Discussion

This chapter has shown that the T-S relationships and the tidally-averaged density-depth relationships in the Middle Estuary of the St. Lawrence are complicated. Although the T-S relationship at an individual station is linear and reflects conservative mixing processes, there is no one T-S relationship that will hold over the whole Estuary. This is mainly because of the variability in the end members, which are the St. Lawrence River and the Lower Estuary. It is not possible to linearly relate the slope of the regression lines at individual stations to any of the parameters, or combinations of parameters, that would normally be considered to be of importance in mixing processes, such as; the tide height, the tidal energy, the properties of the end members, or the location in the estuary. This indicates that the mixing processes in the Middle Estuary are both complicated and nonlinear over both space and time, even though they are conservative and linear at a given instant in space and time.

The implications of the complexity of the T-S relationship to other disciplines are worth considering. Many of the trace metal and particulate matter studies that are done in estuaries relate the concentrations of these materials to the salinity on the basis that both are conservative substances, and that therefore the salinity will act as a tracer for the other. This then allows a very few measurements of a trace metal, for example, to be extrapolated over a much wider area using the more easily made salinity measurements. If then it is impossible to draw convincing 'average' contours of salinity on a chart of the estuary it should also be impossible to draw 'average' contours of any of the substances that are normally related to salinity. In the

case of substances which are known to be nonconservative, such as organic carbon for example, then the situation should be even worse. It seems to be very misleading to draw 'average' contours of, say, salinity on a chart of an estuary such as the Middle Estuary, since the variability is so high at each station. It is very tempting to draw these contours, but this may only be so because there are normally only a very few measurements made, and these measurements are seldom repeated at the same station under different conditions. In the case of the St. Lawrence, it is clearly misleading to draw overall concentration contours which purport to be valid over many time scales and in the case of other, similar, estuaries it may also be as misleading.

In the case of the tidally-averaged density structure, the situation may be thought to be better, if only because the averaging process reduces the variance considerably. However, an examination of Figure 2.6.2 will show that this is not the case. It is not unusual to find a 5 or 6 sigma-t range in the surface densities at a single station and so one would expect the same variability to obtain with any other conservative tracer. Again, in the case of nonconservative substances, the situation should be worse.

There are two unexpected results of the examination of the depth density relationships. The first is that there is no significant difference between the three models when fitted to all of the data. The mathematical properties of the three models are very different, but their ability to predict the tidally-averaged density structure is equivalent. The second unexpected result is not that the separability hypothesis is untenable in a very precise sense, but rather that the

results are so good when it is made. Although the separability hypothesis is mathematically almost necessary if any analytical modelling of the circulation is to be possible, there is no good physical reason for believing that it should hold. The fact that 81% of the tidally-averaged density variance can be explained while retaining the separability hypothesis is quite reassuring.

In Chapter 7, an attempt will be made to show all of the physical processes that control the circulation of the Middle Estuary and their relationship with the tidally-averaged density structure. There are a large number of these processes and they are generally very complex. That a rather simple statistical relationship could hold over an area as large as the Middle Estuary is very reassuring. Over small areas, of course, the separability hypothesis should be quite reasonable. When the exponential cubic was fitted to each individual station, the overall explained variance was 99.4%, and this is almost within the limits of experimental errors, since the standard error of estimate is 0.21 sigma-t units.

Assuming that z is measured negatively downwards from the surface, the three models of the tidally-averaged density structure over the whole Middle Estuary are

$$\bar{\rho} = \rho_o \exp-(0.44297E\text{-}3z - 0.63481E\text{-}5z^2 + 0.30311E\text{-}7z^3) \qquad 2.7.1$$

$$\bar{\rho} = \rho_o \exp(0.3935/(z - 24.676)) \qquad 2.7.2$$

$$\bar{\rho} = \rho_o (1.0 - 0.71594E\text{-}3z - 0.61820E\text{-}5z^2)^{\frac{1}{2}} \qquad 2.7.3$$

where the value of ρ_o is different for each station and time.

The values of ρ_o for the exponential cubic are shown in Figure 2.3.6. This model tends to underestimate the densities at the downstream end of the Estuary and to overestimate the densities at the upstream end of the Estuary.

CHAPTER 3

The Tides of the Middle Estuary

3.0 Introduction

The barotropic, or surface, tides of the St. Lawrence system in general have been the subject of an intensive amount of research over the past 15 years. This interest has been largely due to the necessity of providing accurate tidal predictions but has also been due to interest in the fate of pollutants such as oil spills in Canada's main shipping channel. The work has seldom been restricted to the Middle Estuary, but has usually been concerned with the whole tidal portion from the Straits of Cabot in the Gulf of St. Lawrence to the St. Lambert Lock in Montreal, which is the maximum upstream penetration of a measurable tide.

Work generally connected to the requirements of the Hydrographic Service has been done by Farquharson (1962, 1966), Forrester (1967, 1972, 1974) and Godin (1971, 1979). The work carried out by the National Research Council for the Department of Transport consists of the numerical modelling studies by Kamphius (1968) and Prandle and Crookshank (1974). Other work has been done at various universities by Ouellet and Cheylus (1971), Aubin, Murty and El-Sabh (1979), El-Sabh, Murty and Levesque (1979), LeBlond (1978) and also by Pingree and Griffiths (1980).

All of this work, with the single exception of Forrester (1974), has been concerned with the propagation of the barotropic tide in its passage up the Gulf, Estuary and River. The numerical models that have

been developed have all assumed a homogeneous vertical density structure and have, as a result, been vertically integrated. The one-dimensional models have been integrated both vertically and across the river. As a result, then, the physics of the propagation of the surface tide are fairly well understood, in the sense that the numerical models adequately represent the observed water levels and the analytical models adequately predict the observed distortion of the tidal wave as it progresses upstream. The papers by Godin (1979) and by LeBlond (1978) give extended descriptions of the propagation of the surface tide in the whole system from two different viewpoints. Figure 3.0.1 is a plot of the water level elevations for two months at St. Jean Port Joli, which is slightly upstream of the Middle Estuary but which shows very adequately the type of tidal curve that occurs in the Middle Estuary. The curve is a prediction based on the analysis of one year's data and so represents purely tidal phenomona.

Godin (1979) gives cotidal charts for the two tidal constituents K_1 and M_2, but a brief description of the propagation of the M_2 constituent in the lower part of the system will give an indication of the tidal propagation. There is an amphidromic point about half-way between Prince Edward Island and Anticosti Island in the Gulf of St. Lawrence. The M_2 tide then progresses upstream in the Lower Estuary, becoming a Kelvin wave, and continues as a Kelvin wave through the Middle Estuary, although it loses most of the cross-channel height difference as the Estuary narrows. By the time the wave has reached the Ile d'Orleans, the rotational effects have disappeared and the wave crest is virtually horizontal.

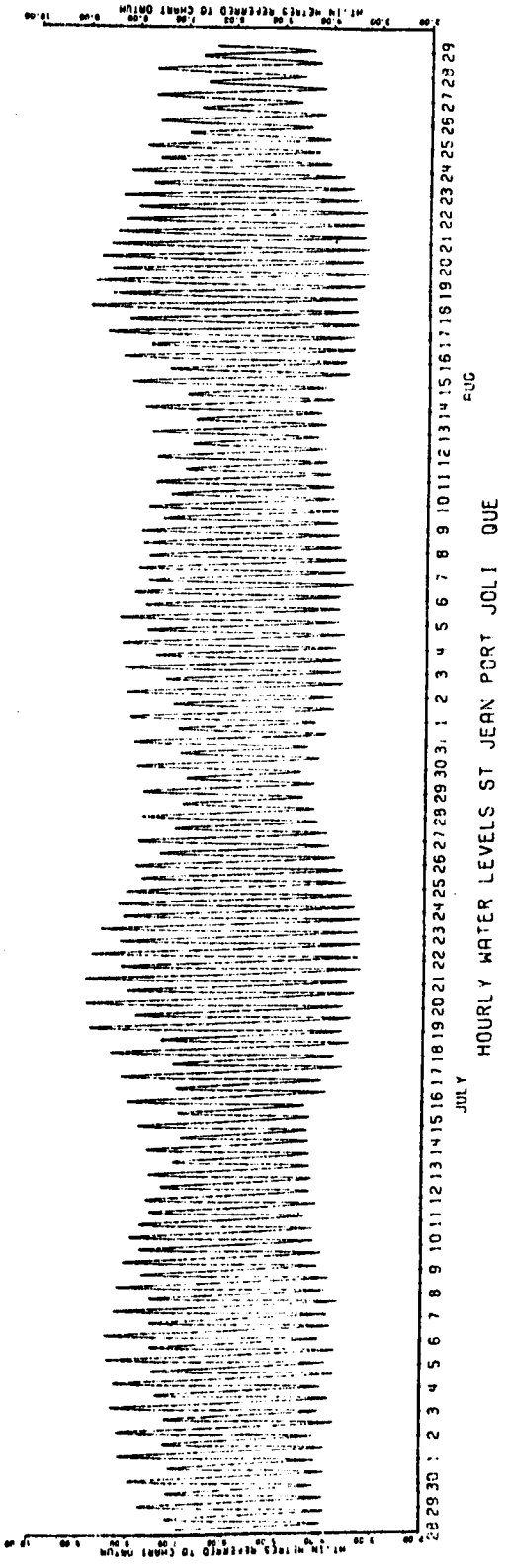

Figure 3.0.1 **Predicted hourly water Levels from St. Jean Port Joli, 1974.**

The phase of the M_2 surface tide at the Saguenay River is 220^o and at St. Joseph de la Rive, near Ile aux Coudres, the phase is 255.5^o, and so the wave takes $35.5 \times 2.07 = 73.5$ minutes to make a passage of 95 km. The mean celerity is therefore 77.6 km/hr. Since the mean water depth in the North Channel is approximately 100m, the phase speed should be about 112.8 km/hr, and so the M_2 surface tide in the North Channel could be considered to be part way between a standing and a progressive wave. The sill stretching from Pte au Pic to the Morin Shoal, which shall be called the Morin Bank, provides an adequate reflector as does the abrupt change in direction of the channel as it goes around Ile aux Coudres. On the south side, the phase at Riviere du Loupe is 224.8^o while at Pte aux Orignaux the phase is 251.1^o so that the time of passage is 54.4 minutes, which gives an average celerity of about 57.4 km/hr. The mean depth in the South Channel is about 25 m which gives a wave speed of about 56.4 km/hr and would indicate that in the South Channel, the M_2 surface tide is a simple progressive wave.

Explanations of the tidal currents in the Middle Estuary have not been very successful. It has been realized for a number of years that the 1939 Tidal Current Atlas is very inaccurate. The verification of the two-dimensional numerical models of Prandle and Crookshank (1974), Oullet and Cheylus (1971), Aubin, Murty and El-Sabh (1979) and El-Sabh, Murty and Levesque (1979) consisted of matching observed with computed water levels, and little attempt was made to match the observed and computed tidal currents. This is primarily because, until the St.Lawrence Tidal Current Surveys of 1974, 1975 and 1977, there has been an almost

total lack of data for verification of the tidal currents. For some of the models computed trajectories of the currents were shown, but these computed currents bear no more than a passing relationship to observed currents and would be completely useless in any operational sense, such as computing the dispersion of oil slicks.

The purpose of this introduction has been to give a brief description of the behaviour of the barotropic tide in the Middle Estuary. In the following sections, attention will be turned to the observed tidal currents and it will be seen that these tidal currents do not behave in the relatively simple manner in which the surface tide seems to behave.

3.1 Harmonic Analysis of the Tidal Currents.

A total of 44 current meter records has been obtained in the Middle Estuary in the course of the three surveys. In 1974 and 1977 the measurements were done using Aanderaa RCM4 or RCM5 instruments, while in 1975 Plessy PC6 instruments were used. The major difference between the two types of meters is that the Aanderaa uses a Savonious rotor while the Plessy uses a Roberts rotor. It has been shown, in the many inter-comparison studies that have been done, that although the frequency response of the two types of rotors is different at high frequencies, there is very little difference at the lower, tidal frequencies. All of the plots and mooring details are to be found in the St. Lawrence Data Reports (Budgell and Muir, 1975; Muir, 1978; and Muir, 1979a), and these details will not be listed here.

The preliminary analysis of the tidal current records was carried out using the standard Canadian Hydrographic Service Tidal Streams

Analysis program, which is described by Godin (1972). The data were filtered and reduced to hourly values which were then analysed for the appropriate tidal constituents, with no related constituents used. In this Chapter, the phase of a tidal constituent is always given in degrees, referred to GMT. The current components are resolved about the east and north axes, while the upstream direction on the St.Lawrence is southwest. Therefore, the phase given is the time of maximum ebb current and not the time of maximum flood current as is usually given by other authors. To convert one system to the other, 180^{o} must be added to both the phase and the inclination of the constituent ellipse. Because of the axes chosen, the inclination of the constituent ellipse gives the direction from which the flooding wave is coming and not the direction in which it is going.

From the statistics of the analyses, the harmonic analyses of the current records were very good. The residual currents were quite small, the coefficient matrices were stiff, and the amount of explained variance was high. However, a closer inspection of the actual constituents showed that there was little consistency in the ratios of the analysed constituents from one record to another; the directions of the mean currents were very different from what would be expected in an estuary; the vertical distribution of the constituents at any given mooring was peculiar; and the phases of the tidal current constituents did not match with the phases of the surface tide constituents. It was expected that the tidal currents would progress up the river as a simple Kelvin wave in the same fashion as the surface tides, but this is clearly not the case, as can be seen from Figure 3.1.1. This Figure gives the phase of the M_2 constituent for the surface tide and for the tidal currents at the

location of the measurements. The number in parentheses after the phase gives the depth of the current meter below chart datum in metres, and the arrow shows the direction of rotation of the constituent ellipse.

If the assumption is made that the tidal currents are simply those directly related to a barotropic surface tide, then there are many anomalous features shown in Figure 3.1.1. First, the phases at any given depth cannot be contoured as a simple Kelvin wave, and, in fact, cannot be contoured in any meaningful way at all. Second, the phase speeds that can be calculated for a wave moving from mooring to mooring vary considerably and do not match with the wave speeds that can be calculated from the water level records. For example, it takes the surface tide about 30 minutes to travel from St. Simeon to Goose Cape, while the tidal current at 5 m depth takes 92 minutes to cover the same distance and, in addition, it arrives on the south shore at Pte. Aux Orignaux about 47 minutes before it arrives at Goose Cape. Third, one would expect that for a barotropic tide, the phase at any given location should be constant throughout the vertical with, perhaps, a slight phase lead for the bottom currents due to the effects of friction (Soulsby,1978). Fourth, since the M_2 surface tide is a Kelvin wave, one would expect there to be no rotation in the ellipse, or, at the very least, for all of the ellipses to rotate in the same direction. The presence of all of these anomalous features throws considerable doubt on the assumption that the tidal currents are due simply to a barotropic surface tide.

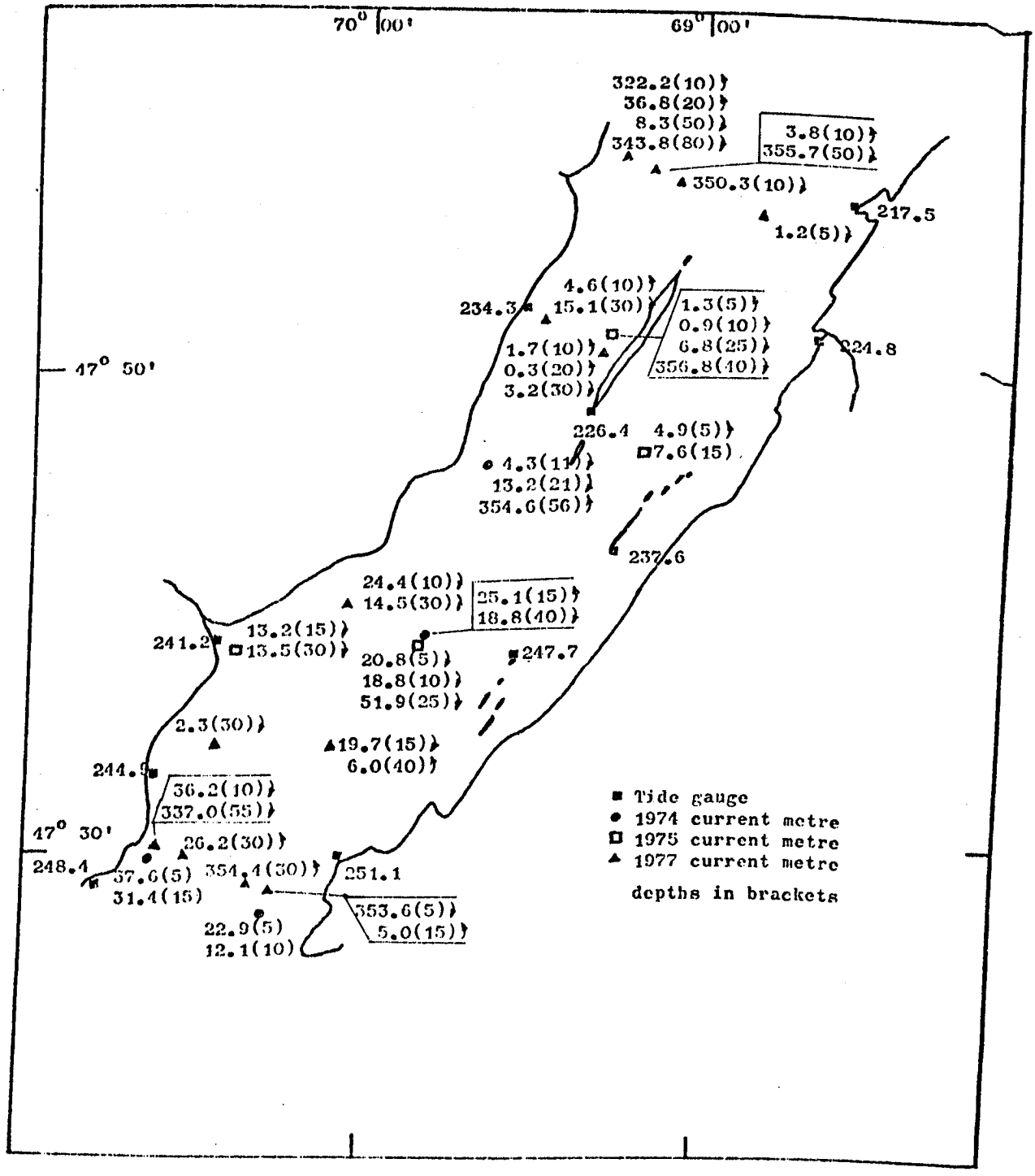

Figure 3.1.1 Phase of the M_2 constituent in degrees (GMT),

3.2 Admittance Analysis of the Tidal Currents

In order to check that there was no error in the harmonic analysis method and also to gain more information from the tidal current records, an admittance analysis was carried out on all of the 1974 current meter records. Since this method is not widely known, a description of it will be given here. The only other complete description that is available is to be found in Godin (1976), where it was used with success in the analysis of tidal currents in Robeson Channel.

The basic idea is the same as the Tidal Spectroscopy methods of Munk and Cartwright (1966), but very much shorter periods of record are used and instead of using the equilibrium tide as an input function, a well-resolved water level record is used. It is not necessary that the water level record be physically very close to the current measurement location, but only that it has the same tidal characteristics as would the current meter record. It is assumed that there is a linear relation between the tidal constituents derived from the water level record and the tidal constituents which make up the tidal current record for each frequency band.

If there are two time series, which may be assumed to be linearly related, then the admittance (or the gain) between them, at frequency σ, is given by

$$G(\sigma) = C_{xy}(\sigma)/X(\sigma)$$

and the coherence is given by

$$\gamma_{xy}(\sigma) = C_{xy}(\sigma)/(X(\sigma)Y(\sigma))^{\frac{1}{2}} \qquad (3.2.1)$$

where C_{xy} is the cross-spectrum between the two series, x and y, and X and Y are the auto spectra of the two time series.

Given the amplitude and phase of the admittance, a component of the series y may be predicted from the corresponding component of the series x simply by multiplying the amplitude of the component of x by the admittance and by adding the phase of the admittance to the phase of x.

Codin (1976) gives the confidence limits for the estimates of the admittance and the phase as

$$e(\sigma) = \left[\left[\frac{1 - \gamma^2(\sigma)}{\gamma^2(\sigma)}\right]\left[\frac{1}{(1-P)^{1/n}} - 1\right]\right]^{\frac{1}{2}} \qquad (3.2.2)$$

where, P is the probability that the error will not exceed $e(\sigma)$, and n is the number of degrees of freedom in the estimate for $G(\sigma)$. This means that there is a probability P that

$$|G| - e \lesssim |G'| \lesssim |G| + e$$

and

$$\arg(G) - e \lesssim \arg(G') \lesssim \arg(G) + e$$

where C is the estimate of the true value G'. Bendat and Piersol (1971) give the confidence limits for the coherence function itself.

In the case of the analysis of tidal current records, the input function is the water level record for a nearby tide gauging station and the u(east) and v(north) components of the tidal currents as the independent output records. So long as the input record can supply a well-resolved set of tidal constituents, it is then possible to calculate $G_u(\sigma)$, $\gamma_u(\sigma)$, $G_v(\sigma)$ and $\gamma_v(\sigma)$ for a given bandwidth Δ.

On the St. Lawrence, in the semidiurnal bands, for a bandwidth of 0.005 cycles/hr, the coherence between the input tidal elevation and the tidal current components is seldom less than 0.98.

Once the admittances have been computed and the coherences found to be satisfactory, the computation of the tidal constituents is straightforward although somewhat tedious. If the input station has a constituent with amplitude C and phase c, then the amplitudes of the u and v components of the same constituent for the currents are

$$A = |G_u|C \quad \text{and} \quad B = |G_v|C$$

and the phases are

$$a = c + \arg(G_u) \quad \text{and} \quad b = c + \arg(G_v)$$

where G_u and G_v are the admittances from the appropriate frequency band. This component form is not too useful, however, and so by going through the standard algebra (Godin, 1972) it is possible to define

$$\begin{aligned} |a_+| &= \left[(A\cos a + B\sin b)^2 + (B\cos b - A\sin a)^2\right]^{\frac{1}{2}} \\ |a_-| &= \left[(A\cos a - B\sin b)^2 + (B\cos b + A\sin a)^2\right]^{\frac{1}{2}} \\ \alpha_+ &= \arctan\left[B\cos b - A\sin a) \;/\; (A\cos a + B\sin b)\right] \\ \alpha_- &= \arctan\left[B\cos b + A\sin a) \;/\; (A\cos a - B\sin b)\right] \end{aligned} \tag{3.2.3}$$

and so the lengths of the major and minor axes of the constituent ellipse are

$$M = |a_+| + |a_-| \quad \text{and} \quad m = |a_+| - |a_-| \tag{3.2.4}$$

and the inclination and phase of the ellipse are

$$\theta = \tfrac{1}{2}\alpha_+ + \tfrac{1}{2}\alpha_- \quad \text{and} \quad g = \tfrac{1}{2}\alpha_- - \tfrac{1}{2}\alpha_+ \tag{3.3.5}$$

It should be realized that these ellipse components are not changed if 180° is added or subtracted to both the phase and the inclination together. However, the inclination of the ellipse is only invariant if one always takes the axes directions on the Earth's surface as a constant. In this way, the inclination is an invariant in the same way as the phase, since the phase is always referred to a standard time, which is the phase of the astronomical constituent at Greenwich. The only effect of using a different reference system is to confuse everyone else and to introduce another source of error into the calculations.

One of the theoretical disadvantages of the admittance method is that the calculated admittances will vary, depending upon the directions chosen for the resolution of the tidal currents. This simply means that the admittance does not have any physical meaning. A second theoretical disadvantage is that if the tidal currents are very nearly rectilinear, as is often the case in estuaries, then the poor signal to noise ratio may result in the poor resolution of one of the components. This would only happen if the direction of resolution was exactly the same as the direction of the current and so different components could easily be chosen for the analysis. In any case, if the current is very near rectilinear, then the semiminor axis of the ellipse would be the only one poorly resolved and this component would be of little importance.

3.2.1 Application to the St. Lawrence

Programs were written for the application of the admittance method to the 1974 St. Lawrence data, in order to check that the harmonic analysis programs were working correctly and also to try to make full use of the information in the tidal current records. The reference water levels used were the actual observed water levels at St. Jean Port Joli, which is somewhat upstream of the Middle Estuary, but which has a very long period of tidal record and whose tidal constituents are very well resolved. The hourly water levels were used as the input function while the filtered, hourly current observations in u and v components were used as the output functions. The admittances and coherences were calculated using a power of two Fast Fourier Transform. The mean and trend were removed from the data using a linear, least squares fit and a cosine taper put on the first and last tenths of the data to remove end effects. The raw spectral estimates were frequency smoothed to produce estimates for both 12 and 36 bands. The estimates from the 36 band analyses were used to ensure that the admittance was not changing significantly within the tidal frequency bands and that the coherences were also constant within the tidal frequency bands.

After the spectral analysis had been done for each of the records, the ellipse parameters were calculated for each of the data sets using the admittances and the 55 tidal constituents from a one-year harmonic analysis of the St. Jean Port Joli water level record. Using these ellipse components, the tidal currents were then predicted for each of the periods of record for the observed currents, and then the residual currents were calculated by subtracting the predicted currents from the observed currents.

Table 3.2.1 shows a comparison between the residuals derived from the harmonic method and the residuals derived from the admittance method. The residuals from the harmonic method are smaller than the residuals from the admittance method and this would indicate that the harmonic analysis provides a better analysis procedure than the admittance method. The reason for this is not difficult to find. Table 3.2.2 provides the coherences computed in three of the frequency bands for each record. The coherences are very high in the semi-diurnal band, poorer in the diurnal band and poorer still in the quarter-diurnal band. Since most of the energy in the tidal signal is in the semi-diurnal band, the signal to noise ratio in the other bands is too much for the admittance method to cope with, and this is why the harmonic method provides a better fit, although both methods reduce the residuals to acceptable levels.

Table 3.2.3 gives a comparison of the M_2 ellipse parameters for each of the 1974 current meter records and since the coherences in the semi-diurnal band are high, these two sets of constituents are quite close. The admittance analysis shows, then, that there is no major fault in the harmonic analysis of the current meter records and that all of the discrepancies mentioned in Section 3.1 require a physical explanation.

The major advantage of the admittance method of analysis is that it allows the analysis of relatively short periods of record in which it would be impossible to separate the individual tidal constituents by means of the harmonic method. This is possible since it is assumed that the relationships between the constituents in any

Mooring Number	OBSERVED VARIANCE		HARMONIC RESIDUALS				ADMITTANCE RESIDUALS			
	U	V	R-u	R-v	V-u	V-v	R-u	R-v	V-u	V-v
01Z005	3485.11	3172.22	76.00	219.00	153.61	698.60	116.57	254.69	338.27	1549.29
01Z015	2319.23	7963.10	55.00	98.00	70.41	158.00	79.10	139.12	149.82	412.37
04Z005	4905.00	5852.45	47.00	49.00	52.11	54.22	71.66	78.93	263.83	190.40
04Z010	2761.41	5343.28	55.00	58.00	62.11	69.89	81.31	74.91	203.18	194.55
07Z015	744.66	2697.96	75.00	78.00	56.01	78.05	92.51	110.57	90.96	145.47
07Z040	334.90	1462.88	48.00	80.00	21.92	50.37	58.44	80.59	32.98	85.02
11Z011	246.30	1794.24	41.00	48.00	31.80	48.41	51.10	60.96	59.09	102.09
11Z021	189.74	472.89	23.00	32.00	14.00	20.39	26.91	46.68	22.93	36.80
11Z056	853.78	1586.43	53.00	68.00	27.59	39.89	50.66	60.97	56.79	103.86

TABLE 3.2.1 Residual Statistics for 1974 St. Lawrence Moorings. Observed Variance is the variance of the observed tide, for east and north components. R-u and R-v give the range in the residuals for the u and v components. V-u and V-v give the variance in the residuals for the u and v components. Admittance residuals calculated using 55 tidal constituents.

Mooring Number	Diurnal Band		Semi-diurnal Band		Quarter-diurnal Band	
	u	v	u	v	u	v
01Z005	.911	.431	.988	.810	.914	.721
01Z015	.910	.947	.992	.990	.780	.312
04Z005	.961	.915	.988	.997	.859	.776
04Z010	.892	.912	.984	.995	.899	.799
07Z015	.557	.947	.995	.997	.832	.903
07Z040	.805	.952	.995	.997	.974	.958
11Z011	.796	.979	.982	.998	.917	.582
11Z021	.919	.971	.990	.996	.852	.802
11Z056	.961	.934	.995	.995	.726	.757

Table 3.2.2 Coherences for three frequency bands, u and v components, for the 1974 St. Lawrence moorings.

Mooring Number	Harmonic Components				Admittance Components			
	M	m	θ	g	M	m	θ	g
01Z005	97.2	5.1	37.6	45.7	90.4	1.9	35.2	48.8
01Z015	136.1	1.6	62.0	31.4	131.4	- .1	61.8	34.8
04Z005	140.3	-9.6	47.3	22.9	133.7	-8.2	47.9	27.1
04z010	121.4	-8.7	54.0	12.1	115.2	-8.1	55.2	16.6
07Z015	77.4	-5.9	62.0	25.1	75.6	-6.0	63.3	29.6
07Z040	52.6	19.4	73.4	18.8	50.7	18.5	73.6	21.7
11Z011	56.0	3.0	74.5	33.2	54.6	3.0	74.6	39.2
11Z021	31.8	6.1	60.9	13.2	30.7	5.7	59.8	19.0
11Z056	64.6	-2.0	54.2	-5.4	62.7	-1.9	54.2	-1.7

Table 3.2.3 Comparison of ellipse components for the M_2 derived from the harmonic analysis and the admittance analysis.

given frequency band are known from the analysis of the water level record. Therefore, some re-analysis of the 1974 data was done in order to examine the assumption that the tidal currents are due to a barotropic surface tide.

The first of the re-analyses was performed on the two sixty-day records 74-12C-07Z015 and 74-12C-07Z040 which were located in the middle of the Estuary, just off Pointe Au Pic. These were analysed in two thirty-day sections and then in four, fifteen day sections. Tables 3.2.4 and 3.2.5 give the results of the analyses for each component along with the associated errors. The errors are in degrees and associated with the error in the estimate of the phase. They are calculated using equation (3.2.2) and if this error is divided by 57.2958, it will give the error in the magnitude of the transfer function.

It should be noticed from these two tables that the amplitude of the semi-diurnal band is fairly stable, but the phase of the semi-diurnal band and the amplitudes and phases of all of the other bands are not at all stable. In particular the third-diurnal and the eighth-diurnal bands are very variable. This instability does not seem to be associated with the coherence estimates as may be thought reasonable. One would expect that the lower coherences should be associated with the more extreme estimates of the phase and amplitude, but this does not seem to be the case.

The immediate inference that can be drawn is that the tidal currents on the St. Lawrence are not very predictable. Using the analysed constituents from any particular one of the 15-day analyses, one could not predict the currents in another of the 15-day periods with any

BAND	RECORD	U-COMPONENT				V-COMPONENT			
		AMP.	PHASE	COHER.	ε	AMP.	PHASE	COHER.	ε
	1st 30 days	2.043	145.56	0.5570	16.88	7.532	124.94	0.9465	3.86
	2nd 30 days	1.815	158.00	0.7496	9.99	6.770	124.17	0.9607	3.25
Diurnal	1st 15 days	1.777	210.85	0.6944	16.77	8.609	124.60	0.9685	4.16
	2nd 15 days	3.453	119.52	0.8256	11.06	6.491	121.62	0.9553	5.01
	3rd 15 days	1.748	172.10	0.8159	11.47	6.914	122.38	0.9623	4.57
	4th 15 days	2.088	137.27	0.7686	13.47	6.643	124.44	0.9611	4.65
	1st 30 days	5.699	120.87	0.9954	1.06	10.986	109.72	0.9967	0.91
	2nd 30 days	5.786	111.90	0.9877	1.82	11.278	102.65	0.9955	1.06
Semi	1st 15 days	5.523	120.36	0.9960	1.45	10.353	109.52	0.9975	1.15
Diurnal	2nd 15 days	5.867	120.07	0.9977	1.10	11.516	109.44	0.9984	0.92
	3rd 15 days	5.239	114.88	0.9974	1.26	11.215	105.07	0.9981	1.00
	4th 15 days	6.308	109.09	0.9890	2.42	11.160	100.95	0.9906	2.23
	1st 30 days	6.442	80.98	0.5022	2.58	26.017	-36.01	0.7428	10.22
	2nd 30 days	5.430	50.49	0.1969	56.39	25.761	-31.23	0.6960	11.66
Third	1st 15 days	3.820	49.87	0.3457	43.93	26.479	-42.84	0.7171	15.73
Diurnal	2nd 15 days	7.975	87.09	0.6094	21.05	22.904	-39.08	0.8010	12.10
	3rd 15 days	14.646	129.19	0.4754	29.95	20.950	-57.23	0.6457	19.14
	4th 15 days	16.742	-26.80	0.6640	18.22	32.842	-17.79	0.8393	10.48
	1st 30 days	21.660	48.81	0.8318	7.57	37.722	- 1.51	0.9029	12.57
	2nd 30 days	17.570	14.14	0.7432	10.14	24.224	- 5.74	0.8006	8.48
Quarter	1st 15 days	29.277	63.24	0.9299	6.40	45.993	1.82	0.9126	7.25
Diurnal	2nd 15 days	16.906	36.80	0.8134	11.57	29.440	- 3.15	0.9607	4.68
	3rd 15 days	10.880	42.57	0.5615	23.85	33.470	- 1.05	0.8826	8.62
	4th 15 days	23.198	7.24	0.8951	8.06	19.024	- 6.40	0.7166	15.76
	1st 30 days	19.765	68.95	0.7587	9.76	28.220	21.84	0.8681	6.51
	2nd 30 days	23.315	56.42	0.7818	9.01	25.201	4.69	0.6877	11.96
Sixth	1st 15 days	25.651	30.99	0.6911	16.92	27.431	8.95	0.8331	10.74
Diurnal	2nd 15 days	23.029	76.67	0.9223	6.78	26.906	22.48	0.9325	6.27
	3rd 15 days	32.517	35.03	0.8251	11.08	15.355	-14.24	0.4794	29.62
	4th 15 days	21.015	61.00	0.8202	11.29	27.356	9.26	0.6945	16.77
	1st 30 days	15.222	24.92	0.3524	30.12	27.297	-43.59	0.6274	14.08
	2nd 30 days	27.326	9.39	0.7345	10.45	22.314	-65.84	0.6857	12.04
Eighth	1st 15 days	68.541	-67.72	0.7745	13.22	45.960	-138.30	0.6916	16.90
Diurnal	2nd 15 days	19.520	48.98	0.5238	26.32	31.030	-33.30	0.7962	12.30
	3rd 15 days	62.661	-18.57	0.7962	12.30	33.920	-92.13	0.6754	17.67
	4th 15 days	25.135	17.09	0.8542	9.85	22.585	-61.57	0.7043	16.31

TABLE 3.2.4 Admittance analysis for mooring 74-12C-07Z015 for various segments of the original record. Errors are for the 90% confidence level.

BAND	RECORD	U-COMPONENT				V-COMPONENT			
		AMP.	PHASE	COHER.	ε	AMP.	PHASE	COHER.	ε
Diurnal	1st 30 days	2.187	47.37	0.8054	8.34	7.011	90.78	0.9523	3.63
	2nd 30 days	2.530	35.48	0.9093	5.19	6.763	88.49	0.9759	2.53
	1st 15 days	3.033	63.60	0.9664	4.30	6.523	91.03	0.9127	3.86
	2nd 15 days	1.637	26.73	0.7439	14.54	7.172	91.80	0.9432	5.70
	3rd 15 days	2.264	34.18	0.8851	8.51	6.856	85.62	0.9848	2.85
	4th 15 days	2.677	40.86	0.9294	6.43	6.380	93.59	0.9664	4.30
Semi Diurnal	1st 30 days	3.725	52.96	0.9954	1.09	7.949	109.64	0.9972	0.85
	2nd 30 days	3.887	45.33	0.9941	1.24	8.140	102.99	0.9941	1.24
	1st 15 days	3.792	52.90	0.9974	1.17	8.050	108.70	0.9990	0.72
	2nd 15 days	3.669	51.64	0.9948	1.66	7.895	109.17	0.9972	1.21
	3rd 15 days	3.816	46.30	0.9983	0.94	8.276	106.03	0.9990	0.72
	4th 15 days	3.970	43.96	0.9923	2.02	8.077	100.22	0.9933	1.88
Third Diurnal	1st 30 days	14.115	170.05	0.7144	11.10	16.289	116.59	0.6147	14.62
	2nd 30 days	20.070	182.98	0.7312	10.57	35.282	120.86	0.8236	17.80
	1st 15 days	9.071	157.58	0.6526	18.79	28.632	124.01	0.7820	12.90
	2nd 15 days	16.714	171.51	0.7639	13.67	9.069	86.79	0.5432	25.01
	3rd 15 days	18.559	176.18	0.7959	12.31	38.432	114.53	0.8845	8.54
	4th 15 days	20.111	184.57	0.6571	18.56	33.189	121.52	0.8023	12.04
Quarter Diurnal	1st 30 days	17.667	-129.88	0.9735	2.66	27.901	129.93	0.9584	3.38
	2nd 30 days	15.019	-129.48	0.9011	5.26	24.215	118.43	0.9129	5.07
	1st 15 days	12.872	-127.85	0.9736	3.79	21.736	125.82	0.8962	8.01
	2nd 15 days	19.695	-132.44	0.9914	2.14	29.955	129.58	0.9771	3.52
	3rd 15 days	11.367	-110.59	0.9714	3.96	30.492	131.50	0.9376	6.00
	4th 15 days	17.792	-137.14	0.9399	5.88	22.636	111.00	0.9359	6.09
Sixth Diurnal	1st 30 days	15.162	213.43	0.6252	14.15	32.715	157.56	0.8786	6.16
	2nd 30 days	11.701	176.08	0.5941	15.34	36.610	136.01	0.9028	5.40
	1st 15 days	19.567	126.23	0.6938	16.80	26.869	121.66	0.8528	9.91
	2nd 15 days	21.756	226.42	0.8793	8.77	37.741	162.20	0.9256	6.62
	3rd 15 days	19.637	142.55	0.6999	16.51	49.012	124.95	0.9164	7.07
	4th 15 days	13.203	194.35	0.7137	15.88	37.392	139.20	0.9183	6.98
Eighth Diurnal	1st 30 days	16.578	-128.91	0.5596	16.78	19.164	132.04	0.4745	21.02
	2nd 30 days	14.842	-123.05	0.4686	21.36	21.316	122.90	0.5589	16.81
	1st 15 days	43.407	-117.75	0.6393	19.46	71.625	71.77	0.8476	10.13
	2nd 15 days	14.045	-132.81	0.6295	19.97	19.164	155.72	0.6021	21.46
	3rd 15 days	68.453	-138.30	0.8900	8.29	85.071	96.74	0.8904	8.27
	4th 15 days	10.935	-110.73	0.4768	29.83	17.002	135.76	0.6471	19.07

Table 3.2.5 Admittance analysis for mooring 74-12C-07Z040 for various segments of the original record. Errors are for the 90% confidence level.

degree of accuracy. The main carrier signal, which is the semi-diurnal band,would not be very far out in terms of amplitude, but its phase would certainly be incorrect and the modulations due to the other frequency bands would be considerably wrong.

A second observation about the analyses is that there does not seem to be any consistency in the variations in the transfer function from one record to the other. These two records were obtained from the same mooring, over the same time period. One of the meters was at 15 metres depth and the other was at 40 metres depth. If the vertical velocity profile due to a barotropic surface tide is considered to be linear or semi-logarithmic, then the ratios of the amplitudes of the admittance should remain more or less constant and the phase differences should also remain constant throughout the vertical, but neither of these things happens.

The third observation that may be made about the analyses concerns the coherences. If the tidal currents at the two meters are caused by the same barotropic tide, then the signals should be related to each other linearly and the coherence between them should be exactly 1. Since the same water level record is used as the input signal for both tables, the coherence over any given period for the u-component, say, should be identical in each table. This does not happen, except possibly in the semi-diurnal band, where the coherences are so high that it is difficult to distinguish between them.

One of the most puzzling features of this first re-analysis of the data is the instability in the phases of the admittances. The major assumption of tidal theory is that the amplitude and phase of a tidal constituent must remain constant with time. Otherwise, there could be no hope of predicting the tides. The success of Tide Tables testifies

to the reasonableness of this assumption. A second re-analysis of the 1974 St. Lawrence data was carried out to determine whether or not there was any pattern in the instability of the admittances.

This second re-analysis consisted of analysing three, contiguous, non-overlapping segments of 236 hours each, for each of the 1974 current records. The length of 236 hours was chosen because it is exactly 19 M_2 tidal cycles; it contains part of a spring tide and a neap tide cycle; and, with 12 frequency bands for the spectral analysis, retains 19.5 degrees of freedom in the estimates so that they have a reasonable amount of significance. For each of the 1974 records, the first three segments were analysed and the phases of the M_2 constituent calculated. The results are in Table 3.2.6. where the difference in phase between the phase of the segment and the phase of the whole record is given along with the error in the calculation of the phase.

Mooring Number	Phase Total Record	Phase Difference			Phase Error		
		1	2	3	1	2	3
01Z005	45.70	1.02	16.46	0.58	5.94	9.70	19.24
01Z015	31.40	3.50	9.62	1.39	3.33	5.60	9.02
04Z005	21.90	2.26	12.68	1.37	5.12	6.44	5.63
04Z010	12.10	0.94	12.00	3.91	4.08	5.86	8.57
07Z015	25.10	4.35	8.10	4.81			
07Z040	18.80	2.45	10.09	1.56			
11Z011	33.20	5.13	9.31	5.00	5.00	7.13	4.65
11Z021	13.20	6.15	6.39	6.36	3.47	4.92	8.06
11Z056	-5.40	3.28	10.72	- .10	7.00	4.49	2.68

Table 3.2.6 Instabilities of the M_2 phase from the 1974 moorings.

The calculated errors for the phase are quite large for each case, which reflects the short period of record used for each of the analyses. However, there is a pattern which emerges from the phase differences. For all of the records, there is a distinct phase shift, which is always in the same direction, from the first to the second ten-day segment and then another phase shift, back again, from the second to the third ten-day segment. The magnitude of these phase shifts is different for each of the records, and some of them, on a purely statistical basis, are not significant phase shifts. However, the fact that all of them are in the same direction is significant. It would argue that this phase shift is related to the differing portions of the spring-neap cycle in each of the ten-day records.

Comparing these phase shifts to the M_2 phase shifts shown in Tables 3.2.4 and 3.2.5 for the successive 15-day segments is revealing. In the 15-day segments, there is one complete spring-neap cycle and the phase shifts are always in the same direction. That is, the phase of the M_2 consistently lags from one 15-day segment to the next. In the 10-day segments, there is an unequal portion of the spring-neap cycle in each of the records and the phase of the M_2 lags from the first to the second segment and then returns almost to its original value by the third segment. Taking the two together it seems that the phase of the M_2 is unstable and that this instability has both a fortnightly component in it as well as a longer period component. To obtain good estimates of these variations in the phase of the M_2, or any other constituent, would require a large number of very long period tidal current records and these are not available at the present time.

The fact that the harmonic analysis and the admittance analysis, on the whole, agree, would argue that there is no error in either method of analysis and that the observed inconsistencies in the tidal constituents and the instabilities of these constituents are a real, physical phenomena in the Middle Estuary of the St. Lawrence. It is necessary, therefore, to find an explanation for them.

3.3 The Propagation of the Tidal Currents.

The use of the admittance method in the analysis of the 1974 tidal current records has shown that neither the amplitude nor the phase of the tidal constituents at a given location in the Middle Estuary is a constant. Since both of the methods of analysis are essentially least-squares, curve fitting exercises, and since neither of the methods makes use of any fluid dynamical principles other than those involved in choosing the frequencies for the curve fits, it is not the fault of the analysis methods that they give results which are inconsistent with our understanding of tidal processes. However, this understanding of tidal processes rests on the assumption that the tidal currents in the Middle Estuary result from the propagation of a simple barotropic tide. On the other hand, it is a simple matter to explain the observed phenomena if this assumption is dropped, and the tidal currents are considered to be the result of not only barotropic tides but also baroclinic tides.

There are two major reasons for expecting to have internal tides present in the Middle Estuary. In Chapter 2 it was shown that there is considerable vertical density structure in the Estuary and, if

there were internal tides generated, these would be allowed to propagate because of this vertical density structure. The second reason for expecting the presence of internal tides is that Forrester (1974) found them present in the Lower Estuary, where they were shown to be generated by the abrupt change in depth associated with the end of the Laurentian Trough which is at the downstream end of the Middle Estuary. LeBlond and Mysak (1978), reporting on the work of Rattray and his co-workers (1960 onward), point out that internal waves may be generated by a step-like change in topography, and although the work of Rattray is concerned with the seaward propogation of these waves, there is also a landward propagation. It is this landward, or upstream, propagating set of waves which would be found in the Middle Estuary.

Given that there are reasons to suspect the presence of internal tides in the Middle Estuary, it is possible to show that they could be used to explain the anomalous features in the amplitudes and phases of the tidal currents. This will be done here in a very simple fashion, and the remaining chapters will be used to make the explanation much more quantitative.

Assume a uniform channel with a constant surface density and an appropriate vertical density structure and that a surface tide of frequency, σ, is generated at one end of the semi-infinite channel. Then if this surface tide also generates internal modes of the same frequency, then at a distance x from the origin, the current will be given by

$$u(x,z,t) = \sum_{i=0}^{m} a_i(z)\cos(\sigma t + k_i x) \qquad (3.3.1)$$

where; a_i is the amplitude of the i^{th} vertical mode at depth z; t is time; k_i is the horizontal wave number associated with the i^{th} vertical mode; x is the distance from the generation point and m is the total number of vertical modes with the zeroth mode being associated with the barotropic tide. Using standard trignometric identities, equation 3.3.1 may be transformed into

$$u(x,z,t) = AMP \cos(\sigma t + PHASE) \tag{3.3.2}$$

where;

$$AMP = \left[\left(\sum_{i=0}^{m} a_i \cos k_i x\right)^2 + \left(\sum_{i=0}^{m} a_i \sin k_i x\right)^2\right]^{\frac{1}{2}}$$

$$PHASE = \arctan\left(\left(\sum_{i=0}^{m} a_i \sin k_i x\right) \Big/ \left(\sum_{i=0}^{m} a_i \cos k_i x\right)\right)$$

and so the current at any distance from the source could still be described by a cosine of the appropriate frequency, but both the amplitude and the phase of this cosine would be functions of the amplitude and phase of the modes as well as a function of the distance from the source.

To give an example of how this process could affect an estuary such as the St. Lawrence, assume that a surface tide at the M_2 frequency generates three internal modes at $x = 0$. If the wave properties are as in Table 3.3.1, then equation (3.3.2) may be used to calculate the amplitude and phase of a 'tidal constituent' at various distances from the source of the internal waves. The values are given in Table 3.3.2. It can be seen, then, that even with very

Mode Number	Max. amplitude (m/sec)	Amplitude at 10 m depth	Wave-number (rad/km)
0	0.50	0.50	0.00406
1	0.21	0.17	0.1093
2	0.15	0.03	0.2389
3	0.08	0.04	0.3570

Table 3.3.1 Wave parameters for the example in Table 3.3.2

Distance (km)	Amplitude (m/sec)	Phase (deg)	Phase Barotropic
60	0.647	19.65	13.96
65	0.647	23.35	15.12
70	0.584	30.07	16.28
75	0.543	42.93	17.45
80	0.506	34.86	18.61
85	0.374	29.89	19.77

Table 3.3.2 Amplitude and phase of a 'tidal constituent' at various distances from the source compared with the phase of the barotropic tide.

modest internal waves in a simple channel, the phase and the amplitude could look quite confusing and bear little resemblance to the amplitude and the phase of the barotropic tide which generates the internal waves. It should also be noted that the same sort of variability would emerge with depth, although there would not be a simple relationship between the amplitudes or the phases at various depths and, in addition, the depth variation would change with location. This is the same sort of pattern that is found on the St. Lawrence.

If the St. Lawrence were a uniform channel with a constant density structure, then the amplitudes and phases of the internal waves could be calculated from a number of simultaneous current meter records in a fairly restricted area. This information could then be used to predict the tidal currents at any point in the Estuary from the knowledge of the amplitudes, phases and wave numbers at the source. However, quite apart from the fact that the St. Lawrence is not a simple channel and has large and important topographic features, it was shown in Chapter 2 that the density structure itself is quite complicated. Since the density structure is a complex function of both space and time, then the wave numbers and the modal structure at the generation point would be a function of time and the propagation properties of the internal tides would also be a function of both space and time. Hence the tidal currents at any given location will be a function of time as well as a function of the density structure which lies between the measuring point and the generation point.

The final piece of evidence that the observed currents in the Middle Estuary are not due to simple progressive waves is that some of the analysed tidal vectors rotate the wrong way. In a channel, there are only two types of waves possible and these are Kelvin waves and Poincare waves (Vermersch and Beardsley, 1976). Kelvin waves only produce currents parallel to the direction of propagation and so the ellipses associated with them have a zero minor axis. Poincare waves do have a cross-channel current component, but they can only produce current ellipses which rotate in a counter-clockwise direction in the Northern Hemisphere (Proudman, 1952; Mortimer, 1973). This means that the sign of the minor axis of the current ellipse must be positive, but in any

list of the tidal constituents for the St. Lawrence (and for many other locations) the sign of the minor axis is frequently negative, which indicates that the current ellipse rotates the wrong way.

One way in which this could happen is for the 'tidal constituent' to be the sum of two progressive, plane waves which are of the same frequency, σ, different phase, and which have an angle θ between their propagation directions. If the two waves are

$$U_1 = u_1 \cos(\sigma t + \phi_1)$$

$$U_2 = u_2 \cos(\sigma t + \phi_2)$$

then taking the components parallel and perpendicular to U_1 gives the resultant current components

$$u = \sqrt{A^2 + B^2}\, \cos(\sigma t - \phi_3)$$

$$v = u_2 \sin\theta \cos(\sigma t + \phi_2)$$

where

$$A = u_1 \cos\phi_1 + u_2 \cos\theta \cos\phi_2$$

$$B = u_1 \sin\phi_1 + u_2 \cos\theta \sin\phi_2$$

$$\phi_3 = \arctan(B/A)$$

Using the definitions 3.2.3 and 3.2.4, the length of the minor axis is $m = |a_+| - |a_-|$ and so the direction of the ellipse rotation

depends upon the balance between $|a_+|$ and $|a_-|$. Substituting and carrying out the algebra shows that the rotation will be clockwise if

$$\tan\phi_3 < \tan\phi_2$$

and doing some more algebra shows that the rotation is clockwise if

$$\tan\phi_1 < \tan\phi_2$$

There will be no rotation of the ellipse if the 'less than' sign is an equality and it will be counter-clockwise if the sign is 'greater than'.

Since the St. Lawrence is not a manmade channel, it does have some fairly definite changes in direction. At the mouth of the Saguenay there is a bend in the main channel of about 15^o, and there are further bends at Gros Cap à l'Aigle,Pte au Pic and at Goose Cape. These bends could give rise to sidewall reflections that would allow both direct and reflected waves to be present in some parts of the Estuary. Since the reflected wave has further to travel, its phase should lag the phase of the direct wave and so the ellipse will rotate in the clockwise direction. A direct wave alone will, of course, rotate in the proper, counter-clockwise, direction. Hence it is possible to have current ellipses rotating in either direction, depending upon the location in the Estuary.

3.4 Discussion

The purpose of this Chapter was to draw out some of the information available from the tidal current records that have been collected on the Middle Estuary. The admittance method of analysis of tidal currents has been very useful in revealing the inconsistencies in these records. However, the inconsistencies are due to the assumption that the tidal currents in the St. Lawrence are due to surface, or barotropic, tides alone. It has been shown that the inconsistencies may be explained in a qualitative manner if it is assumed that there are baroclinic, or internal, tides present which also contribute to the observed tidal currents. Unless the internal tides are taken into account, it will be impossible to predict the currents in the Middle Estuary even though the statistics of the tidal analyses indicate that very good least-squares fits are obtained. In addition an explanation has been offered for the observed phenomena of current ellipses which rotate the wrong way.

CHAPTER 4

Theory of Internal Gravity Waves

4.0 Introduction

In the past ten to fifteen years, internal gravity waves have been seen to be a ubiquitous feature of the circulation processes in the oceans. Although G.G. Stokes (1847) gave the first mathematical theory of free waves on the interface of a two-layer fluid, it was not until 1904 that the first oceanographical applications were found. Ekman (1904) described the phenomena of 'dead water' in some Norwegian Fjords and E.R. Watson (1904) described internal seiches in Loch Ness in terms of internal gravity waves. In 1933, J.E. Fjeldstad developed a theory of internal gravity waves for oceanographic applications which included both arbitrary vertical density structures and geostrophic forces. However, there was very little activity in the field until the 1960's.

This lack of activity in recognizing the importance of internal waves can easily be ascribed to the consensus view that the oceans moved on large space and time scales. In addition to this view, the crudity of measuring instruments led to measuring programs which tended to filter out processes with the length and time scales of internal waves, and so there were very few measurements made in which the effects of internal waves were obvious. With the rise of the nuclear submarine as a major weapon in the Cold War, a large amount of money became available for oceanographic research and new developments in instrumentation and data processing techniques led to more closely-spaced measurements, and these were quickly followed by an explosive

interest in internal gravity waves.

In 1963, the American Geophysical Union started its series of reviews of the internal wave literature. Cox (1963) listed 9 papers written between 1960 and 1963, while in the next review Cox (1968) listed 28 papers published between 1963 and 1968. Wunsch (1971) listed 41 papers published between 1968 and 1971; while Briscoe (1975) listed 406 published between 1971 and 1975 and Gregg and Briscoe (1979) in the latest of these reviews, listed about 325 published between 1975 and 1979.

A great many of these papers have very little application to the problems of internal waves in estuaries, since the scales of motion and the energetics of estuaries are very different from those in the deep oceans. In Table 3.2.1 it was shown that, once the tidal energies are removed from the records, there is very little energy left. On average, the tidal frequencies account for 94% of the energy observed on the St. Lawrence. In addition, an examination of the amplitudes of the tidal constituents shows that almost all of the energy lies in the diurnal, semi-diurnal, quarter-diurnal, and sixth-diurnal bands. In Chapter 3, it was shown that in any one of these frequency bands, some of the energy is in the internal waves and some is in the barotropic waves, but even though the distribution of energy between the surface and internal wave structure is not clear, it is the tidal frequencies that contain the energy. Further, it has already been mentioned that the only types of long waves that can propagate in a channel are Kelvin or Poincare waves. Hence the major portion of the energy in the St. Lawrence will be in either Kelvin or Poincare waves, of tidal frequency.

This chapter will be concerned with the development of the

equations of motion of internal gravity waves and the related eigenvalue problems associated with the vertical equation. The results of the investigations into the vertical density structure that were carried out in Chapter 2 will be used to solve this vertical velocity equation. The following chapters will concern themselves with the horizontal propagation of internal gravity waves in estuaries and the application of this theory to the circulation processes in the St. Lawrence.

4.1 The Equations of Motion

There are a number of ways of deriving the equations of motion of internal gravity waves, but for the purposes here it suffices to begin with the linear, inviscid, Boussinesq equations for a rotating earth. Using a right-handed coordinate system the equations are

$$\frac{\partial u}{\partial t} - fv + \frac{1}{\bar{\rho}} \frac{\partial P}{\partial x} = 0$$

$$\frac{\partial v}{\partial t} + fu + \frac{1}{\bar{\rho}} \frac{\partial P}{\partial y} = 0$$

$$\frac{\partial w}{\partial t} + \frac{1}{\bar{\rho}} \frac{\partial P}{\partial z} + g \frac{\rho}{\bar{\rho}} = 0$$

where the variables have their usual meaning, that is; u,v,w are the long channel, cross channel and vertical components of velocity; f is the inertial or Coriolis frequency; P is the pressure excess; $\bar{\rho}$ is the reference density; ρ is the density; and g is the acceleration due to gravity. By eliminating the pressure from these equations

$$\frac{\partial}{\partial t}\left[\frac{\partial u}{\partial z} + \frac{\partial v}{\partial z} - \frac{\partial w}{\partial x} - \frac{\partial w}{\partial y}\right] - f\left(\frac{\partial v}{\partial z} - \frac{\partial u}{\partial z}\right) + \frac{g}{\bar{\rho}}\left(\frac{\partial \rho}{\partial x} + \frac{\partial \rho}{\partial y}\right) = 0$$

and then a further differentiation with respect to time and taking the horizontal divergence, $\nabla_h = \frac{\partial}{\partial x} + \frac{\partial}{\partial y}$, results in

$$\frac{\partial^2}{\partial t^2}\left[\frac{\partial}{\partial z}\left[\frac{\partial u}{\partial x} + \frac{\partial v}{\partial y}\right] - \nabla_h^2 w\right] - f\frac{\partial}{\partial z}\frac{\partial}{\partial t}\left[\frac{\partial v}{\partial x} - \frac{\partial u}{\partial y}\right] + \nabla_h^2 \frac{g}{\bar{\rho}}\frac{\partial \rho}{\partial t} = 0$$

The first two terms may be combined through the continuity equation. If the fluid is assumed to be irrotational except for the vorticity induced by the Earth's rotation, then the third term may be reduced using the vertical component of the vorticity equation, which is

$$\frac{\partial}{\partial t}\left[\frac{\partial v}{\partial x} - \frac{\partial u}{\partial y}\right] = f\frac{\partial w}{\partial z}$$

and the final term is dealt with using the incompressibility condition

$$\frac{\partial \rho}{\partial t} + u\frac{\partial \rho}{\partial x} + v\frac{\partial \rho}{\partial y} + w\frac{\partial \rho}{\partial z} = 0$$

and the definition of the Brunt-Vaisala frequency

$$N^2 = -\frac{g}{\bar{\rho}}\frac{\partial \rho}{\partial z}$$

so that the structure equation for internal gravity waves becomes

$$\frac{\partial^2}{\partial t^2}\nabla^2 w + N^2\nabla_h^2 w + f^2\frac{\partial^2 w}{\partial z^2} - \frac{g}{\bar{\rho}}\left[u\frac{\partial^3 \rho}{\partial x^3} + v\frac{\partial^3 \rho}{\partial y^3}\right] = 0 \qquad (4.1.1)$$

In most derivations, the final term is lumped in with all of the other nonlinear terms and dropped on the basis of its nonlinearity and assumed negligible size. In this derivation, however, it has been kept until this stage since it is not immediately obvious that horizontal density gradients are negligible in an estuary.

By definition, any estuary does have a longitudinal density gradient since it is the meeting area of fresh and salt water. In addition, it would seem reasonable to suppose that if there were any bends in the channel, or if Coriolis forces were to play an important role, then there should also be lateral density gradients. Since, by Taylor's Theorem, any continuous function may be represented by a polynomial, it is only necessary to consider polynomial representations of the density gradients. If then, the horizontal density variations may be represented by linear or quadratic forms, then this last term is identically zero and may be ignored. However, if the density structure is complicated enough to require a polynomial of more than second order, it cannot be dropped without further consideration.

If the final term is kept in equation 4.1.1 the vertical structure equation is nonlinear and non-separable. It will be shown in the next chapter that there is at least one particular solution that may be found for the complete equation. However, for the moment, the usual expedient of dropping the final term from equation 4.1.1 will be followed.

Assuming, then, that the final term in 4.1.1 is zero and that the solution is separable in the form $w(x,y,z,t) = (W(z)F(x,y)\exp(i\sigma t)$ then

$$\frac{1}{\sigma^2 - f^2} \frac{\nabla_h^2 F}{F} = \frac{1}{N^2 - \sigma^2} \frac{\partial^2 W}{\partial z^2 W} = \frac{-K^2}{\sigma^2 - f^2}$$

where the separation constant has been chosen from the assumption that the solution will be wave-like in the horizontal. Therefore, the vertical and the horizontal structure equations may be entirely decoupled

and the two equations are

$$\frac{d^2W}{dz^2} + \left(\frac{N^2(z) - \sigma^2}{\sigma^2 - f^2}\right)K^2W = 0 \qquad (4.1.2.)$$

$$\frac{\partial^2F}{\partial x^2} + \frac{\partial^2F}{\partial y^2} + K^2F = 0 \qquad (4.1.3.)$$

These two equations are well known in Mathematical Physics. The vertical structure equation is known as the Schrodinger Equation while the horizontal structure equation is an inhomogeneous form of the Laplace equation. Rather surprisingly, the only authors to comment on the fact that the vertical structure equation is a time independent form of the Schrodinger Equation have been Lighthill (1978) and Malvestuto (1979). The equation is of no little importance in Quantum Mechanics and so it has an extensive literature, reference to which may be found in almost any book on modern physics.

4.2 Properties of the Vertical Structure Equation

In this section, a brief list of the important properties of the vertical structure equation will be given, but not all of them will be proved.

Assuming that the horizontal wave number, K, is real, then if $N^2 > \sigma^2 > f^2$, $\frac{d^2W}{dz^2}$ and W must have different signs and so the function W must be 'wavey' and always concave to the z-axis. If σ is outside the interval (N,f) then $\frac{d^2W}{dz^2}$ and W must have the same sign and then W will show an exponential type of behaviour and will monotonically increase or decrease from the surface to the bottom. Hence internal waves can only propagate as waves for $N^2 > \sigma^2 > f^2$.

If the relative displacement of an isopycnal is given by $Z(x,y,z,t)$, then by definition, $w = \frac{dZ}{dt}$ and so

$$Z(x,y,z,t) = \frac{1}{i\sigma} F(x,y)\, W(z)\, \exp(i\sigma t)$$

so that at any particular depth, the relative displacement of an isopycnal is proportional to the vertical velocity and 90^{o} out of phase with the vertical velocity.

Assuming that at a time, t, in a small region about the origin there is no y-dependence in the motion so that $F(x,y) = F(x)$ and assuming that

$$w = F(x)W(z)$$

$$u = G(x)U(z)$$

then, from the continuity equation and integrating

$$U(z) \int_0^x \frac{dG}{dx}\, dx = - \frac{dW}{dz} \int_0^x F(x)\, dx$$

and so at the point, x

$$U(z) = - \frac{\int_0^x F(x)\, dx}{G(x) - G(o)} \frac{dW}{dz}$$

and so the horizontal velocity is proportional to the z-derivative of the vertical velocity and the constant depends upon x.

Appropriate boundary conditions are easy to find for the vertical velocity equation. At the bottom there must be no vertical velocity, and so

$$W(H) = 0$$

At the surface, assuming constant atmospheric pressure and a sinusoidal disturbance with the same horizontal wave number as the internal wave, the boundary condition is (Fjeldstad, 1933)

$$\frac{dW}{dz} + \left(\frac{K^2}{\sigma^2 - f^2}\right) gW = 0$$

An approximation that is frequently made to these boundary conditions is to set the surface boundary condition to $W = 0$, which is known as the rigid lid assumption.

The vertical velocity equation, together with the boundary conditions, make up a Sturm-Liouville system. Volume 1 of Courant and Hilbert (1937) is almost entirely devoted to systems of this type, and they prove a great number of theorems about Sturm-Liouville problems and the eigenvalue problems associated with them. Five theorems are important enough to be stated explicitly.

1. If λ_n is the n^{th} eigenvalue of the vertical velocity equation under the rigid lid assumption and μ_n is the n^{th} eigenvalue under the free surface boundary conditions, then; $\lambda_n < \mu_n$.

2. The asymptotic behaviour of the eigenvalues of the vertical velocity equation is independent of the boundary conditions, and if n is sufficiently large,

$$\lambda_{n+1} = \frac{(n+1)^2}{n^2} \lambda_n \quad .$$

3. If $N^2 > \sigma^2 > f^2$, then all of the eigenvalues of the system will be real and positive.

4. The eigenfunctions are orthogonal. That is, if ϕ_i and ϕ_j are two eigenfunctions, then $\int_0^H \phi_i \phi_j dz = 0$, if $i \neq j$.

5. The eigenfunctions form a complete set. That is, all possible motions may be produced by linear combinations of the eigenfunctions.

The eigenvalues of the vertical velocity equation 4.1.2 are the horizontal wave numbers, K_i and there are, in general, a countable infinite number of them. They are related to the phase speed of the wave by

$$c_i^2 = \frac{\sigma^2 - f^2}{K_i^2}$$

and $c_i > c_j$ if $i < j$. The $i+1^{st}$ eigenvalue will correspond to an eigenfunction that has i zero crossings of the z axis, not counting the zero value at the bottom. Application of the rigid lid assumption has the practical effect of making the smallest eigenvalue computed correspond to the first internal mode rather than the barotropic mode. If the free surface conditions are used, the smallest eigenvalue corresponds to the barotropic, or surface, mode.

When $N(z)$ is a constant, the vertical velocity equation is an ordinary differential equation with constant coefficients, and is, therefore, easily solved in terms of a simple sine function. The application of the boundary conditions then results in a very simple dispersion relation. In general, however, the vertical velocity equation is nonlinear because of the functional form of $N^2(z)$, and so it is not easily soluble in analytical form, except in a few special cases.

Roberts (1975) has a section devoted entirely to solutions of the vertical velocity equation for various density distributions that are to be found in the deep ocean. Most of these are not applicable to the density structures that have been found in estuaries. One of the major reasons for Chapter 2 was to establish a vertical density structure for the St. Lawrence in order to calculate the

vertical modal structure. The next three sections of this chapter will be devoted to computing the vertical modal structure that occurs in the St. Lawrence.

4.3 The Exponential Cubic

In Chapter 2 it was shown that, of all of the exponential polynomials, the exponential cubic, in the form

$$\bar{\rho} = \rho_o(x,y)\exp(az + bz^2 + cz^3)$$

provided the best statistical fit to the observed density structure on the St. Lawrence. If the Brunt-Vaisala frequency is calculated and substituted into the vertical velocity equation, 4.1.2, then

$$\frac{d^2W}{dz^2} + (c_1z^2 + b_1z + a_1)W = 0$$

where

$$c_1 = \frac{3gc}{\sigma^2 - f^2} K^2$$

$$b_1 = \frac{2gb}{\sigma^2 - f^2} K^2$$

$$a_1 = \frac{(ga-\sigma^2)}{\sigma^2 - f^2} K^2$$

By making the coordinate transformation

$$x = 4c_1z + \frac{b_1}{2c_1}$$

the vertical structure equation becomes

$$\frac{d^2W}{dx^2} + (\tfrac{1}{4}x^2 - d)W = 0 \qquad (4.3.1)$$

with $$x = \left(\frac{12gc}{\sigma^2 - f^2} K^2\right) z + \frac{b}{3c}$$

$$d = \frac{b^2}{36c^2} - \left(\frac{ga - \sigma^2}{\sigma^2 - f^2}\right) K^2$$

The solutions to 4.3.1 are the Parabolic Cylinder Functions (Abramowitz and Stegun, 1965). The boundary conditions for the vertical velocity equation must also be transformed, and they become

$$W = 0 \quad \text{at} \quad x_H = \frac{12gcK^2}{\sigma^2 - f^2} H + \frac{b}{3c}$$

$$\frac{dW}{dx} + \frac{W}{12c} = 0 \text{ at } x_o = \frac{b}{3c}$$

Since the boundary conditions are no longer given at the surface and bottom, the solutions can be neither strictly even or odd, and so the general solution to the vertical structure equation is

$$W = Ay_1 + By_2 \tag{4.3.2}$$

where y_1 is the even solution and y_2 is the odd solution and these Parabolic Cylinder Functions are given by their series forms

$$y_1(x) = 1 + d\frac{x^2}{2!} + (d^2 - \tfrac{1}{2}) \frac{x^4}{4!} + (d^3 - \frac{7}{2}d) \frac{x^6}{6!} \ldots$$

$$y_2(x) = x + d\frac{x^3}{x!} + (d^2 - \frac{3}{2}) \frac{x^5}{5!} + \ldots$$

and where the non-zero coefficients a_n of $x^n/n!$ are connected by the recursion relation

$$a_{n+2} = d\, a_n - \tfrac{1}{4}n(n-1)\, a_{n-2}$$

Alternatively, the solution may be written in terms of Kummer's Confluent Hypergeometric Function, $M(c_1,c_2,c_3)$, as

$$W = \exp(ix^2) \left| AM\left(\frac{-id}{2} + \tfrac{1}{4}, \tfrac{1}{2}, \frac{ix^2}{2}\right) + Bx^{\pi i/4}\, M\left(\frac{-d}{2} + \tfrac{3}{4}, \frac{3}{2}, \frac{ix^2}{2}\right) \right|$$

However, in this age of computers, there is no real advantage in using the Hypergeometric form, since the power series for the Parabolic Cylinder Function converges very rapidly for the range of values that are of interest in the St. Lawrence or any other estuary.

It is still necessary to determine the integration constants, A and B . One of them must remain as a scaling factor, but the other may be eliminated by applying the bottom boundary condition to obtain

$$A = - B \frac{Y_2(x_H)}{y_1(x_H)}$$

Substituting this into the surface boundary condition and rearranging gives the dispersion relationship

$$\frac{y_2(x_H)}{y_1(x_H)} \left[y_1'(x_o) + \frac{1}{12c}\, y_1(x_o)\right] + y_2'(x_o) + \frac{1}{12c}\, y_2(x_o) = 0 \qquad (4.3.3)$$

where the primes denote differentiation with respect to the transformed variable x .

The only unknown in this dispersion relation is the wave number, K , but it is expressed implicitly within the arguments of the Parabolic Cylinder Function. This dispersion relation is not too useful in an analytical sense since the relationships are not only implicit and nonlinear, but also, the properties of the Parabolic Cylinder Function are not particularly well-known. On the other hand, it does have the advantage that neither the rigid lid assumption nor

the long wave assumption has been made and so it is applicable to any frequency for which internal waves are possible. In practice, the dispersion relationship could be very simply programmed on a small computer and, with this to do the arithmetic, the wave number for any particular mode could then be calculated, and used in equation 4.3.1 to calculate the modal structure.

4.4 Forrester's Density Structure

It will be recalled that Forrester (1974) proposed a particular form for the vertical density structure on the Lower Estuary which was based on a few bottle casts that were obtained while setting out current meter moorings. In terms of the explained variance, there was no significant difference between the model obtained by using Forrester's equation for the density structure in the Middle Estuary and the model obtained by using the exponential cubic.

Forrester's density structure may be expressed in the form

$$\rho = \rho_o(x,y)\exp(a/(z + b))$$

and so the Brunt-Vaisala frequency is given by

$$N^2(z) = \frac{g}{\rho}\frac{\partial \rho}{\partial z} = \frac{ag}{(z + b)^2}$$

Substituting this expression for N^2 into the vertical velocity equation 4.1.2, and making the long wave approximation, by neglecting σ^2 in the top line with respect to the much larger N^2, results in a nonlinear ordinary differential equation. The solution to this differential equation is

$$W = A\sqrt{z + b}\ \sin\left(\sqrt{\frac{ag}{c^2} - \tfrac{1}{4}}\ \ell n(z + b) + B\right) .$$

In this equation, the constants a and b are due to the density structure and the constants A and B are the constants of integration. The eigenvalue for this solution is the phase speed c, of the wave.

There should be countable infinity of eigenvalues, c_n, for this problem, the lowest numbered eigenvalue is for the barotropic mode and the higher eigenvalues are for the internal modes.

If the rigid lid is applied as the surface boundary condition, then the argument of the sine function in the solution must be zero, and after a little algebra,

$$c_n^2 = \frac{4ag\ \ell n^2(b)}{4B_n^2 + \ell n^2(b)}$$

Applying the bottom boundary condition at $z = H$, means that there must be $n - 1$ crossings of the z axis and so the value of the argument of the sine function must be $n\pi$, and so

$$c_n^2 = \frac{4ag\ \ell n^2(H + b)}{4(n\pi + B_n^2) + \ell n^2(H + b)}$$

Since the value of the eigenvalue must be the same at the surface and at the bottom, these two values may be equated and B_n eliminated from further consideration, since

$$B_n = \frac{n\pi(\ell n^2(b) + \ell n(b)\ell n(H + b)}{\ell n^2(H + b) - \ell n^2(b)}$$

Substituting this value for B_n into the surface boundary condition gives an expression, after a little manipulation, for the phase speed of the internal wave modes in the Middle Estuary of the St. Lawrence, which is

$$c_n^2 = \frac{4ag(\ell n(H + b) - \ell n(b))^2}{(2n\pi)^2 + (\ell n(H+b) - \ell n(b))^2}$$

and from this, the dispersion relationship is easily calculated as

$$K_n^2 = \frac{(\sigma^2 - f^2)((2n\pi)^2 + (\ell n(H + b) - \ell n(b))^2)}{4ag(\ell n(H + b) - \ell n(b))^2}$$

Due to the rigid lid boundary condition, the barotropic mode has been ignored, but since this mode has a phase speed of $c_o^2 = gH$, there is not too much point in doing any more complicated mathematics to obtain it. If, instead of the rigid lid assumption, the free surface boundary condition were used, the phase speed of the modes would be very slightly slower. This statement is proved by the first theorem in 4.2.

At first sight, the long wave approximation seems to be a critical assumption. The long wave assumption neglects the wave frequency on the basis that it is very small in comparison to the Brunt-Vaisala frequency. In this study, however, it is only waves of tidal frequency that are of interest and the largest of these frequencies is about 1.57 rad/hr (sixth diurnal). A typical Brunt-Vaisala frequency for the St. Lawrence would be about 280 rad/hr (80 seconds). Hence, for the tidal frequencies of interest, there is no difficulty with the long wave assumption since $N^2 >> \sigma^2$. The errors due to the long wave assumption would, of course, grow if the wave period of interest became very short.

4.5 Magaard's Density Structure

Magaard (1962) used a model of the form

$$\bar{\rho} = \rho_o(x,y)\ \sqrt{1 + az}$$

for the density structure, and he showed that it had solutions

$$W_n(z) = A \sin\left[\frac{n\pi(4g - 2a^2z)^{\frac{1}{2}} - \sqrt{4g}}{(4g + 2a^2H)^{\frac{1}{2}} - \sqrt{4g}}\right]^{\frac{1}{2}}$$

and a dispersion relationship

$$K_n^2 = \frac{\sigma^2 - f^2}{g}\left[\frac{n\ a}{(4g + 2a^2H)^{\frac{1}{2}} - 4g}\right]^2$$

Unfortunately, this model was not particularly successful at explaining the observed variance in the St. Lawrence density structure, and so the model was extended to the form

$$\rho = \rho_o(x,y)(1 + az + bz^2)^{\frac{1}{2}}$$

which may be substituted into the vertical structure equation, to obtain

$$\frac{d^2W}{dz^2} - \left[\frac{b\sigma^2z^2 + (a\sigma^2 - bg/2)z + (\sigma^2 - ga/2)}{2(bz^2 + az + 1)}\right]c_n^2\ W = 0$$

and this is very unpromising. Since the equation is still of the Sturm-Liouville type, it does have an integral, and all of the theorems about the eigenvalues still hold, but it does not necessarily have an integral that is easily expressible in terms of elementary functions. No progress has been made towards finding a simple integral for this particular differential equation.

4.6 Vertical Structure on the St. Lawrence

Up to this point, this Chapter has been concerned with the purely theoretical aspects of the internal wave structure for the three different models which, given the separability hypothesis, do not differ significantly in their ability to explain the vertical density structure of the Middle Estuary. It has proved impossible, so far, to obtain any satisfactory results about the vertical modal structure from Magaard's model, and so this model will have to be ignored in what follows. The vertical structure, for tidal frequencies, obtained from the Exponential Cubic and that obtained from using the Forrester's model do not differ when the same depth of water and the same mode numbers are used. Numerical experiments have shown that they agree to well within any practical limits when they are used in the same circumstances.

To give an idea of the magnitude of the various wave properties that would be encountered on the St. Lawrence, the vertical structure equation has been solved for a number of frequencies and modes. The density structure assumed was the exponential cubic, equation 2.7.1 and Table 4.6.1 gives the results of the calculations. It is worth noting that although the waves are dispersive, since the long wave approximation has not been made, the dispersive aspect does not show up at all. It is only in very high frequency waves that the difference in phase speed begins to show up. For this example, the water depth was assumed to be 55.m, the phase speed, c , is given in m/sec, and the wave length, λ , in km. Any other conditions of interest may be easily calculated from the formulae given by Forrester's equations.

Mode Number	12.42 hr.		2.00 hr.		0.25 hr.	
	c	λ	c	λ	c	λ
0	23.30	1049.40	23.29	168.99	23.29	20.96
1	0.724	32.60	0.724	5.25	0.722	0.65
2	0.350	15.77	0.350	2.54	0.349	0.32
3	0.232	10.43	0.232	1.68	0.227	0.20
4	0.172	7.67	0.172	1.25	0.172	0.16
5	0.137	6.15	0.137	0.99	0.135	0.12
6	0.114	5.15	0.114	0.83	0.114	0.10

Table 4.6.1 Wave properties for the St. Lawrence density structure, for three different wave periods.

To show how insensitive the vertical modal structure is to the precise density profile, the shapes of the first and third modes were calculated for the overall density structure given by Forrester's density model and for the density structure given by Forrester's model fitted to the single station 75-001C. Since this station provided the maximum errors in the overall fit, it should give the worst agreement for the modal structure. The results are shown in Figure 4.6.1. It is fairly obvious that the vertical modal structure is quite insensitive to the precise nature of the vertical density structure. This, then, lends support to the assumption of the separability hypothesis. If there is very little change in the vertical modal structure when the density is perturbed somewhat, then it should not matter too much that there is a slightly better statistical fit by ignoring the separability hypothesis.

By assuming a bottom boundary condition of $W = 0$ at $z = H$, it is also assumed that the bottom of the estuary is flat. Quite clearly, the bottom of a real estuary is anything but flat and this assumption cannot, in general, be made. The proper boundary condition is that there should be no flow normal to the bottom. Fortunately, some work has been done on the problem of flow over bottom topography

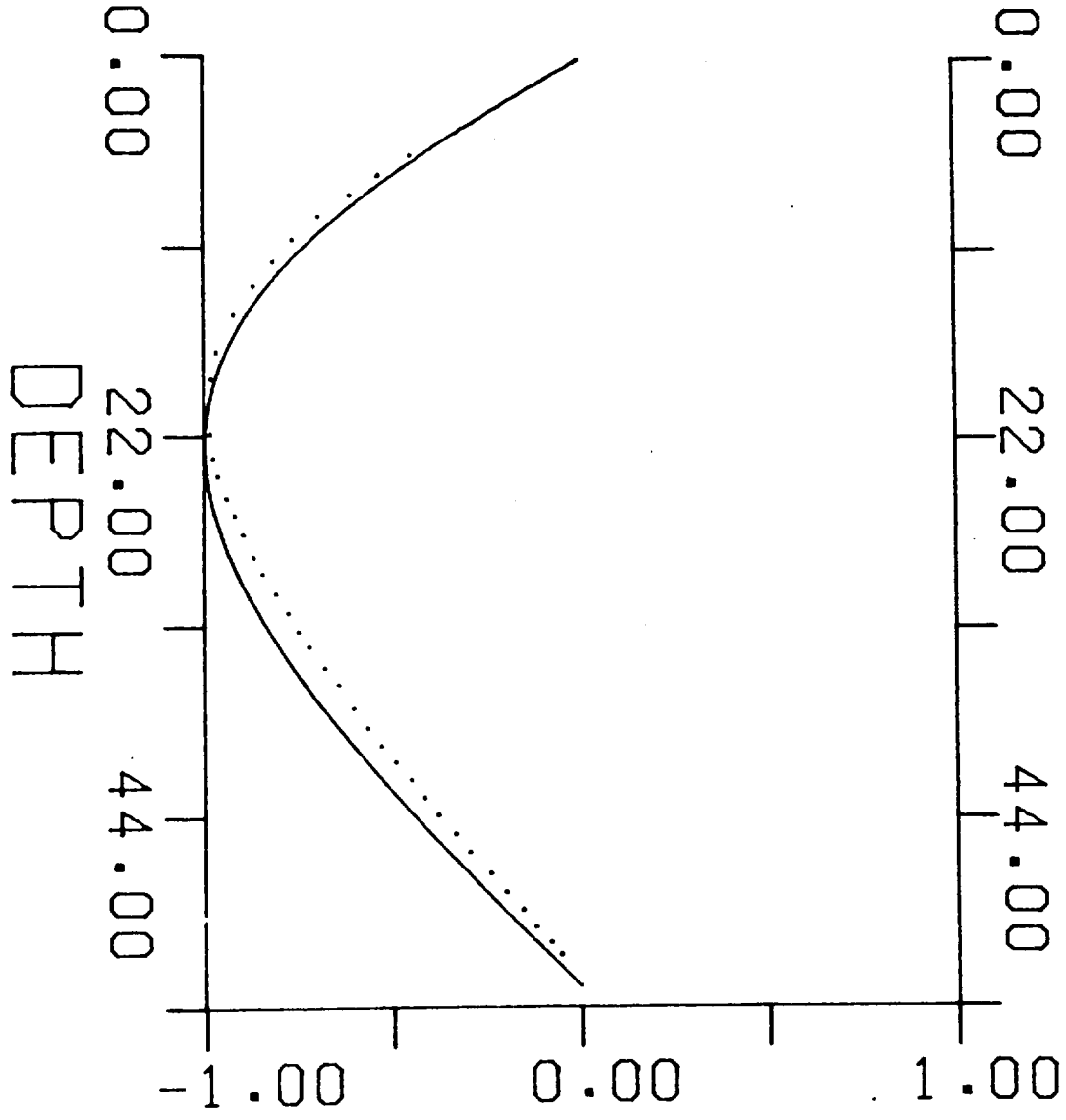

Figure 4.6.1 Comparison of Modal Structure due to different density structure. (Modal structure for the overall density structure is shown as a solid line).

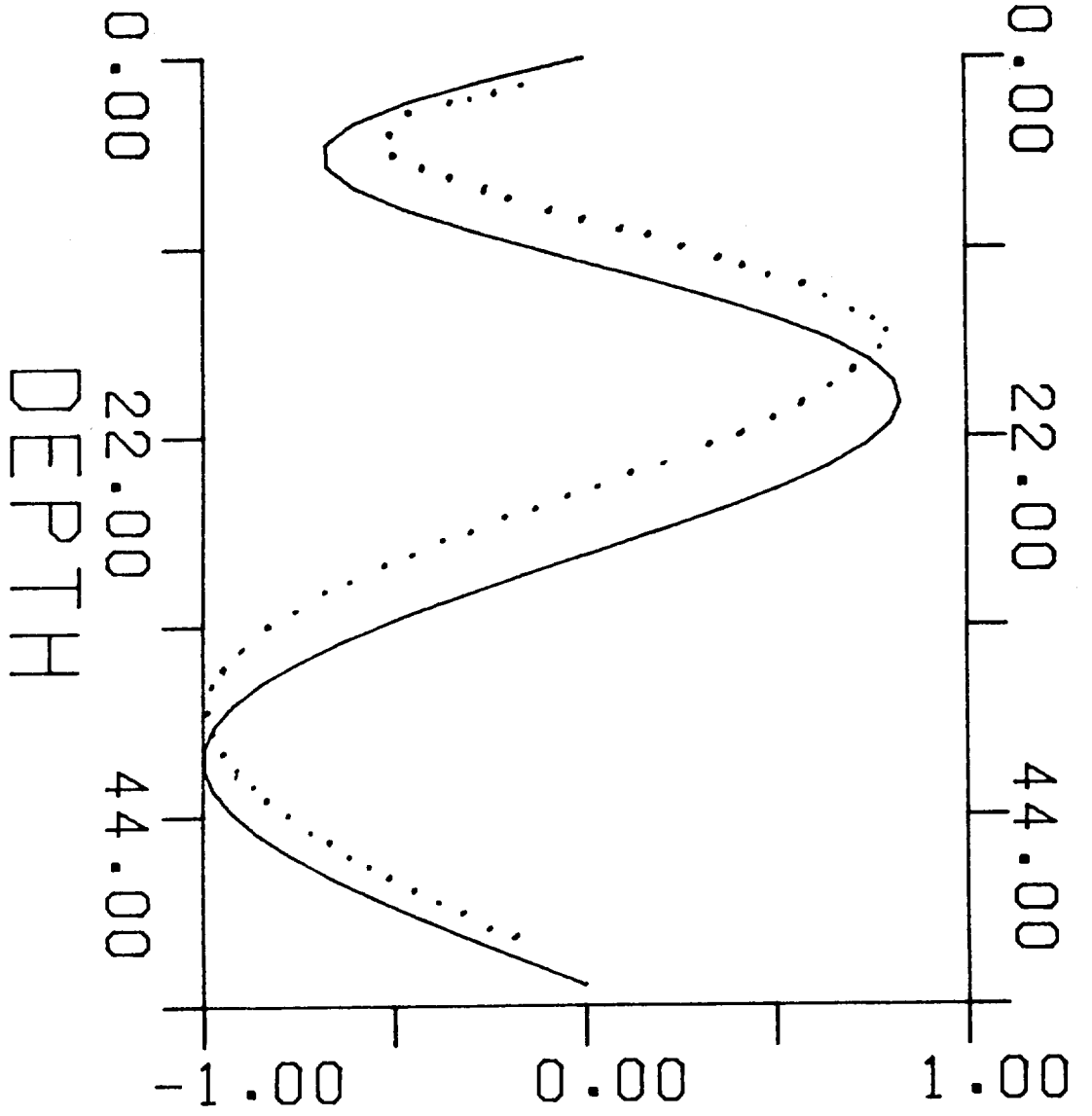

Figure 4.6.1 (Con't).

which is relevant to estuaries in general, and the St. Lawrence in particular.

The cross-sectional shape of the North Channel, which is the primary area of concern, is more or less triangular. The north side-wall is vertical, but the bottom slopes quite evenly from its maximum depth on the north side to a minimum on the south side-wall, with a mean slope of less than 0.01. Vermersch and Beardsley (1976) have solved exactly this problem for a channel which has a small cross-channel bottom slope. They found that it makes very little difference to the vertical structure, since the internal Kelvin and Poincare wave solutions applicable to the flat-bottom case are still applicable to the sloping bottom case. The effect of the sloping bottom is to allow the propagation of a very low frequency, bottom-trapped Rossby wave, which decays quickly away from the bottom. Their analysis is for a density structure where N^2 is constant, but the analysis should not change very much for a higher order exponential density gradient, so long as the separability hypothesis holds.

Of much more concern is the longitudinal bottom slope on the Morin Bank. Sandstrom (1966) has shown that a longitudinal bottom slope will reflect an internal wave if the bottom slope is more than

$$s^2 = \frac{\sigma^2 - f^2}{N^2 - \sigma^2}$$

and, assuming a very long Brunt-Vaisala period of 10 minutes, the maximum transmissive bottom slopes are 0.01 for a semi-diurnal wave and 0.02 for a sixth-diurnal wave. The mean slope on the Morin Bank is about 0.008 and the maximum slope is about 0.07. Hence, it is

very possible that many of the internal waves coming up the St. Lawrence would be reflected off the Morin Bank. On the other hand, there is no distinct tidally-averaged density difference observable in the water on either side of the Bank, and so some of the waves must propagate up and over the Bank. Wunsch (1968,1969) has shown that for small slopes, in the case of a constant Brunt-Vaisala frequency, the solutions are asymptotic to the case of a flat bottom.

Thus it is entirely possible that the longitudinal bottom slopes on the St. Lawrence are large enough to significantly distort the solutions that arise from assuming that the bottom is flat. In addition, it is probable that internal tides that are observed downstream of the Morin Bank are the sum of a direct and a reflected wave, and could not be considered to be purely progressive waves.

Chapter 5

Horizontal Propagation of Internal Gravity Waves

5.0 Introduction

In Chapter 4, the equations of motion and the vertical properties of internal gravity waves were examined. In this Chapter, the horizontal properties of these waves will be discussed and, in particular, the effects of horizontal density gradients will be examined. These horizontal density gradients will have two effects. The first is to affect the properties of the waves themselves, and the second is to affect the measurements that will be made at a particular location, since the density gradient will be advected back and forth past the measuring point by the waves.

5.1 No Horizontal Density Gradients

If it is assumed that there are no horizontal density gradients, the horizontal structure of the internal waves is given by equation 4.1.3 which is

$$\nabla_h^2 F + K^2 F = 0 \qquad (5.1.1)$$

Theorem 3 of Section 4.2 ensures that K^2 will be real and positive so long as $N^2 > \sigma^2 > f^2$, and so the solutions will be wave-like.

Assuming that the function, F, is separable in the form $F(x,y) = X(x)Y(y)$, and substituting this form into the horizontal structure equation

$$\frac{1}{X}\frac{d^2X}{dx^2} + \frac{1}{Y}\frac{d^2Y}{dy^2} + K^2 = 0$$

and so

$$\frac{1}{X}\frac{d^2X}{dx^2} = -\frac{d^2Y}{dy^2} - K^2 = -k_x^2$$

where; K is the total horizontal wave number and is the eigenvalue from the vertical velocity equation, and k_x is the wave number in the long stream direction. The long stream and cross stream wave numbers k_x and k_y, are related by

$$K^2 = k_x^2 + k_y^2 \qquad (5.1.2)$$

and the separated horizontal equations are therefore

$$\frac{d^2X}{dx^2} + k_x^2X = 0$$

$$\frac{d^2Y}{dy^2} + k_y^2Y = 0$$

Since the longstream solution will be evanescent and hence of no interest if $k_x^2 < 0$, in all future work, k_x^2 is always assumed to be positive. Hence the solution for the long stream direction may be written in the form

$$X(x) = A\cos(k_x x)$$

The solution for the y-dependence is determined by the value of k_y^2 which could be positive or negative. If k_y is imaginary, then the wave is a Kelvin wave and the amplitude of the wave decays exponentially across the channel. If k_y is real, then the wave is a Poincare wave and the amplitude has a sinusoidal cross channel dependence. In a channel, the only allowable waves are Kelvin and Poincare waves, since they are the only ones which

satisfy the boundary conditions of no flow through the sides of the channel, and these boundary conditions provide additional constraints on the magnitude of k_y (Proudman, 1952).

In a channel, then, one solution of the full equations of motion, assuming no horizontal density gradients, is given by

$$w(x,y,z,t) = -\sigma H \exp(ik_y y)W(z) \sin(\sigma t + k_x x + \phi)$$

$$u(x,y,z,t) = U \exp(ik_y y)W'(z) \cos(\sigma t + k_x x + \phi)$$

$$v(x,y,z,t) = iV \exp(ik_y y)W'(z) \sin(\sigma t + k_x x + \phi)$$

where; σ is the wave frequency, H is the wave amplitude, $W(z)$ is the solution to the vertical velocity equation, normalized so that its maximum value is 1, $W'(z)$ is the vertical derivative of W also normalized so that its maximum value is 1, $i = \sqrt{-1}$, and U and V are the maximum horizontal wave velocities.

5.2 Effects of Horizontal Density Gradients

There is one particular case in which the effects of horizontal density gradients may be determined, and this case will be examined here. If the w and the $\vec{u}$ components of velocity are assumed to be

$$w = W(z)F(x,y)\exp(i\sigma t)$$

$$\vec{u} = \vec{U}W'(z)F(x,y)\exp(i\sigma t)$$

and these are substituted into equation 4.1.1 the result is

$$(N^2 - \sigma^2)W\nabla_h^2 F + (f^2 - \sigma^2)\, F\frac{d^2W}{dz^2} = \frac{g}{\rho} F\frac{dW}{dz}\, \vec{U}.\nabla_h^3\rho \qquad (5.2.1)$$

Now, assuming that the horizontal density gradient will not have any effect upon the vertical structure, the vertical structure equation is assumed to be

$$\frac{d^2W}{dz^2} = - \frac{N^2 - \sigma^2}{\sigma^2 - f^2} K^2 W \tag{5.2.2}$$

and this may be substituted into 5.2.1 to get a separable equation which is

$$\frac{K^2F + \nabla_h^2 F}{\frac{g}{\bar{\rho}} F \vec{U}.\nabla_h^3 \rho} = \frac{\frac{dW}{dz}}{(N^2 - \sigma^2)W} = \frac{1}{\psi}$$

i.e. there are two separated equations:

$$\frac{dW}{dz} - \frac{N^2 - \sigma^2}{\psi} W = 0 \tag{5.2.3}$$

$$\nabla_h^2 F + \left(K^2 - \frac{\frac{g}{\bar{\rho}} \vec{U}.\nabla_h^3 \rho}{\psi}\right) F = 0 \tag{5.2.4}$$

The separation constant ψ may be eliminated from the equations, since there are now two equations, 5.2.2 and 5.2.3, which control the vertical velocity and so both must hold simultaneously. Differentiating 5.2.3 with respect to z and substituting into 5.2.2 and then solving for the separation constant results in

$$\psi^2 - \frac{2NN'(\sigma^2 - f^2)}{K^2(N^2 - \sigma^2)} \psi + \frac{(N^2 - \sigma^2)(\sigma^2 - f^2)}{K^2} = 0$$

where the prime denotes differentiation with respect to z. However, since ψ is a constant of separation, it cannot depend upon the variable z. The only case in which ψ does not depend

upon z, occurs when N is a constant. Hence in the case where N is a constant the assumption in 5.2.2 is justified and the horizontal density gradients do not affect the vertical structure but will influence the horizontal structure through equation 5.2.4.

When the vertical structure is such that N is a constant, then ψ is purely imaginary and equation 5.2.4 is a nonlinear partial differential equation, which is not separable into two components in the usual manner. However, it is possible to examine the equation in a qualitative way. Setting

$$F(x,y) = A\ X(x)\ Y(y)$$

$$a = \left(U \frac{\partial^3 \rho}{\partial x^3} + V \frac{\partial^3 \rho}{\partial y^3}\right) \frac{W'(z)}{\psi} \frac{g}{\bar{\rho}}$$

and substituting into 5.2.4, results in

$$\nabla_h^2(XY) + \left(1 - \frac{W'aA}{K\sqrt{(N^2 - \sigma^2)(\sigma^2 - f^2)}}\, i\right) K^2 XY = 0$$

Now, $W'(z)$ has a maximum value of 1 and the maximum value of A is almost always less than 2 m/sec, so that for an M_2 barotropic tide, which would be the worst case, the equation would become

$$\nabla_h^2(XY) + \left(1 - \frac{a}{5.0 \times 10^{-10}}\, i\right) K^2 XY = 0 \qquad (5.2.5)$$

If the horizontal structure of the tidally-averaged density may be represented by a polynomial which is either linear or quadratic, $a = 0$ and equation 5.2.5 is exactly the same as equation 5.1.1 and all of the analysis of Section 5.1 holds. In general, however, equation 5.2.5 is a nonlinear, non-separable partial differential

equation, when the third derivative of the horizontal tidally-averaged density structure is allowed to be any arbitrary function.

It will be shown in Chapter 6, that a value of $a \lesssim 1\times10^{-14}$ produces quite typical estuarine density structures, and for many estuaries a very small value of a would be appropriate. There are, of course, situations where a small value of a would not be appropriate, such as near a source of fresh water or in a location where the tidal mixing is particularly strong. If a is assumed to be very small, such as 1×10^{-14}, and the functions X and Y are assumed to be 'wavey' and to have maximum values near $+1$ or -1, then the partial differential equation 5.2.5 may be quasilinearized to

$$\nabla_h^2(XY) + (1 \pm \varepsilon i)K^2XY = 0$$

where ε is a very small real number, less than 1×10^{-4}.

The result of this would be that the analysis in section 5.1 would still be applicable, with the modification that the horizontal wave number, K, would be modulated by a very small damping factor, εi. This means that in the case of a constant Brunt-Vaisala frequency and with 'reasonably small' horizontal density gradients, the horizontal density gradients do not affect the horizontal propagation or the horizontal structure of the internal waves very much. Although this argument is qualitative, it would seem to be reasonable. One would not really expect large changes in the wave structure if the density gradients were not very extreme, but that there should be fairly large changes if the horizontal density gradients were quite large. One could think

of the normal mode solution given by Chapter 4 and Section 5.1 as a first approximation to the correct solution, and the evidence seems to point to the fact that one would not be too far wrong. It seems unlikely that a full analytical solution is possible for arbitrary vertical and horizontal density structure and that numerical methods would be required for a full solution.

5.3 Advection of the Horizontal Density Gradients

The previous section has shown that the horizontal density gradients do not affect the horizontal structure of the internal tides to a very great extent. That is, if a wave has a basic sinusoidal shape, then the presence of 'reasonably small' horizontal density gradients will not change this basic shape very much. It does not follow that a measuring instrument which is fixed to the bottom of the estuary will register the same sinusoidal shape if it is measuring the time-dependent density at its fixed location in the channel.

The tidal excursion in a typical estuary is usually quite long in comparison to the length of the estuary, since in many cases it is of the order of 10 to 15 km. Considering the flow in a Lagrangian sense, a marked particle of water may move a significant distance up and down the estuary during the course of a tidal cycle due to the particle motion of the wave. The tidally-averaged density gradients in a body of water are fixed to the water itself, like a marked particle, and not to the channel in which the water moves. Hence, the effect of a wave passing through an estuary would be to advect this tidally-averaged density structure back and forth over the course of a complete tidal cycle.

Assume that the tidally-averaged density structure in an estuary is given by

$$\bar{\rho} = \rho_o(x,y)D(z)$$

and the properties of the water in the estuary are to be measured at the location (x,y,z) as shown in Figure 5.3.1. Consider a plane wave, whose frequency is σ, and whose wave number is K, to be propagating from right to left past the measuring point. The tidally-averaged density structure in the estuary is shown in the figure and increases downstream, to the right.

If there were no waves present, the density registered

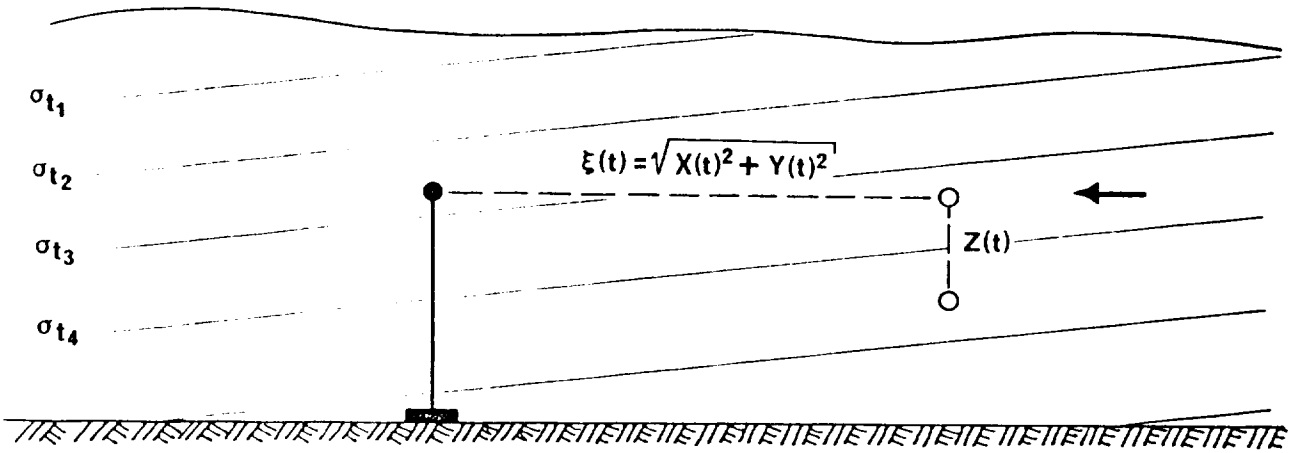

Figure 5.3.1. Advection past a measuring instrument.

at the instrument would remain constant at $\bar{\rho}$. However, when there is a wave present, after a time, t, the instrument will record a value of the density which is perturbed from the tidal mean, since the wave will have advected a parcel of water from the point (x',y',z')

a horizontal distance

$$\xi^2 = (X^2(t) + Y^2(t))^{\frac{1}{2}}$$

while at the same time, advecting it a vertical distance $Z(t)$. At time, t, then, the instrument measures the density of a parcel of water whose tidal mean position is at (x',y',z').

The instrument measures the time-dependent density at the point (x,y,z) and this may be expressed as

$$\rho(x,y,z,t) = \bar{\rho}(x + X(t), y + Y(t), z + Z(t))$$

which may be expanded in a three-dimensional Taylor Series as

$$\rho(x,y,z,t) = \bar{\rho}(x,y,z)(1 + \mathfrak{L} + \tfrac{1}{2}\mathfrak{L}^2 + \frac{1}{3!}\mathfrak{L}^3 + \frac{1}{4!}\mathfrak{L}^4 + \ldots) \qquad (5.3.1)$$

where the operator, $\mathfrak{L}$ is given by

$$\mathfrak{L} = X(t)\frac{\partial}{\partial x} + Y(t)\frac{\partial}{\partial y} + Z(t)\frac{\partial}{\partial z}$$

$$\mathfrak{L}^2 = X^2 \frac{\partial^2}{\partial x^2} + Y^2 \frac{\partial^2}{\partial y^2} + Z^2 \frac{\partial^2}{\partial z^2} + 2XY \frac{\partial^2}{\partial x \partial y} + 2XZ \frac{\partial^2}{\partial x \partial z} + 2YZ \frac{\partial^2}{\partial y \partial z}$$

and the higher powers of the operator are given by the Trinomial Theorem. This expansion will be exact and converge so long as there are no discontinuities in the tidally-averaged density structure that could be advected past the measuring point.

In general, of course, the tidally-averaged horizontal portion of the density structure may be represented by a polynomial and so, in general, equation 5.3.1 is an infinite series. In practice the higher derivatives of the horizontal density structure would be small, and so the series could be truncated after an appropriate

number of terms. The error involved in truncating the series is given by the Remainder Theorem, and if the series is truncated after n terms, the error is

$$R_n \leq \frac{1}{(n+1)!} \xi^{n+1} \bar{\rho}(x,y,z)$$

Unlike the effects of the horizontal density gradient that were discussed in the previous section, the linear and quadratic terms in the horizontal density gradient have a very large effect here. In practice, one would expect the linear and quadratic portions of the horizontal density gradient to be the largest terms, and although they would not affect the shape of the internal waves, they would very strongly affect the instantaneous densities measured at a given location in an estuary.

5.4 Advective Transport in a Channel

Equation 5.3.1 describes the density that would be measured at a fixed point when a tidally-averaged density structure is advected past that point. There were no assumptions made about the nature of the advecting disturbance, and although the discussion was conducted in terms of a tide wave in a channel, the mathematics are perfectly general. When it comes to actually computing the advection in the three dimensions, however, the exact nature of the advection process becomes important. In this section, the advection process will be confined to tidal waves in a channel. These waves may be either Kelvin or Poincare waves, or linear combinations of the two.

A solution to the equations of motion in a channel is

$$Z = H_{m,n}\exp(ia_m y)W_n(z)\cos(\sigma t + k_{m,n}x + \phi_{m,n}) \qquad (5.4.1)$$

$$w = -\sigma H_{m,n}\exp(ia_m y)W_n(z)\sin(\sigma t + k_{m,n}x + \phi_{m,n}) \qquad (5.4.2)$$

$$u = U_{m,n}\exp(ia_m y)W_n'(z)\cos(\sigma t + k_{m,n}x + \phi_{m,n}) \qquad (5.4.3)$$

$$v = iV_{m,n}\exp(ia_m y)W_n'(z)\sin(\sigma t + k_{m,n}x + \phi_{m,n}) \qquad (5.4.4)$$

where , $i = \sqrt{-1}$ and the real part of the solution is understood. $H_{m,n}$, $U_{m,n}$, $V_{m,n}$ are the maximum amplitudes of the vertical displacement and the velocity components for the n^{th} vertical mode and the m^{th} cross channel mode; $k_{m,n}$ and a_m are the long and cross-channel wave numbers; σ is the wave frequency; $\phi_{m,n}$ is the phase of the wave at the origin. $W_n(z)$ is the solution to the vertical velocity equation 4.1.2 and $W_n'(z)$ is the z-derivative, both normalized so that the maximum value is 1.0. When the cross-channel wave number is real, $K_n^2 = k_{m,n}^2 + a_m^2$, and the wave is a Poincare wave. When the cross-channel wave number is imaginary, the wave is a Kelvin wave and the real part of the cross-channel velocity is zero.

It is, therefore, very easy to calculate the vertical advection, since it is given by 5.4.1 and is proportional to the solution to the vertical velocity equation. The equations for the horizontal advection distances will depend upon the type of wave. For a Kelvin wave, the cross-channel wave number, or wave number analogue, is imaginary and has nothing to do with the horizontal wave number calculated as the eigenvalue of the vertical structure equation. For a Poincare wave, the cross-channel wave number is real and is connected to the total horizontal wave number calculated

from the vertical structure equation via equation 5.1.2. So long as the distinction is kept in mind, the same analysis will do for both types of waves.

Considering only the long-channel advection for the moment, ignoring the z-dependence, and assuming that the measuring instrument is at the origin of the co-ordinate system, then, after a time, t, the displacement of a water particle is

$$X(t) = \int_o^t u(x,t)dt$$

where

$$u(x,t) = U\cos(\sigma t + kx + \phi) \tag{5.4.5}$$

and this velocity may be expanded in an asymptotic series about the origin to give the displacement as

$$X(t) = \int_o^t \left(u(0,t) + X(t)\left.\frac{\partial u}{\partial x}\right|_{x=0} + \tfrac{1}{2}X^2(t)\left.\frac{\partial^2 u}{\partial x^2}\right|_{x=0} + \ldots\right)dt$$

Truncating this expression at first order (Longuet-Higgins, 1953) and resubstituting gives

$$X(t) = \int_o^t \left(u(0,t) + \left(\int_o^t u(0,t)dt\right)\left.\frac{\partial u}{\partial x}\right|_{x=0}\right)\,dt \tag{5.4.6}$$

and this may be evaluated by substituting equation 5.4.5 and carrying out the integration.

The first term in the expansion of 5.4.6 is given by

$$\int_o^t u(0,t)dt = \frac{U}{\sigma}(\sin(\sigma t + \phi) - \sin\phi)$$

while the second term is given by

$$\int_o^t \left(\left(\int_o^t U\cos(\sigma t + \phi)dt \right)(- Uk\sin(\sigma t + \phi)) \right) dt$$

$$= - \frac{U^2k}{\sigma} \int_o^t (\sin^2(\sigma t + \phi) - \sin\phi\sin(\sigma t + \phi))dt$$

Collecting everything together, then, gives an expression for the long-channel advection, which is

$$X(t) = \frac{U}{\sigma}(\sin(\sigma t + \phi) - \sin\phi) - \frac{U^2k}{4\sigma^2}(2\sigma t - \sin 2\phi + 2\sin\sigma t$$

$$- \sin 2(\sigma t + \phi) + 2\sin(\sigma t + 2\phi)) \qquad (5.4.7)$$

and represents, to first order, how far a particle of water has travelled horizontally in time t.

The term $\frac{U^2kt}{2\sigma}$ is the Stokes Drift that arises because the wave is assumed to be a progressive wave. In an estuary, there cannot be a steady flow upstream as would be indicated by this term, since the mass cannot increase without limit. Over a suitably long period of time, the total Stokes Drift due to all of the tidal frequencies and modes must be balanced by a net estuarine circulation, which would be made up of the long period river discharges, the wind drift, the non-tidal estuarine circulation and the river flows due to the sloping bed. During any reasonably long time period, it should not be expected that the tidally-averaged density structure of an estuary should remain constant, but these low frequency changes are not properly the subject of this discussion. Hence they may be ignored for the moment, noting that the Stokes Drift belongs with these low frequency flows and may therefore be dropped from the long channel advection equation.

The cross-channel advection is computed in exactly the same

way as the long-channel advection. The cross-channel velocity is given by

$$v = iV\exp(iay)\sin(\sigma t + \phi)$$

and so the cross-channel advection is given by

$$Y(t) = \frac{V\sin(ay)}{\sigma}(\cos(\sigma t + \phi) - \cos\phi) - \frac{aV^2\sin(2ay)}{4\sigma^2}(2\cos\sigma t + 2\cos(\sigma t + 2\phi) - \cos 2(\sigma t + \phi) - 2\cos 2\phi - 2) \qquad (5.4.8)$$

and this part of the advection does not have a Stokes Drift term since the cross-stream component of a Poincare wave is actually a standing wave across the channel. For a Kelvin wave, the cross-channel velocity is exactly zero everywhere, and so there is no cross-stream advection.

The expressions 5.4.7 and 5.4.8, without the Stokes Drift term, may now be substituted into equation 5.3.1 to obtain an expression for the time history of the density fluctuations that would be measured at a given location in an estuary which has a single progressive tidal wave, of either Kelvin or Poincare type, and arbitrary horizontal and vertical density gradients.

5.5 Consistency Relationship

In section 4.2, it was shown that the horizontal velocity is proportional to the z-derivative of the vertical velocity, but more than this can be proved. In fact, there is a very definite relationship between the amplitude of a wave and the horizontal velocity associated with the wave. Writing a solution to the equations of motion in the form

$$Z = H\cos(ay)W(z)\cos(\sigma t + kx + \phi)$$

$$w = \frac{\partial Z}{\partial t} = -\sigma H\cos(ay)W(z)\sin(\sigma t + kx + \phi)$$

$$u = US(z)\cos(ay)\cos(\sigma t + kx + \phi)$$

$$v = VS(z)\sin(ay)\sin(\sigma t + kx + \phi)$$

and substituting these into the continuity equation, which is

$$\frac{\partial u}{\partial x} + \frac{\partial v}{\partial y} + \frac{\partial w}{\partial z} = 0$$

results in $$- US(z)k + VS(z)a - \sigma H \frac{\partial W}{\partial z} = 0$$

where $S(z)$ is a nondimensional shape factor, U and V have the dimensions m/sec, $W(z)$ is also a non-dimensional shape factor, and so $\partial W/\partial z$ has the dimensions m^{-1}. However, the shape factor $S(z)$ is proportional to the vertical derivative of the vertical velocity, $\partial W/\partial z$ and so could be given by

$$\frac{\partial W}{\partial z} = TS(z)$$

where $S(z)$ is the vertical derivative of the vertical velocity which has been scaled so that its maximum value is 1.0, and T is a dimensionalizing factor with dimensions m^{-1}. Hence in the notation of all of the other sections,

$$S(z) = W'(z)$$

and so the relationship between the horizontal velocities and the vertical amplitude is

$$Uk - aV + \sigma TH = 0$$

In the special case of the Kelvin wave, it is possible to get a very simple relationship, since the cross-channel velocity is zero, and so

$$U = -\frac{\sigma}{k} HT \quad .$$

5.6. Discussion

This Chapter has been primarily concerned with the horizontal aspects of the internal waves in a channel. It has been shown that as long as the third and higher derivatives of the horizontal density structure are reasonably small, they will not affect the shape of the internal waves. On the other hand, any horizontal density gradient at all will affect the instantaneous densities measured at a recording instrument which is fixed to the channel bottom. The distances both vertically and horizontally that the tidally-averaged density gradients are advected by the waves passing through the channel have been calculated, and a relationship between the vertical amplitude of a wave and the horizontal current velocity associated with the vertical displacement has been given.

It should be pointed out that the processes that have been considered in the past two Chapters have been linear processes. A complete description of the circulation would include all of the nonlinear processes that are possible, beginning with the full, nonlinear equations of motion. There are, however, two nonlinear processes that could be considered. The first is the nonlinearity in the horizontal propagation equation that was considered in Section 5.2, and the second is the weak wave-wave interaction process, which has been described briefly by LeBlond and Mysak (1978).

The mathematics of the wave-wave interactions and the effects due to a horizontal density gradient would be formidable, but the essential process is fairly clear and involves a clear understanding of the process of 'tidal averaging'. For example, the M_2 waves deform the mean density gradient, and so another wave, say the S_4, would see a different 'tidally-averaged' density gradient than it would if the M_2 wave were not present. Of course, if the waves are linear and the propagation process is truly linear, then the principle of superposition holds and allows adding the effects of each wave separately, and so the whole problem of wave-wave interactions does not arise.

Chapter 6

Prediction and Analysis

6.0 Introduction

In the previous four chapters, enough theory has been developed to tackle two problems of flow in estuaries. The first problem is quite simple, and will be considered first. This is, given the tidally-averaged density structure in an estuary and all of the wave parameters applicable, 'What will be measured at an instrument fixed to the bottom of the channel?'. The second problem is much more difficult and is the inverse problem. Given the observations at a fixed location in the channel, and the density gradients, ' What are the waves which produce the observations?'. It will be seen that the first is a simple problem, while the second can only be solved in a very limited way.

6.1 The Prediction Problem

In Chapter 5, the prediction equations for a single frequency and mode were developed. Due to the principle of superposition, since the original equations are linear, the result of a series of waves is simply the sum of the effects from each wave separately. Hence, for a series of waves, each one of either Kelvin or Poincare type, and each with its appropriate vertical and horizontal mode, the prediction equations are

$$\rho(x,y,z,t) = \bar{\rho}(x,y,z) + \frac{\partial\bar{\rho}}{\partial x}\sum_j X_j(t) + \frac{\partial\bar{\rho}}{\partial y}\sum_j Y_j(t) + \frac{\partial\bar{\rho}}{\partial y}\sum_j Z_j(t)$$

$$+ \tfrac{1}{2}\left[\frac{\partial^2\bar{\rho}}{\partial x^2}\sum_j X_j^2(t) + \frac{\partial^2\bar{\rho}}{\partial y^2}\sum_j Y_j^2(t) + \frac{\partial^2\bar{\rho}}{\partial z^2}\sum_j Z_j^2(t) + \right.$$

$$\frac{\partial^2\bar{\rho}}{\partial x\partial y}\sum_j X_j(t)Y_j(t) + \frac{\partial^2\bar{\rho}}{\partial y\partial z}\sum_j Y_j(t)Z_j(t)$$

$$\left. + \frac{\partial^2\bar{\rho}}{\partial x\partial z}\sum_j X_j(t)Z_j(t)\right] + \frac{1}{3!}\left[\frac{\partial^3\bar{\rho}}{\partial x^3}\sum_j X_j^3 + \ldots\right] + \ldots. \qquad (6.1.1)$$

$$u(x,y,z,t) = \sum_j U_j W_j'(z)\cos(a_j y)\cos(\sigma_j t + k_j x + \phi_j) \qquad (6.1.2)$$

$$v(x,y,z,t) = \sum_j V_j W_j'(z)\sin(a_j y)\sin(\sigma_j t + k_j x + \phi_j) \qquad (6.1.3)$$

$$w(x,y,z,t) = \sum_j -\sigma_j H_j W(z)\cos(a_j y)\sin(\sigma_j t + k_j x + \phi_j) \qquad (6.1.4)$$

with

$$Z_j(t) = H_j W_j(z)\cos(a_j y)\cos(\sigma_j t + k_j x + \phi_j) \qquad (6.1.5)$$

$$X_j(t) = \frac{U_j W_j'(z)\cos(a_j y)}{\sigma_j}\left(\sin(\sigma_j t + k_j x + \phi_j) - \sin(k_j x + \phi_j)\right)$$

$$- \frac{k_j U^2 W_j'^2(z)\cos(2a_j y)}{4\sigma_j^2}\left(2\sin(\sigma_j t) + 2\sin(\sigma_j t + 2k_j x + 2\phi_j)\right.$$

$$\left. - \sin 2(k_j x + \phi_j) - \sin 2(\sigma_j t + k_j x + \phi_j)\right) \qquad (6.1.6)$$

$$Y_j(t) = \frac{V_j W_j'(z)\sin(a_j y)}{\sigma_j}\left(\cos(\sigma_j t + k_j t + \phi_j) - \cos(k_j x + \phi_j)\right)$$

$$- \frac{a_j V_j^2 W_j'^2(z)\sin(2a_j y)}{4\sigma_j^2}\left(2\cos(\sigma_j t) + 2\cos(\sigma_j t + 2k_j x + 2\phi_j)\right.$$

$$\left. - 2\cos 2(k_j x + \phi_j) - \cos 2(\sigma_j t + k_j x + \phi_j) - 2\right) \qquad (6.1.7)$$

and

$$U_j k_j - a_j V_j + \sigma_j T_j H_j = 0 \qquad (6.1.8)$$

In the above set of prediction equations, the origin of the co-ordinate system is assumed to be the generation point of the internal waves, where the phase of the waves at this point, in relation to some convenient time origin, is ϕ_j . All of the other notation is consistent with the previous notation, and each individual wave is indexed by j. If the individual wave is a Poincare wave, then the cross-channel wave number, a_j , has its usual meaning, but if the wave is a Kelvin wave, then the maximum amplitude of the wave, on the right hand side of the channel, is H_j; the factor $\cos(a_j y)$ is adjusted to fit the exponential decay of the wave across the channel, and $V_j = 0$. $W_j(z)$ is the solution to the vertical structure equation, normalized to a maximum value of 1.0, and $W_j'(z)$ is the z-derivative of W_j also normalized to a maximum value of 1.0. T_j is the dimensionalizing factor for $W_j'(z)$.

The truncation that must be made is in equation 6.1.1 where it must be decided to which order of derivative the density gradient must be taken. This can only be decided for a particular estuary and location in that estuary. If the only requirement is to produce test data, then the

decision is arbitrary. If the requirement is to represent a particular estuary, then, in order that the higher order derivatives may be calculated a great deal of synoptic data over a complete tidal cycle must be known to very great accuracy and this information is very seldom, if ever, available.

In order to give an idea of the complexities produced by a very simple system, Equations 6.1.1 to 6.1.8 were put into a computer program which performed all of the calculations and plots necessary for display purposes. The example shown here consists of a uniform channel, 65 m deep and 8.4 km wide, where the measuring instruments are 3.1 km north of the south side of the channel. The channel is in an east-west direction, with downstream to the east, and the waves propagating upstream, to the west. The tidally-averaged density structure, taking the measuring point as (0,0,z), is:

$$\bar{\rho}(x,y,z) = a_1 \exp(a_2/z + a_3)(1 + a_4 x + a_5 x^2 + a_6 x^3 + a_7 y + a_8 y^2) \qquad (6.1.9)$$

where;

a_1 = 1.03029938	(gm/ml)	a_5 = 0.0	(m^{-2})
a_2 = -0.3934996	(m)	a_6 = -6.63713143 E-16	(m^{-3})
a_3 = 24.67621	(m)	a_7 = 3.333333333 E-8	(m^{-1})
a_4 = 3.98227886 E-7	(m^{-1})	a_8 = 3.111111111 E-11	(m^{-2})

and Figure 6.1.1 gives a plot of this density structure in terms of depth and distance along the estuary. Although this density plot is not exactly the same as on the St. Lawrence, it does seem typical of the type of density structures that could be measured in partially-mixed estuaries. Owing to the nature of the density structure chosen, it was only necessary to calculate the density derivatives to third order. It was from density structures such as this that the

approximations used in equation 5.2.5 were derived.

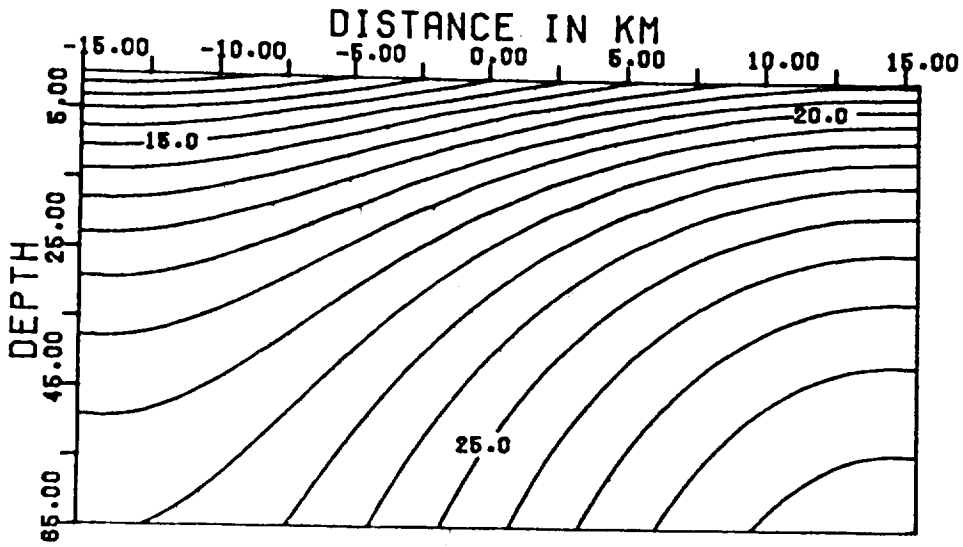

Figure 6.1.1 Example estuarine tidally-averaged density structure.

Table 6.1.1 Wave properties for the examples.

Const.	Period	Vert. Modal No.	Amp.	Phase (deg)	V-vel. (m/sec)	Wave-length (km)
1	12.42	0	1.1	0.0	0.0	1746.9
2	12.42	1	1.2	17.2	0.0	54.7
3	12.42	2	0.8	22.9	0.0	27.8
4	12.42	3	0.4	57.3	0.0	18.6
5	6.21	0	0.2	-5.8	0.0	610.7
6	6.21	1	0,6	5.8	0.0	19.1
7	6.21	2	0.4	149.0	0.3	9.7
8	6.21	3	0.2	252.1	0.2	6.5
9	4.14	0	0.1	-189.1	0.0	389.2
10	4.14	1	0.6	-137.5	0.2	12.2
11	4.14	2	0.4	57.3	0.1	6.2
12	4.14	3	0.2	-217.7	0.1	4.1

The wave properties that were used for the examples were as in Table 6.1.1, and again, these are not exactly the wave parameters applicable on the St. Lawrence, but they are derived from the St.Lawrence, in that the amplitudes of the barotropic modes are the same as the St. Lawrence and the phases were derived by assuming that all of the waves at a particular frequency were phase locked to the barotropic mode at the end of the Laurentian trough and then the measuring point was assumed to be near St. Simenon. The baroclinic amplitudes were obtained by making a number of runs with different amplitudes and adjusting them until 'reasonable' plots were obtained.

The first example, shown in Figure 6.1.2, used constituents 1,5 and 9 only. That is, it is the result of propagating purely barotropic waves through the density structure. Since the waves are Kelvin waves, there is no cross channel velocity, and since they are barotropic, the long channel velocity contours are vertical. The density plot would seem to show the presence of an 'internal wave' which is approximately 40. m high. This 'internal wave' however, is due entirely to the advection of the horizontal density gradient and has nothing to do with baroclinic motions, since there are none in the example. The asymmetry in the density structure is due to the phases of the waves and is not due to the asymmetry of the density structure, since the coefficient of x^2 in equation (6.1.9) is zero.

The second example, shown in Figure 6.1.3, used all twelve constituents, but assumed that all twelve were Kelvin Waves whose amplitudes at the measuring point were given in Table 6.1.1. This example looks much more like a typical estuarine structure. Again, since all of the waves

were assumed to be Kelvin waves, there is no cross-channel velocity. The long-channel velocity shows that there are quite strong instantaneous shears in the flow and that the tide at the bottom lags the tide at the surface by between 45 minutes and one hour. At any given time, the vertical structure is not linear or semi-logarithmic, but rather there is a very complicated vertical flow pattern. In the density plot, the amplitude of the density fluctuations is partially due to the internal waves, but is also partly due to the advection of the density gradients. The maximum vertical displacement that could be due to the internal waves is 6.2 m, but it looks like a 30 m internal wave is passing the measuring point. Most of this is due to the advection of the density gradient.

The third example is given by Figure 6.1.4, which used all twelve of the constituents, but assumed that constituents which could be Poincare waves were of the first cross-channel mode and so had a cross-channel wave length of 16.8 km. The contours of the long-channel velocity are much simpler than in the previous example, but the same sort of features are shown, and the lack of complexity is due to the reduction in long-channel velocity, since the amplitudes of the Poincare waves are given at the centre of the channel and not at the measuring point. In the cross-channel velocity plot, a quite reasonable amount of structure is shown, and there is a large amount of shear in the vertical. The density plot looks very like the density plot in the previous example.

Of course, it is possible to invent an infinite number of examples and to predict measurements for each one of these examples. However, the important points have been shown in these quite simple cases. If, as is usually assumed, there is no baroclinic component to the flow,

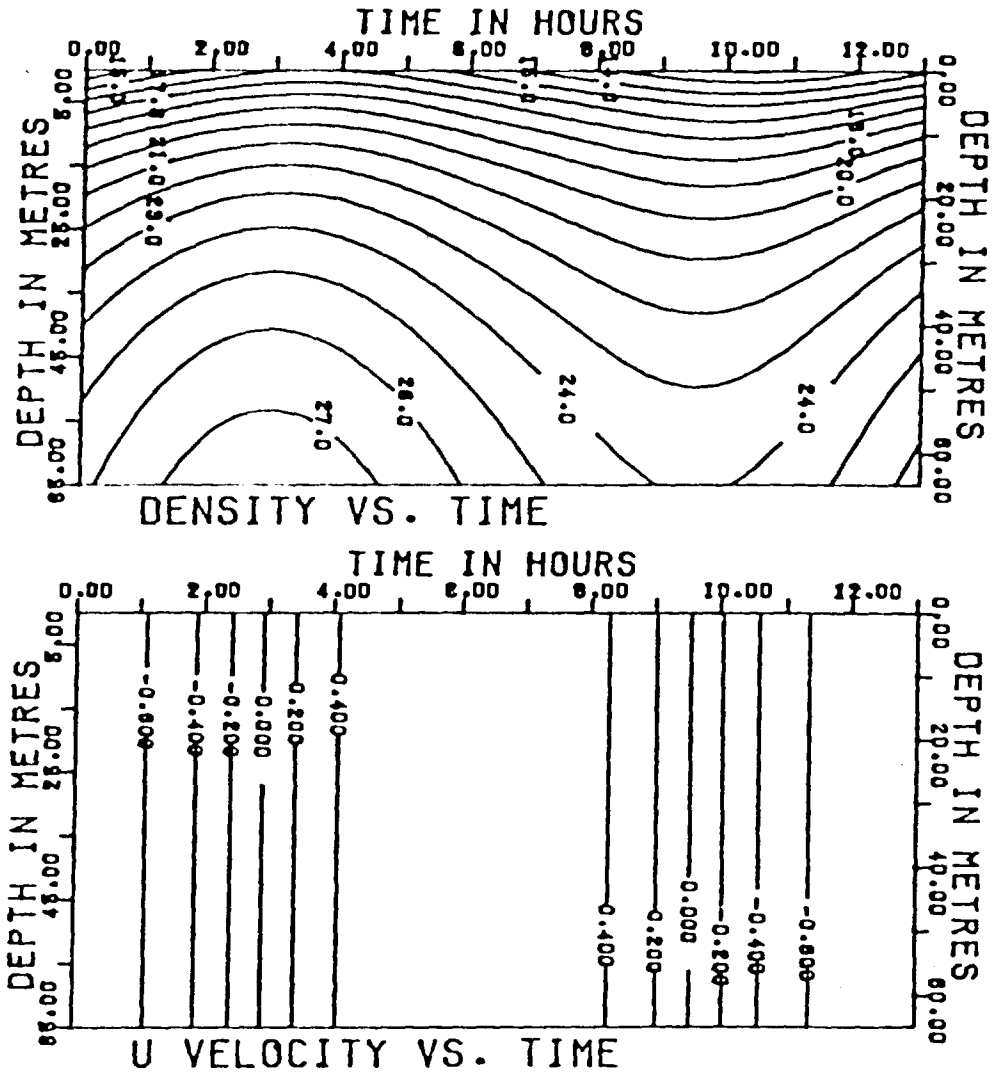

Figure 6.1.2 Density and velocity structures produced by barotropic tides.

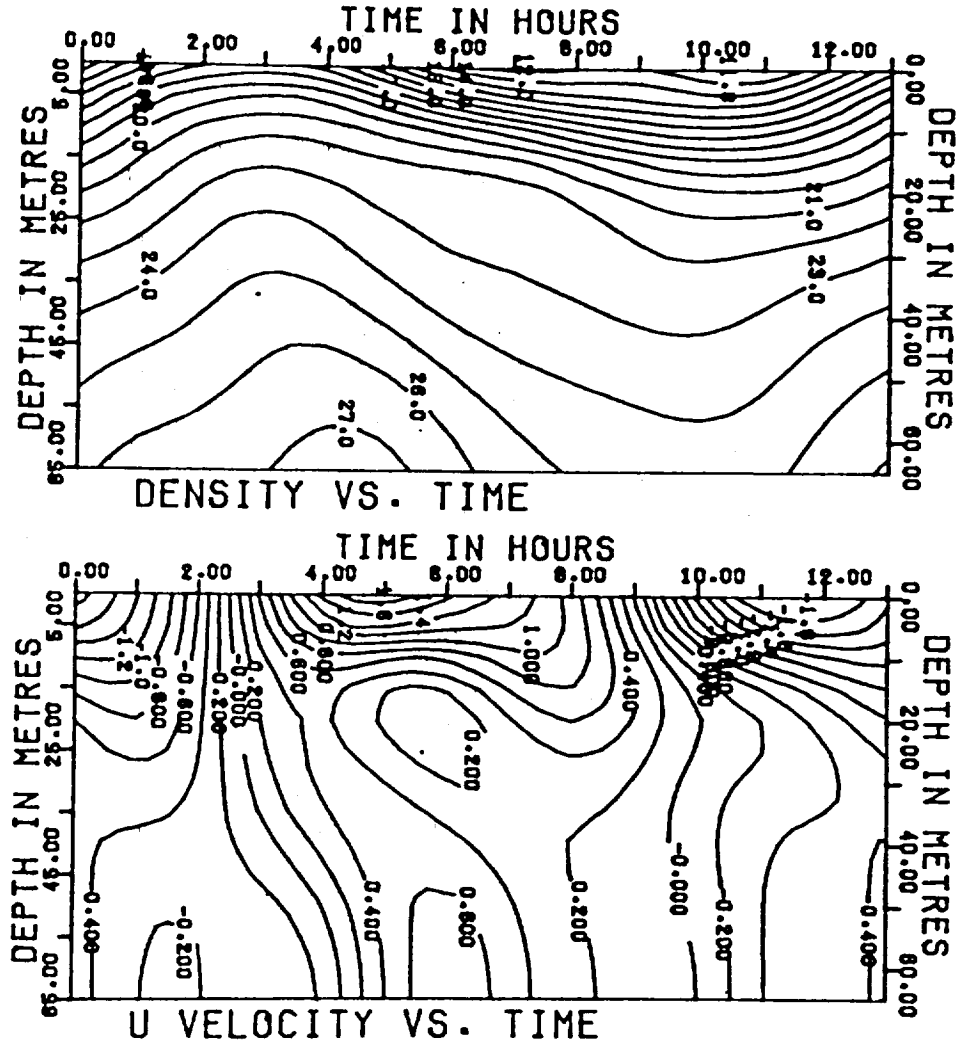

Figure 6.1.3 Density and velocity structures produced by barotropic and baroclinic Kelvin waves.

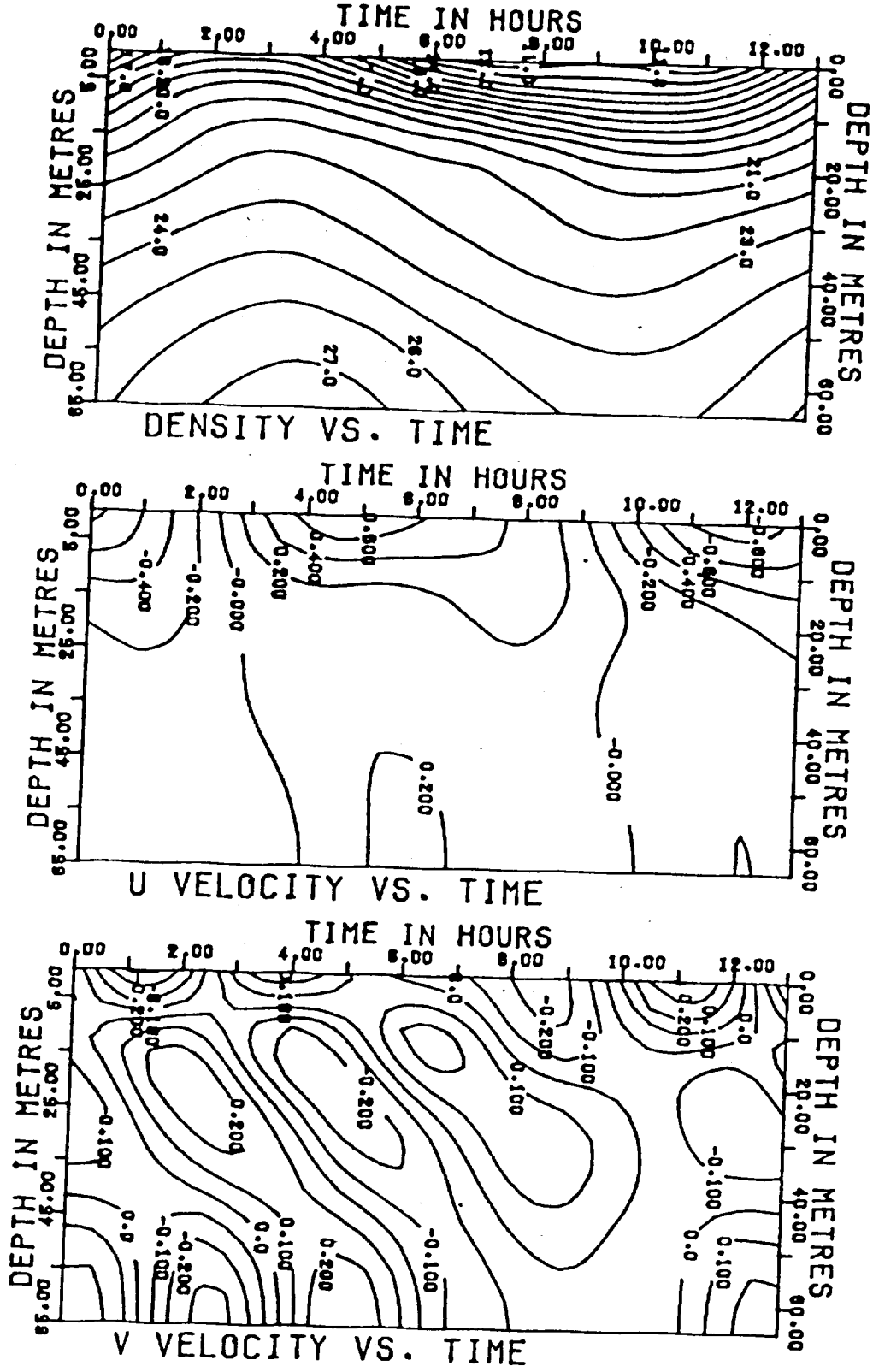

Figure 6.1.4 Density and velocity structures produced by barotropic and baroclinic Kelvin and Poincare waves.

and the horizontal density gradients may be ignored, then the density contours would remain horizontal, the velocity contours would remain vertical, and there could be no cross-channel velocity. This situation is very seldom seen in the observations from partially-mixed estuaries, and so the two assumptions cannot hold. On the other hand, the fact that the density contours rise and fall with time is not sufficient evidence for assuming that the movement of the isopycnals is due to internal waves, since it could very easily be due to the advection of horizontal density gradients. It is also an error to measure the displacement of the isopycnals and use this measurement as the amplitude of 'internal waves' even if there is evidence for the presence of internal waves. The interpretation of the movements of the isopycnals is very dependent upon the horizontal structure of the density gradients. On the other hand, vertical complexity in the instantaneous velocity structures could be taken to be prima facia evidence for the presence of internal waves.

6.2 The Inverse Problem

Although it is quite easy to set up the prediction problem, and it is very useful in discovering the sorts of structure that could be present in an estuary, it is the inverse problem which is of major interest. Typically, one has the observed density and velocity at a given location over a period of time, and one wishes to determine the density and wave fields that gave rise to these observations. In principle, the inverse problem may be solved by the method of least-squares.

In general, a fair number of the variables in the prediction equations, 6.1.1 to 6.1.8, are usually known from measurements. From an analysis of the long period current meter records, it is possible to make a determination of the relevant frequencies. The vertical tidally-averaged density structure is generally known, and so the vertical velocity equation may be solved to obtain the total horizontal wave numbers, the vertical shape functions, $W_j(z)$ and $W_j'(z)$ and the dimensionalizing factors, T_j. From here on, however, there are still a very large number of variables which are unknown. For the moment, it will be assumed that it is also possible to determine the appropriate horizontal and vertical mode numbers that are present in the observations and that the tidally-averaged density structure is known to the required accuracy.

The unknowns, then consist of the wave amplitudes, H_j, the long channel velocities, U_j, the phases of the waves at the generation point, ϕ_j and the directions of the waves, θ_j. It may seem strange that the wave direction is an unknown, but it cannot be assumed, in general, that the wave direction is directly up the estuary. If there are distinct bends in the estuary or if the incident waves are not parallel to the estuary's axis at the generation point, then they will not propagate directly up the estuary. At a given location inside the estuary the inclination of the waves may not lie along the axis of the estuary. There is much evidence in the analysis of the current meter records of the St. Lawrence for this statement. Hence, for each wave, there are, in general, four unknowns.

If the subscript c refers to calculated values from the prediction equations, the subscript o refers to observed values and

the variable q takes on the unknowns in turn, then the least squares equations are of the form

$$\sum_{obs} (\rho_o - \rho_c) \frac{\partial \rho_c}{\partial q} + \sum_{obs} (u_c - u_o) \frac{\partial u_c}{\partial q} + \sum_{obs} (v_c - v_o) \frac{\partial v_c}{\partial q} = 0 \qquad (6.2.1)$$

where the sums are taken over each of the observed depths and times. There are 4n equations in 4n unknowns, for n waves, and so, in principle, these equations may be solved for the unknowns.

Since the least-squares solution technique is a statistical one, some thought must be given to the significance levels and the statistical errors. The only difficulty here is to determine the correct number of degrees of freedom in the fits. Since the density and the two components of velocity are statistically independent, and there are four unknowns for each wave, then the number of degrees of freedom is

$$df = 3 \times \text{no. of observations} - 4 \times \text{no. of waves}$$

Hence there should be no difficulties with the statistical analysis.

There is, however, a difficulty with solving the equations. If the prediction equations 6.1.1 to 6.1.8 are substituted into 6.2.1 and the indicated differentiations performed, then it is immediately obvious that the equations are not only nonlinear, but also transcendental. In addition, the predicted values which would have to be calculated for each of the observed times and depths are very complicated. Hence there will obviously be some difficulty in carrying out the entire operation.

6.3 Numerical Experiments With the Inverse Problem

In order to minimize these difficulties, numerical experiments were carried out which analysed invented data. Since the data are invented, the parameters which were used to make up the data should be the solutions in the analysis of the data. If an attempt were made to analyse real data from the beginning, there would be no absolute check on whether or not the answers were correct.

The computer program that was written for Section 6.1 will generate data in the form of density and the two components of velocity at a given location for a number of depths and times. A second computer program was written to read in these values and to solve the nonlinear least-squares equations for the wave parameters. To reduce the complexity even further for the numerical experiments, the first simplification was to use only Kelvin waves in the prediction and the analysis programs. The second simplification that was made was to assume linear density gradients in the horizontal directions. These two simplifications have been made in all of the numerical experiments.

By assuming that all of the waves are Kelvin waves, a considerable linearization of the equations may be carried out by setting the origin of the co-ordinate system to the measurement point and defining two new variables as

$$C_j = H_j \cos\phi_j$$

$$S_j = H_j \sin\phi_j$$

This means that the velocity portions of the least-squares equations are linear in C_j and S_j, the density portion is considerably simplified,

and the only transcendental nonlinearities are in terms of the directions, θ_j , and the advection distances. This is the same substitution that is used in the harmonic method of tidal analysis to make those least-squares equations linear.

In the first computer program that solved the least-squares problem, the equation solver chosen was the one employing Brown's Method that was used in Chapter 2 (Brown, 1967, 1969; Muir, 1975). Unfortunately, it proved impossible to get the equation solver to converge upon an answer. The difficulty was that the Jacobian matrix for the Quasi-Newton's method was almost singular. The most common cause of singularity is that the equations have no solution or that there is an error in the programming that has the same effect. The second most common cause is that there are multiple solutions of the equations which are near the starting solution. Since the equations are not only nonlinear, but also transcendental, and they most definitely do have at least one solution, the second reason seemed to be entirely possible.

A second equation solver was chosen which would eliminate this possibility. This second solver chosen was one developed by Powell (in Rabinowitz, 1970) which is available through the NAG library. It employs a mixed method of solution, commencing with gradient search technique and then switching over to a Newton's method when very close to a solution. The major difficulty with the technique is that,due to the gradient search method, it uses large amounts of computer time. On the other hand, since the step sizes are very small, if there is a solution near to the

starting point, it will find this solution. There were very few difficulties in finding solutions using the gradient search method.

Since the equation solver took up large amounts of computer time, a fairly restricted data set was used for the tests. The data set was computed using the vertical structure from the St. Lawrence and linear density gradients in the long- and cross-channel directions. Six waves were used to generate the density and velocity observations. The M_2 frequency contained the barotropic and the first two baroclinic modes, the M_4 frequency contained the barotropic and the first baroclinic mode and the M_6 frequency contained only the barotropic mode. Various trials were run, but the solutions were computed to only a small number of significant digits since each of the tests described here took about 500 seconds of CDC 7600 time and so all of the tests were very expensive in terms of computer time. The complete sequence of development and testing used in excess of 7 hours of CDC 7600 time. All of the calculations were done using 64-bit word lengths, and the data files were generated to 8 decimal places. Hence roundoff and truncation errors should not be a factor in the answers.

The first series of tests was to use an initial guess to the solution that was fairly close to the correct solution. The initial phase was chosen to be 90° away from the phase of the true solution and then the initial guess was taken to be a multiple of the true solution. It was anticipated that these tests would provide answers very close to the true solution.

The results of four tests are shown in Table 6.3.1. The column headings are the factors by which the true solution was multiplied

		True Solution	0.99	0.95	0.50	0.10
AMPLITUDE	1	3.00	3.0003	3.0001	0.0504	0.0521
	2	2.50	2.596	2.4957	0.01997	0.00199
	3	1.00	0.70658	0.95736	0.00297	0.00128
	4	2.00	1.9992	1.9993	0.0787	0.000552
	5	0.50	0.4025	0.53125	0.00741	0.000350
	6	1.50	0.000989	1.5001	0.00150	0.000375
PHASE	1	32.704	33.063	33.008	115.00	114.90
	2	61.352	37.738	61.046	100.50	93.00
	3	90.00	107.510	82.200	-26.96	156.20
	4	-24.59	-23.84	-23.98	61.60	64.20
	5	4.06	32.33	8.94	57.20	64.70
	6	20.28	112.25	21.21	104.4	98.4
DIRECTION	1	57.30	57.37	57.29	-31.3	-31.9
	2	0.00	-3.70	-0.08	-14.0	-17.4
	3	-57.30	-58.64	-59.28	-35.5	-39.1
	4	57.30	57.82	57.30	-32.4	- 0.63
	5	28.65	67.62	26.34	-15.90	-11.8
	6	-28.65	34.49	-28.65	-13.30	0.54
ITERATIONS			163	163	235	235
Σres^2			1.770	0.0187	0.0454	0.0111
MAX. ERROR	ρ		-0.00095	-0.00006	0.00259	0.00274
	u		0.84	±0.01	2.25	2.28
	v		-0.46	±0.01	-2.75	-2.76

TABLE 6.3.1 KELVIN WAVES - Solving for amplitude, phase and direction. Initial guess to solution as a factor of true solution.

to give the initial starting solution after the phase had been shifted by 90^{o}. The amplitudes are in metres, the phases and directions are given in degrees, the densities are in gm/ml and the velocities in metres/second. The number of iterations is given and the sum of the squares of the residual errors is also given along with the maximum errors for the density and the two velocity components.

The only answer that is close to the 'true' solution is the one which started at 95% of the true solution. However, the other answers are in fact solutions, in that the sum of the squares of the residuals are small, and they are converging. The difficulty here is that the least-squares solution requires that the sum of the squares of the residuals be a minimum, and not that the observations exactly match the computed values. The solution surface in the eighteen dimensional solution space is very complicated and has local minima that the least-squares technique finds.

It may be thought that the multiplicity of 'solutions' is not a major problem, since it is fairly obvious from an inspection of the maximum errors that these alternative solutions are 'wrong' and that it would be time-consuming, but possible to try various initial guesses until the maximum errors are minimized. There is , however, another practical problem that has not been considered in these tests.

The assumption made in these tests was that it was known beforehand which were the appropriate modes to use for each frequency. It is very simple to determine the appropriate frequencies to use for the fits from the long period tidal records, but it is not easy to determine exactly which vertical modes are appropriate for each frequency.

The second set of tests shows the difficulties that can arise if the correct frequencies or number of modes are not known. Test 1 used only four constituents to fit the data set, the proper M_2 constituents and the M_4 barotropic only. Test 2 used the correct number of constituents but tried to substitute the second baroclinic mode for the M_4 in place of the M_6 barotropic mode. Tests 3 and 4 used nine constituents, adding in the second M_4 baroclinic mode and the first two M_6 baroclinic modes. The difference between tests 3 and 4 is in the starting guess to the true solution.

In all four of the tests, the sum of squares of the residuals is very small, and so the equation solver has found local minima. In Tests 1 and 2, the maximum errors would indicate that the solution is inappropriate, but in Tests 3 and 4, there would be no indication that the solutions are wrong, since the maximum errors are very small, and, in both cases, the answers look quite reasonable. Tests 1 and 2 are, however, unrealistic, in that one whole frequency band has been missed out of the solution, but this would not be a problem in practice. Tests 3 and 4 are very realistic, in that it would usually be the case that one would look for more modes than are in the observations. If the problem were a linear one, looking for more modes than are in the solution could be overcome by a stepwise regression technique, but this will not work for the nonlinear case, since the solution is not unique. Therefore, an optimum number of vertical modes for one solution is not necessarily an optimum number of vertical modes for a different solution, and there is not necessarily any way of determining which one of the many possible solutions is the correct, physical solution.

		True Solution	4 Constituents	TEST 1	TEST 2	TEST 3
AMPLITUDE M2	1	3.00	3.215	3.124	2.9736	2.9683
	2	2.50	0.2570	2.850	2.2360	0.5373
	3	1.00	0.4629	0.684	1.6076	0.7634
M4	4	2.00	0.0063	0.003706	1.9884	1.9780
	5	0.50	-	0.003497	0.27676	0.9751
	6	-	-	0.05644	1.1974	1.1699
M6	7	1.50	-	-	1.4989	1.4772
	8	-	-	-	0.6159	0.3931
	9	-	-	-	1.0099	3.0609
PHASE	1	32.704	29.274	29.19	32.939	32.887
	2	61.352	-48.026	37.26	64.885	3.449
	3	90.00	-10.767	73.29	75.413	32.904
	4	-24.59	63.982	63.36	-24.048	-24.037
	5	4.06	-	67.71	99.42	89.846
	6	-	-	85.43	152.14	83.484
	7	20.282	-	-	21.141	21.181
	8	-	-	-	11.580	1.765
	9	-	-	-	-17.306	5.932
DIRECTION	1	57.30	57.508	57.485	57.279	57.288
	2	0.0	-13.396	4.588	0.2633	35.552
	3	-57.30	22.717	-55.337	-86.026	-55.411
	4	57.30	50.704	62.068	57.334	57.181
	5	28.65	-	0.99995	7.611	65.296
	6	-	-	-30.509	-22.816	-15.432
	7	-28.65	-	-	-28.582	-28.348
	8	-	-	-	-39.749	3.862
	9		-	-	-44.186	67.446
ITERATIONS			145	145	145	145
Σres^2			12.074	1.2513	1.887	5.080
MAX ERROR	ρ		-0.00185	-0.00154	-0.00047	0.00110
	u		-1.49	-1.47	-0.05	-0.09
	v		1.52	1.51	-0.04	-0.05

TABLE 6.3.2 Kelvin waves using incorrect number of constituents. Solving for amplitude phase and direction.

In general, then, the conclusion is that it is impossible to solve the inverse problem in the way that it has been set, or in a more general setting, such as allowing Poincare waves or trying to solve for the density gradients as well as the wave parameters.

If the problem is restricted to Kelvin waves as before, but the direction of the waves is assumed to be known, then the solution space is considerably simpler. Using the same data set as before, it was found that the true solution would be obtained for the first set of trials if the initial guess to the solution was between 0.8 and 1.5 of the true solution. Outside of this range, different solutions would be obtained. As in the previous case, if too many frequencies or modes were used, the wrong solutions were obtained.

Even if the correct number of modes is used at each frequency, the waves are known to be Kelvin waves, the correct number of frequencies is known, the horizontal density gradients are linear and known and the direction from which the waves are coming is known, it is impossible to solve the inverse problem in general. This is simply because the solution space is complicated enough that it has local minima which are very close together. In the analysis of data from a real estuary, of course, almost none of the simplifying assumptions would hold. In general it would not be possible to know which modes are important, the waves are unlikely to be pure Kelvin waves, the horizontal density gradients would not be linear and they probably would not be known to any great degree of accuracy. In addition, it would be impossible to know, in advance, the directions of the waves. Hence the solution of the inverse problem in an estuary is impossible in any practical sense.

The final objection that could be raised against the practicality of a solution, at the present time, is the large amount of computer time that would be required. Most of the computer time in the above solutions is taken up in calculating the density and velocity information at each depth and time for each iteration. This would increase linearly with the number of constituents used and the number of observations. The test cases above used 11 depths, 9 times and 6 constituents and each trial used up about 500 seconds of CDC 7600 time. Doubling the number of constituents would double the amount of time used in calculating the densities and velocities and would increase the time for the equation solver by a factor of four. Twelve constituents use up about 1200 seconds of computer time per trial.

It would seem reasonable that if a number of stations were solved simultaneously, then the solution space may be simplified enough that the true solution would appear. However, going to a solution involving, say, three simultaneous stations, would increase the computer time required to about 4000 seconds per run and this would be a very expensive experiment to try. In any case, there is no data set from the St. Lawrence that has three or more simultaneous stations, and there are no precise data on the horizontal density gradients in the St. Lawrence. For these reasons, the experiment was not tried.

6.4 Linearization of the Inverse Problem

There is one major simplification of the inverse problem that yields results. This is simply to ignore the horizontal density gradients. If they can be ignored, then the advection terms do not appear

in the problem, and the inverse problem becomes considerably easier to handle mathematically. Since the velocities do not appear in the density equation, there is then no need to involve all of the observations in one equation as is done in equation 6.2.1, and there will be three separate least-squares problems, one for the density, one for the long-channel velocity and one for the cross channel velocity. In addition, all of these problems are linear, and so they each have a unique solution. The results of the two velocity fits may be combined into constituent ellipses using equations 3.2.4, and 3.2.5. There is very little problem carrying out the programming for the three fits and solving the equations and so this was done and tests made on the St. Lawrence data. The results presented here are also to be found in Muir (1979b).

The results shown in Table 6.4.1 are from station 75-001B which is 10 km downstream from Pointe au Pic and 2 km from the north shore. The observations covered 13 hours of a spring tide cycle. The fit to the density observations is shown in Figure 6.4.1. The results shown in Table 6.4.2 are from station 75-001C, which is in the same location, but covered 13 hours of a neap tide cycle. The fit to the density observations for this station is shown in Figure 6.4.2. The standard error of estimate for the major and minor axes of the ellipses is 1.86 cm/sec for station 75-001B and 2.1 cm/sec for station 75-001C.

Clearly the fits are very good. Since there were a large number of frequencies and modes used in the fits, the results are what would be expected from what is, after all, a Fourier analysis of the observations. What is more interesting are the numbers in the tables.

Table 6.4.1 (from Muir, 1979b)

Internal Wave Parameters for Station 75-001B. Standard Error for Major and Minor Axes of Ellipse is 1,86 cm/sec. Phase is in Hours after High Water at Pointe-au-Pic. Spring Tide Conditions.

Const. name	Mode No.	Frequency (rad/hr)	Wavelength (km)	Density		Velocity			
				Amp. (m)	Phase (hrs)	Major (cm/sec)	Minor (cm/sec)	Inclination (degrees)	Phase (hrs)
M_2	0	0.50589	1619.5	8.23	1.14	78.62	2.49	41.4	-4.42
	1	0.50589	47.7	8.28	4.18	9.37	2.29	40.7	6.57
	2	0.50589	22.0	1.87	6.05	23.31	-2.40	37.3	0.19
	3	0.50589	14.8	4.04	2.47	3.24	-1.08	58.1	2.99
M_4	0	1.01178	563.5	9.72	-1.76	13.35	-0.68	34.4	-1.49
	1	1.01178	16.60	1.19	-2.96	27.18	-2.98	28.6	-1.50
	2	1.01178	7.73	2.40	1.11	4.62	-2.60	69.3	-2.35
	3	1.01178	5.15	2.68	-3.05	5.79	2.89	169.5	1.81
M_6	0	1.53248	355.2	5.58	-1.92	5.72	0.21	28.6	1.16
	1	1.53248	10.46	8.56	-1.66	14.51	-1.31	70.0	1.43
	2	1.53248	4.87	2.15	-0.64	9.59	-2.34	10.7	0.01
	3	1.53248	3.25	2.04	2.00	3.56	0.20	124.0	3.41
M_8	0	1.99466	269.2	3.35	0.76	8.24	1.64	49.0	0.76
	1	1.99466	7.93	2.56	1.09	9.97	-2.88	25.7	0.54
	2	1.99466	3.69	2.69	0.92	5.36	-3.03	15.8	0.83
	3	1.99466	2.46	1.64	1.12	3.94	0.41	36.8	1.64
M_{10}	0	2.57507	206.9	1.74	0.01	2.49	1.93	9.0	0.33
	1	2.57507	6.09	2.67	0.01	4.28	1.63	84.7	0.02
	2	2.57507	2.84	0.69	0.17	4.72	-2.19	80.56	0.46
	3	2.57507	1.89	0.16	1.11	7.15	-1.16	25.23	-0.81
M_{12}	0	3.06496	173.2	3.35	-0.24	1.86	-0.63	86.9	-0.31
	1	3.06496	5.10	4.05	-0.36	5.24	-1.59	157.2	-0.04
	2	3.06496	2.38	1.53	-0.20	4.41	-1.43	90.0	0.35
	3	3.06496	1.58	2.17	-0.33	2.30	1.18	119.3	1.45

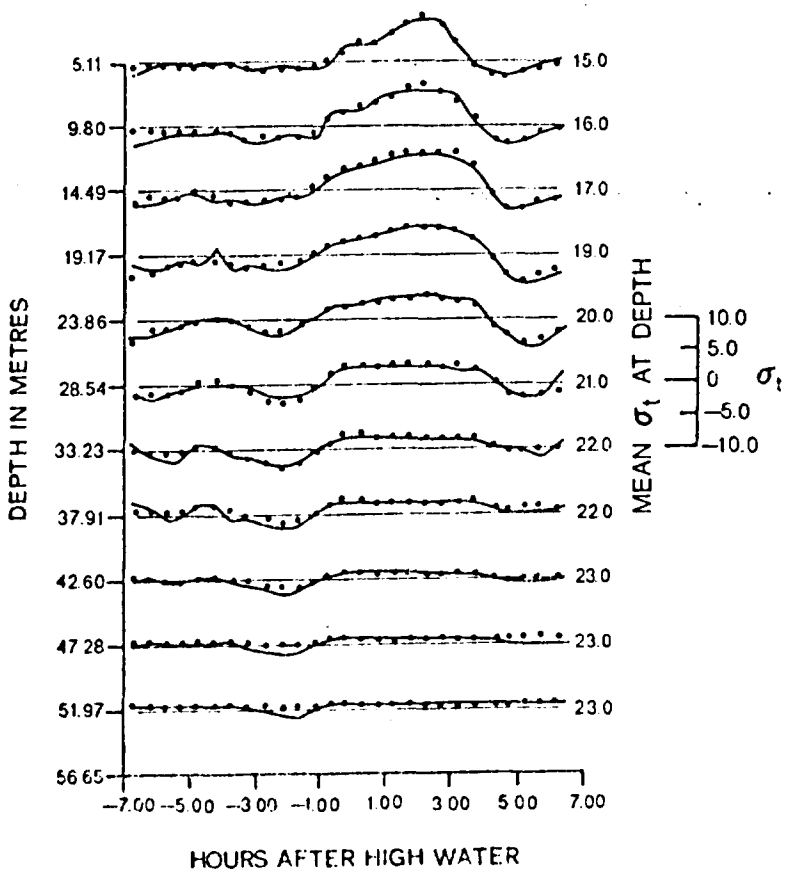

Figure 6.4.1 Density structure at station 75-001B. Spring tide conditions. (from Muir, 1979b)

Table 6.4.2. (from Muir, 1979b)
Internal wave parameters for Station 75-001C. Standard error for major and minor axes of Ellipse is 2.1 cm/sec. Phase is in hours after high water at Pointe-au-Pic. Neap tide conditions.

Const. name	Mode No.	Frequency (rad/hr)	Wavelength (km)	Density		Velocity			
				Amp. (m)	Phase (hrs)	Major (cm/sec)	Minor (cm/sec)	Inclination (degrees)	Phase (hrs)
M_2	0	0.50589	1547.1	7.49	5.25	50.0	0.51	37.9	1.65
	1	0.50589	57.5	10.97	4.71	21.0	2.0	30.6	-3.73
	2	0.50589	26.3	3.85	5.88	14.9	8.3	61.9	5.51
	3	0.50589	17.6	3.38	5.28	7.9	-5.6	79.6	2.20
M_4	0	1.01178	538.3	6.82	-0.38	5.9	-0.1	56.6	2.81
	1	1.01178	20.0	8.51	-0.15	19.2	2.8	31.1	-2.07
	2	1.01178	9.16	5.38	-0.14	19.6	1.7	52.5	-0.59
	3	1.01178	6.12	1.79	-1.14	9.1	-2.6	128.7	3.20
M_6	0	1.53248	339.4	7.02	0.67	3.5	-1.5	173.1	0.35
	1	1.53248	12.6	8.75	0.74	9.9	-6.8	55.5	-1.23
	2	1.53248	5.77	4.15	0.61	7.2	-0.8	102.9	2.89
	3	1.53248	3.86	1.60	0.12	7.0	-0.8	6.3	2.06
M_8	0	1.99466	257.2	3.42	0.53	3.0	-2.0	48.8	1.86
	1	1.99466	9.56	2.39	0.63	4.2	-1.4	3.6	0.95
	2	1.99466	4.38	0.97	0.70	8.9	0.8	83.1	-0.84
	3	1.99466	2.92	1.72	0.39	7.5	-1.7	79.4	-0.61
M_{10}	0	2.57507	197.6	2.72	-0.92	1.7	-0.9	116.4	0.90
	1	2.57507	7.35	3.38	-1.02	9.4	0.6	72.6	1.17
	2	2.57507	3.36	1.85	-0.84	3.6	1.4	32.1	0.78
	3	2.57507	2.25	0.24	-1.09	3.1	2.2	31.3	0.47
M_{12}	0	3.06496	165.5	4.69	0.29	1.01	-0.62	75.6	0.43
	1	3.06496	6.15	4.39	0.25	1.9	1.1	53.1	0.64
	2	3.06496	2.82	3.21	0.33	2.2	1.0	91.6	-0.10
	3	3.06496	1.88	1.96	0.23	4.2	-3.2	178.9	0.79

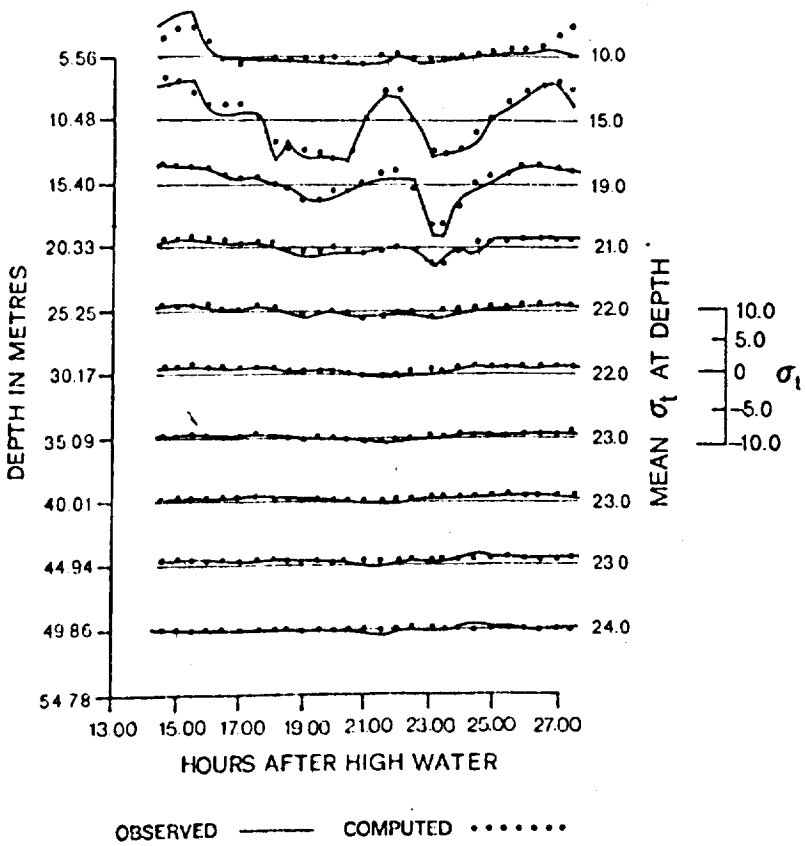

Figure 6.4.2 Density structure at station 75-001C. Neap tide conditions.
(from Muir, 1979b)

The waves amplitudes are much too high, which is simply because the horizontal density gradients have been ignored. The density gradients do not affect the velocities however, and these are very interesting. If the waves were propagating directly up the Estuary, the inclination of the ellipses should be about 55^{o} and so these tables show that the wave directions are seldom directly up the Estuary.

The negative signs for the minor axis of many of the ellipses indicate that these ellipses rotate clockwise, which is the wrong direction for a Poincare wave, as explained in Section 3.3. Therefore, it is not the case that the waves are either purely Kelvin or Poincare waves. In many cases, the length of the minor axis is not significant, since it is less than the standard error of estimate but for the 3rd internal mode of the M_2 at station 75-001C, not only is the minor axis significant, but it also rotates the wrong way. In addition, it is impossible for a Poincare wave to exist for this mode, and so the wave, if it is simply one single wave, must be a Kelvin wave. This is good evidence for the hypothesis that there are reflected waves in the Estuary, and that these reflected waves do induce rotation in the wrong direction as suggested in Section 3.3.

The distribution of the energy in the internal waves through the modal structure is not uniform in very many of the frequency bands and such phenomona as the high energy in the second internal mode of the M_2 frequency of station 75-001B, for example, may be instances of local resonances which occur due to the wave number matching the local topography. The high energy for this wave is not seen in the other table, where the wave number is different due to the different tidally-averaged density structure.

The final comment to be made on the two results is that the internal wave field is distinctly different in the two tables. This could well be simply due to the different tidally averaged density structure in the two cases, which give rise to different wave numbers and hence to very different resonances and energy distributions in the Estuary. Whatever the reason, it is very obvious that the internal wave field in the Estuary varies with the state of the Spring-Neap tidal cycle.

This linearization of the inverse problem is very unsatisfactory from a mathematical point of view and from an oceanographic point of view, since the simplification made by neglecting the horizontal density gradients cannot be justified. However, this only means that the density observations cannot be used for the fit. On the other hand, since the velocities are not affected by the density gradients, the fit of the velocities is very useful. It has shown that in an actual estuary, the St. Lawrence, the waves are not necessarily simple Kelvin or Poincare waves, which propagate directly upstream. It has also shown that the internal wave structure of the Estuary is not a constant field, but varies with time and so could be very complicated. One of the problems with using the observations from a single thirteen hour station is that it is impossible to separate out all of the tidal frequencies that are known to be in the signal. If the period of record was of the order of thirty days, to allow the separation of all of the relevant tidal constituents, and if a number of these stations were analysed simultaneously, to reduce local effects and to allow separation of direct and reflected waves, then it may be possible to describe the internal wave field in a more satisfactory manner.

6.5 Discussion

The purpose of this Chapter has been to attempt the solution of the prediction problem and the inverse problem. The prediction problem is quite simple and can be used to show that very simple systems can produce observations which are very similar to those found in typical partially-mixed estuaries.

The inverse problem, on the other hand, is very difficult indeed. By considering a quite simple portion of the problem it is possible to show that the problem cannot be solved by a direct solution of the full nonlinear, transcendental equations, due to a multiplicity of roots near the 'correct solution'. A useful and partially satisfactory result may be obtained by decoupling the velocity from the density, solving for the velocity and then solving the density equation. This result, however, would only be satisfactory if the observations are completely noise-free, the waves are purely progressive Kelvin or Poincare waves, and the horizontal density gradients are unimportant. In an estuary such as the St. Lawrence, these assumptions may be shown to be false.

It may well be that the inverse problem could be solved in general if there were a number of synoptic stations which could all be solved simultaneously. Having a number of simultaneous stations would not only simplify the solution space considerably, but also would provide enough information to compute the density gradients to the required degree of accuracy and also would allow the separation of direct and reflected waves. A further requirement would be that each of the

stations had a sufficiently long record, one month at least, to allow the separation of all of the important tidal constituents. The only difficulty with this approach would be the massive amounts of computer time required for the solution. This difficulty may not be of much importance in a few years' time, given the development of more sophisticated computing systems and methods.

Chapter 7

Physical Processes in the St. Lawrence

7.0 Introduction

The original purpose of the St. Lawrence Current Surveys was to discover and relate all of the physical processes which control the circulation of the Middle Estuary.

The previous five chapters have gone to considerable lengths to discuss the effects of the tidally-averaged density structure and the internal wave structure in partially-mixed estuaries in general, and the St. Lawrence in particular. The processes that have been of interest have been confined to the tidal frequencies in the interval (N,f), with the length scale of one tidal excursion. Although the two processes, discussed previously, are of major importance in the circulation of the Estuary, there are many other processes which are also of major importance and which interact with the tidally-averaged density structure and the internal wave structure.

In this Chapter, an attempt will be made to put the circulation processes in perspective and to show the inter-relationships between all of the various processes which affect the circulation of the Middle Estuary of the St. Lawrence.

7.1 Tidal Processes

In order to guide the discussion, Figure 7.1.1 is a diagram of all of the important physical mechanisms which operate in the Middle Estuary of the St. Lawrence. The interactions in the diagram

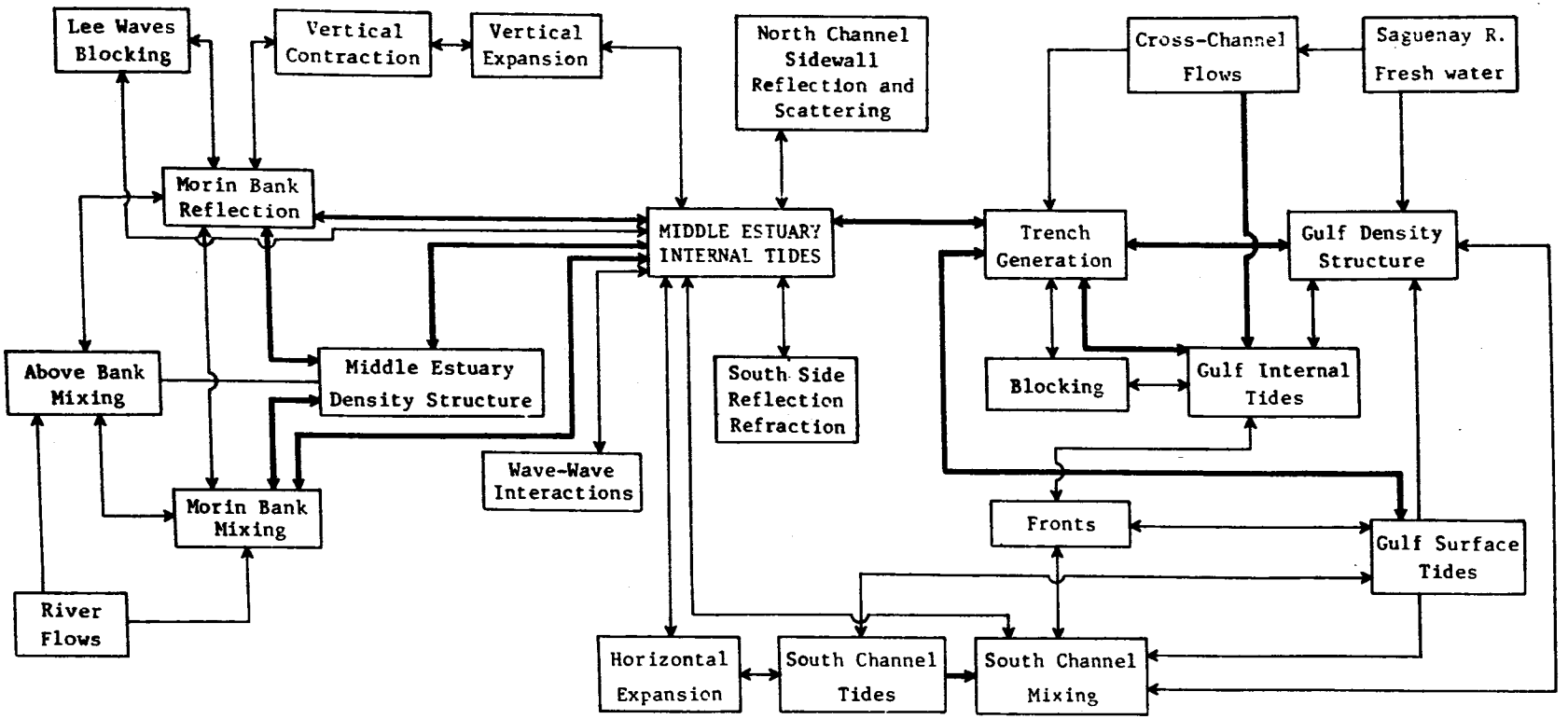

Figure 7.1.1 Physical Processes in the Middle Estuary of the St. Lawrence

are shown by arrows which indicate the direction of the interaction and which attempt to give a qualitative estimate of the importance of the interaction by the weight of the arrow. Many of these processes have been mentioned in the previous chapters but major discussion on them has been left until now. In some of the cases, there is no direct observed evidence for the processes, although in all cases there is good theoretical evidence that they should play some role in the circulation of the Middle Estuary.

Because of the many interactions in the diagram, it is arguable that there is a best way of discussing all of them. A natural place to start is in the Atlantic Ocean and the Gulf of St. Lawrence with the surface tides. These tides propagate up the Gulf and the Lower Estuary, unaffected by the density structure of the water, but very influenced by the topography of the channel, and the Coriolis Forces. They do not propagate directly up the channel, parallel to its axis, due to the bends in the channel but are reflected and refracted in accordance with the shape of the sidewalls and the bottom. The nonlinear effects of friction and advective accelerations cause the creation of shallow water constituents which interact with the original surface tides. Although these surface tides are not strongly affected by the density structure in the Lower Estuary, they do induce mixing and the formation of a typical partially-mixed estuarine circulation pattern. Due to the nature of the tides, they contain frequencies up to 19 years in length and have a very definite Spring-Neap frequency and diurnal inequality. By the time the tides reach the upper end of the Laurentian Trough then, they already possess considerable complexity. The structure of the tides in the Lower Estuary is dealt with by Godin (1979), the

generation of shallow water constituents by Dronkers (1964), and the formation of partially-mixed estuarine circulation by Dyer (1973) and Officer (1976).

The upper end of the Laurentian Trough is the generation point (or area) for the internal tides (Forrester, 1974), and at this point a number of mechanisms interact. The generation mechanism at a sloping shelf region has been discussed by Prinsenberg and Rattray (1975) for the inviscid case and for a steplike structure in the viscous case by Prinsenberg, et al (1974). The effects of refraction have been discussed by Wunsch (1969). The results are that the surface tides generate internal tides which propagate both upstream and downstream, as well as creating new shallow water constituents due simply to the nonlinear effects of the topographic changes.

At the upper end of the Laurentian Trough is the Saguenay River, which inputs a considerable amount of fresh water into the Lower Estuary. The variations in this runoff contribute significantly to the mean density structure of the Lower Estuary (Neu, 1975 and El-Sabh, 1979). In addition, this input of water provides cross-channel flows which interact with the internal tides generated at the Laurentian Trough to provide the cross-channel momentum for Poincare waves, and could somewhat deflect the direction of propagation of the waves. The seaward propagating waves cause shears and mixing in the Lower Estuary which affect the mean density structures in the Lower Estuary, which in turn affect the propagation of the internal waves. The final major effect of the Laurentian Trough on the propagation of both the internal and surface tides in the Lower Estuary is through the mechanism of blocking and the possible formation of internal hydraulic jumps (Turner,

1973). The whole subject of uptide influence is difficult (Baines, 1977) and is mentioned here only for completeness.

The effect of all of the processes in the Lower Estuary is to generate internal tides and to modify the surface tides that propagate into the Middle Estuary. As these tides propagate into the Middle Estuary, they are in turn affected by processes in the Middle Estuary and the interactions are passed back into the Lower Estuary. The total effect is to modify in a continuous way the mean density structure of the Lower Estuary, which influences the propagation of the internal tides in the Lower Estuary and is also the source of relatively dense water which penetrates the Middle Estuary. Hence the downstream boundary conditions for the Middle Estuary are very variable in that the amount of energy, the distribution of the energy between the surface and the internal tidal modes, the direction of propagation of the waves, and the water properties in the Lower Estuary are changing all of the time in a way which depends upon the conditions in both the Middle and the Lower Estuary.

Upon arrival in the Middle Estuary, the tides are immediately split by Hare Island. In the relatively shallow South Channel, considerable mixing occurs and the 1977 Data Report (Muir, 1979a) shows that the vertical density structure is generally quite well mixed. In the lower part of the South Channel, fronts are frequently observed and Ingram (1976) notes that they are formed when the relatively warm, fresh water in the South Channel meets the colder water upwelled at the Laurentian Trough during the flood tide. Since the water in the South Channel is vertically well mixed, no internal tides are able to propagate in the South Channel. Hence the South Channel acts as an energy sink in the system and provides a source of well-mixed relatively

warm, fresh water for the Lower Estuary.

In the North Channel, both the surface and the internal tides propagate without hindrance, since there is a well-developed vertical tidally-averaged density structure, as was shown in Chapter 2. The energy distribution between the barotropic and the baroclinic waves as well as the modes present, vertical as well as horizontal (cross-channel) will be determined by the conditions at the head of the Laurentian Trough. However, due to the changing topography and the relatively long length of the waves, the waves will not necessarily be in dynamic balance at any point in the North Channel. The total length of the North Channel is of the order of 70 km, and this is less than two wavelengths long for the first internal mode of the M_2 and only about ten wavelengths long for the M_6 internal constituents. In this length there are significant changes in the width and depth of the Middle Estuary and so the waves could always be in a process of adaptation to the topography.

In particular, the cross channel wavelengths must adjust at the beginning of Hare Island and at the end of Hare Island where the width of the Estuary changes abruptly. The vertical wavelengths must also adjust from the 50 metre depth passing over the top of the Laurentian Trough to a maximum depth of about 180 metres at the south-west end of Hare Island and back to the 38 metre depth over the Morin Bank. Each adjustment in the cross-channel or vertical wave number must be matched by a corresponding adjustment of the long channel wave number.

The north sidewall of the North Channel is very steep, and combined with the bend in the channel at the mouth of the Saguenay

River, should allow sidewall reflexions to occur. Since the edge of the channel is not perfectly straight, a certain amount of scattering could occur, although the exact amount would depend strongly upon the match between the length of the topographic features and the wave number of any particular wave.

The sloping bottom in the North Channel does not strongly affect the propagation of the Kelvin and Poincare waves although there will be a cross-channel adjustment in the vertical wave number (Vermersch and Beardsley, 1976). However, since the waves do not propagate directly parallel to the axis of the channel, they should be refracted on the south side in the same way that surface waves are refracted when approaching a shelving beach (Wunsch, 1969). Whether or not the waves are dissipated by viscous effects and boundary layer formation on the south side of the channel, or whether they are reflected and refracted back into the channel must presumably depend upon the particular wave in question, its frequency, wavelength, and modal structure and total energy. At the low frequency end of the spectrum, there should be some energy absorbed in the generation of bottom-trapped Rossby waves, due to the sloping bottom (Vermersch and Beardsley, 1976), but no evidence for these Rossby waves has been found.

Due to the changes in topography and also due to the changes in the mean density structure with time in the North Channel, there is a continual variation in the wave numbers of the internal modes. Some of these wave numbers are quite near the length scales of various topographic features, and so it is possible that resonances could be set up. These resonances would not necessarily be present at all times, but when present could strongly affect the mixing and observed properties of the water at certain locations. In particular, the 'hole' in front

of the Morin Bank seems to be a prime candidate for resonance to occur in the form of standing waves, if the particular wave is reflected from the Morin Bank without too much loss of energy. A second effect of the continual adjustment of wave number due to the changing topography and density structure would be the occasional presence of wave-wave interactions (Phillips, 1966). These wave-wave interactions could be a mechanism for the transfer of energy to the smaller scales and the creation of new modes or augmentation of existing modes at higher frequencies.

As the waves pass up the Estuary, their interaction with the Morin Bank is critical. The downstream face of this Bank is steep enough that many of the waves will be reflected back downstream as discussed in Section 4.6. Upon reflection the reflected amplitude of the wave is almost equal to the incoming amplitude (reduced only by frictional losses), but the reflected wave number is different from the incoming wave number (Phillips, 1966). This, then, provides another wave number to be adjusted as it passes down the Estuary and interacts with all of the previously discussed factors. However, the Estuary presents quite a different shape to the wave during the downstream trip compared with what it was during the upstream trip, and so the effects upon a downstream travelling wave will be different from the effects upon an upstream travelling wave.

Wunsch (1968,1969) has discussed extensively the mechanisms of an internal wave interacting with a sloping bottom. Of particular interest in the case of the Middle Estuary is the development of a frictional boundary layer on the slope, and the apparent decrease in wavelength up the slope. In the cases Wunsch was discussing, the slopes were very long in comparison to the wavelengths of his internal waves.

and on the St. Lawrence, the length of the slope would be quite short. However, the results should hold in a qualitative manner at least.

As in the discussion on the head of the Laurentian Trough, the phenomena of blocking may be quite important. Of perhaps more importance, since the water above the Morin Bank is also stratified, is the possibility of lee waves. De Guise (1977) discusses lee waves downstream of the Morin Bank which have periods on the order of 2 to 5 minutes, but does not discuss waves of tidal frequencies. Bell (1975) and Baines (1973, 1979) discuss the problems and theory of lee waves generated by topography, but they consider only 'small' bumps and 'slightly' stratified fluids, whereas in the Estuary, the Morin Bank is large and the tidally-averaged stratification is strong. However, the strong effects produced by small bumps and slight stratification are an indication that this effect may be very important upon the St. Lawrence.

Even though the downstream slope of the Morin Bank is large enough to reflect internal tides most of the time, the observations show that there is no appreciable difference in the water on either side of the Bank. This would indicate that there is flow over the Bank at some times and for some waves. In addition, since the Bank is approximately 70% of the depth of the channel, there must be extremely strong mixing taking place at some portions of the tidal cycle to take the dense water from the bottom on the downstream side of the Bank to the upstream side of the Bank. This then raises the possibility of breaking internal waves and the creation of internal hydraulic jumps

on the Morin Bank. There is no direct evidence for these two processes, but the circumstantial evidence would indicate that they do occur.

Fronts are a quite common feature on both sides of the Morin Bank on the changes of the tide. These are produced by the shears that are set up due to the difference in time at which the tide changes on the surface and at the bottom. The high density gradients that are set up by the fronts could have strong effects on the internal waves by the mechanisms discussed in Section 5.2.

The mixing that occurs above and on the Morin Bank is very strongly influenced by the properties of the upstream water and by the internal waves coming over the Morin Bank. The strength of the mixing processes could vary from being very weak, when the internal tides are mostly reflected from the Bank, to quite strong if the internal tides are breaking over the Bank. This process could be catastrophic in the sense that the resultant effect would be quite different in each case and would have far-reaching effects upon the downstream density structure, which would in turn affect the wave numbers of the internal tides in the downstream section.

All of the above effects are complicated in themselves, and because of their interactions with the other effects, it would be very difficult to quantify each and every one of them. In Figure 7.1.1 an attempt has been made to indicate all of the possible interactions, and to quantify the strengths of the interactions into strong and weak effects, by the weight of the arrows. However, the discussion above is very qualitative and by no means exhaustive. Many of the interactions are very sensitive to each other and small changes in one could have serious repercussions on another process.

For example, a small decrease in the upstream density could change the density downstream of the Morin Bank enough that one particularly strong internal wave mode would break over the Morin Bank instead of being reflected by it. This could then introduce dense water from the bottom over the Bank and mix it with the water above the Bank which would then change the mean density of the water above the Bank and equilibrium would be restored. On the other hand, an increase in the fresh water from the Saguenay River could decrease the density in the Lower Estuary enough that the entire modal structure of the waves in the Middle Estuary could be changed, which could affect all of the mixing in the Middle Estuary and the amount of resonance of various modes. These changes could be quite important in the circulation of the Middle Estuary, over a fortnightly or monthly time scale.

Although the previous five Chapters were concerned with the interaction between the tidally-averaged density structure and the surface and internal tides, it will be seen from the discussion so far that these processes are not the only controlling processes in the circulation of the Middle Estuary. They are very important, but they do not explain everything. The long time scale variation in the tidally-averaged density structure is also of great importance and this is controlled by a large number of factors, only one of which is the internal wave structure. On the other hand, the time variation in the internal wave structure is also of great importance, and this variation is only partially controlled by the tidally-averaged density structure.

7.2 Non-Tidal Processes

In the previous section, the tidal processes which contribute to the circulation of the Middle Estuary have been discussed. The tidally-averaged density structure is a tidal process on the basis that the exact amount and location of the mixing that occurs is controlled by the surface and internal tides, but there are other non-tidal processes which also have an effect on the mixing and on the tidally-averaged density structure. The two most important of these are the hydrological and the meteorological conditions.

Until now there has been no mention of the hydrological conditions in the Middle Estuary of the St. Lawrence. This has been because the effects of the hydrological cycle could not be seen in the data collected from the St. Lawrence Current Surveys. Neu (1975) has discussed the effects of the hydrological cycle on the St.Lawrence and the effects of runoff regulation on the environment over the long term.

The total catchment basin of the St. Lawrence system is 1.5×10^6 km^2 and about 40% of this is directly into the Great Lakes, while the remainder is directly into the St. Lawrence. Due to the vast storage capacity of the Great Lakes, their discharge varies little over the year, although the discharge directly into the St. Lawrence is much more variable. Regulation of the direct discharge into the St. Lawrence for Hydroelectric power generation has reduced this variability significantly. There are long-term variations over the year, and in 15 to 20 year cycles, and the effects of these

varying discharges will be important since they are the major input of fresh water to the system.

Over the course of one survey, however, the variation in freshwater discharge is very small. During the course of the 1975 St. Lawrence Survey, the average daily discharge at Montreal was 14,840 m^3/sec with a maximum variation of 7.5% (Water Survey of Canada, personal communication). The variation is barely outside the expected limits of accuracy of a stage-discharge curve and so the discharge at Montreal could be taken to be a constant, over the period of the surveys.

The cross-sectional area of the Estuary, below chart datum near Pointe au Pic is approximately 7.08×10^5 m^2 , and this gives an average nontidal velocity of 2.1 cm/sec downstream due to the discharge. This is, of course, only the cross-sectional average and would be modified at any particular location by the topography.

Although the amount of water entering the Middle Estuary from upstream does not vary too much over the yearly cycle, the heat content does vary considerably. Section 2.1, discusses the temperature variation in some detail. The minimum temperature of the Great Lakes outflow is about $1^{\circ}C$ from January to March and rises to about $20^{\circ}C$ in August (Webb, 1975). This temperature is modified considerably in the St. Lawrence River and contributes to the density variation in the Middle Estuary.

At the lower end of the Middle Estuary, the variation in the discharge of the Saguenay River has a considerable effect upon the density conditions in the Lower Estuary (El-Sabh, 1979), and this has already been discussed.

Meteorological conditions are variable throughout the Estuary over any given time scale. Aubin, et al (1979) have discussed the effects of the wind on the surface currents in the Riviere du Loupe area. In general, easterly winds prevail in the spring and westerly or southwesterly winds prevail over the summer, with mean wind speeds of about 8 m/sec. Due to the topography of the north side of the Estuary, the winds seem to blow more or less up and down the Estuary, and the circulation and mixing effects of these winds must, at times, be considerable.

The formation of ice in the winter months will affect the wind-induced circulation and mixing. Ice formation starts in December, and there is almost complete ice cover of the Middle Estuary from about January to March. In addition to its effects in reducing the wind-induced mixing and circulation, the ice cover should provide another boundary layer which will increase the effects of friction and the concomitant generation of turbulent mixing processes.

No surveys have ever been carried out in the winter months. The result is that there is no information upon which to base speculation concerning the seasonal variations in the circulation of the Middle Estuary.

7.3 Dissipation Processes

The dissipation processes in the Middle Estuary are no different from the dissipation processes in any other body of water. Of particular importance, however, would be the boundary layer formation due to the internal tides propagating up the slopes (Wunsch, 1969) and the form drag (McDowell and O'Connor, 1977) due to the bed

shape of the Estuary. In addition to these two processes, the usual effects of bottom and sidewall friction, viscous dissipation and the generation of turbulent motions should all be important. These processes do, however, depend very strongly upon the precise tidal processes that are occurring in the Estuary at a given time and would interact with them to modify the tidal processes.

7.4 Discussion

The tidal frequencies contain approximately 94% of the energy in the Middle Estuary, and for any convincing description of the circulation processes in the Middle Estuary to be given it is necessary that this tidal energy be properly accounted for. It is of long-term interest to consider the effects of the non-tidal processes and the dissipation processes, and it is very important to consider them if any predictive work of practical use is to be done, but of primary importance, over the course of one tidal cycle, are the tidal processes as discussed in Section 7.1.

Much time and effort has gone into the numerical modelling of the circulation of the Middle Estuary, but it should be clear from the interactions displayed in Figure 7.1.1 that the problem is essentially a spatially three-dimensional one and that vertically-integrated models cannot expect to do more than they have done in considering only the barotropic tide. The interaction of the horizontal density gradients and the barotropic tide is fundamental to an understanding of the circulation patterns within the Middle Estuary.

There is no theoretical reason that would preclude the three-dimensional modelling of the Estuary, given the proper specification of the boundary conditions at either end of the Estuary. It would not be enough to simply specify the water levels at either end, but rather the boundary conditions must be truly radiation boundary conditions, in order to specify the proper number of internal modes and their directions of propagation. Once this is done, a solution to the complete nonlinear equations of motion is, in theory, quite straightforward.

Chapter 8

Summary and Conclusions

The objectives of the St. Lawrence tidal current survey were to explain the physical processes controlling the circulation of the Middle Estuary of the St. Lawrence and to provide means whereby the tidal currents could be predicted with a reasonable degree of accuracy. It is shown here that the most important determinants of the circulation are the tidally-averaged density structure and the barotropic and baroclinic tidal fields. It is also shown that the physical processes controlling the circulation are very much more complicated than was first envisaged. They occur on many time and length scales, and their interaction is very complicated. Although the aim of predicting the tidal currents has not been achieved, much progress has been made towards the aim of explaining which physical processes are of importance and what must be done before the prediction of the tidal currents is possible.

The T - S relationships from single tidal profiling stations show conservative mixing over one tidal cycle, but the properties of the end members change sufficiently rapidly that there is no generally applicable T - S relationship that would hold over the whole Estuary for periods longer than one tidal cycle. The tidally averaged depth/density relationship allows the separation of the vertical from the horizontal variation. The vertical variation may be expressed by any one of three functional forms, but there is not enough information to allow the expression of the horizontal variation in a simple functional

relationship. The horizontal density gradients vary considerably with time, and it would be quite misleading to draw charts showing the 'average' density structure of the Estuary, since the horizontal density structure of the Estuary depends in a complex way upon many factors.

An examination of the 44 current meter records that have been collected in the Estuary shows that the tidal currents cannot be explained by a theory of purely barotropic tides, but that it is necessary to take into account the baroclinic motions that are sustained by the vertical density gradients and generated by the topography of the Estuary. The analysis of the current meter records shows that 94% of the energy is contained within the tidal frequencies. However, the traditional methods of tidal analysis cannot distinguish between the surface and the internal tides, and so the tidal currents are not predictable from the tidal constituents which arise from the traditional forms of tidal analysis. On the other hand, many of the anomalous features which are present in the traditional tidal analysis of the current meter records may be explained, in a qualitative manner, by assuming a combination of barotropic and baroclinic tides.

In Chapters 4 and 5, an examination is made of the propagation of internal tides in the Middle Estuary. By using the functional forms of the vertical-density variation, the modal structures and the dispersion relations are calculated for the appropriate tidal frequencies and it is shown that these forms are not particularly sensitive to the inaccuracies in the vertical-density structure. It is shown that the horizontal density gradients that are observed in the Middle Estuary do not affect the horizontal propagation of the internal waves, but equations are

derived which show that in general, strong horizontal density gradients will affect the horizontal propagation of internal waves. On the other hand, the topography of the Middle Estuary is such that the internal tides should be reflected and may be in resonance with some of the topographic features.

Although the horizontal density gradients observed in the Middle Estuary are not strong enough to significantly modify the horizontal propagation of the internal tides, these horizontal density gradients are advected up and down the Estuary. The advection of the horizontal density gradients will considerably affect the measurements that are made by a fixed sensor. A set of equations is developed which allows the prediction of observations that would be made by a fixed sensor, given the density and wave fields in an estuary. Examples in a hypothetical channel give rise to structures that are very like those observed in partially-mixed estuaries. These examples also show that both the internal wave field and the horizontal density gradients are important and that neither can be neglected if the observed features are to be reproduced.

Although the direct problem of prediction is quite straightforward, it is the inverse problem that is of most interest; that is, given the observations, to deduce the wave field that produced the observations. If the inverse problem were solved, it would be a fairly simple task to predict the tidal currents in the Estuary. Unfortunately, it can be shown that the inverse problem does not have a unique solution, since the equations are not only nonlinear but also transcendental. In addition, there are enough physically realistic solutions that it would be impossible to discover the 'true' solution without further information.

It may be possible to simplify the solution space if synoptic information is available, but at the present time it seems that the computer time required would be excessive. Some progress is possible if the horizontal density gradients are ignored, since the equations become linear and so the solutions are unique. On the St. Lawrence, this procedure shows that the internal tides are reflected and that the direction of propagation of the waves is not directly parallel to the axis of the Estuary. To separate the direct and the reflected waves adequately, synoptic information is required and this is not presently available. In addition, there is not enough information available over long enough time periods to allow the separation of the tidal constituents and so there is not enough information available to adequately resolve the internal wave field either in time or in space.

The two most important factors controlling the circulation of the Middle Estuary are the tidally-averaged density field and the internal wave field. However, these are not the only factors which need to be taken into account if the currents of the Middle Estuary are to be predictable. There are many other processes which interact with each other and with the tidally-averaged density structure and the internal wave field. The quantitative assessment of these other factors, the degree of interaction, and the sensitivity of all of the processes to one another await a major synoptic survey of the entire Middle Estuary.

REFERENCES

1. ABRAMOWITZ, M. and STEGUN, I. 1965 Handbook of Mathematical Functions. Dover, N.Y.

2. AUBIN, F., MURTY, T.S. and EL-SABH, M.I. 1979 Numerical Simulation of the Movement and Dispersion of Oil Slicks in the Upper St. Lawrence Estuary: Preliminary Results. Le Naturaliste Canadien, 106(1), pp.37-44.

3. BAINES, P.G. 1973 The Generation of Internal Tides by Flat Bump Topography. Deep-Sea Research, Vol. 20, pp.179-205.

4. BAINES, P.G. 1977 Upstream Influence and Long's Model in Stratified Flows. J.F.M. Vol. 82, part 1, pp.147-159.

5. BAINES, P.G. 1979 Observations of Stratified Flow past Three-Dimensional Barriers. J. Geophysical Res., 84, C12, pp.7834-7838.

6. BELL, T.H. 1975 Lee Waves in Stratified Flows with Simple Harmonic Time Dependence. J.F.M. Vol. 67, part 4, pp.705-722.

7. BENDAT, J.S. and PIERSOL, A.G. 1971 Random Data: Analysis and Measurement Procedures. Wiley Interscience.

8. BRISCOE, M.G. 1975 Internal Waves in the Ocean. Reviews of Geophysics and Space Physics, Vol. 13, No. 3, pp.591-598.

9. BROWN, K.M. 1967 Solution of Simultaneous Non-Linear Equations. Communications of the ACM, Vol. 10, No. 11. Algorithm # 316, pp.728-729.

10. BROWN, K.M. 1969 A Quadratically Convergent Newton-Like Method Based upon Gaussian Elimination. SIAM J. Numer. Anal., Vol. 6, No. 4, pp.560-569.

11. BUDGELL, W.P. and MUIR, L.R. 1975 St. Lawrence River Current Survey 1974 Data Report. Ocean & Aquatic Sciences, Cent. Region, Dept. Fish. Envir., 335 p.

12. COURANT, R. and HILBERT, D. 1937 Methods of Mathematical Physics. Interscience, N.Y. Vol. I.

13. COX, C.S. 1963 Internal Waves. EOS Transactions of the American Geophysical Union, 44, pp.488-489.

14. COX, C.S. 1968 Internal Waves. EOS Transactions of the American Geophysical Union, Vol. 48, pp.588-591.

15. DE GUISE, J.C. 1977 High Frequency Internal Waves in the St. Lawrence Estuary. M.Sc. Thesis, McGill University, 93 p.

16. DRONKERS, J.J. 1964 Tidal Computations in Rivers and Coastal Waters. North Holland, Amsterdam.

17. DYER, K.R. 1973 Estuaries: A Physical Introduction. John Wiley, London.

18. EKMAN, V.W. 1904 On Dead-Water. Scientific Results of the Norwegian North Polar Expedition 1893-1896 5(15), pp.1-152.

19. EL-SABH, M.I. 1979 The Lower St. Lawrence Estuary as a Physical Oceanographic System. Le Naturaliste Canadien, 106(1), pp.55-73.

20. EL-SABH, M.I., FORRESTER, W.D. and JOHANNESSEN, O.M. 1969 Bibliography and Some Aspects of Physical Oceanography in the Gulf of St. Lawrence. McGill University, Montreal, Quebec, Marine Sciences Centre, Report 14.

21. EL-SABH, M.I., MURTY, T.S.and LEVESQUE, L. 1979. Mouvements des Eauxs Induits Par La Marée et le Vent dans l'Estuaire du Saint-Laurent. Le Naturaliste Canadien, 106(1), pp 89-104.

22. FARQUHARSON, W.I. 1962 Tides, Tidal Streams and Currents in the Gulf of St. Lawrence. Canadian Hydrographic Service, Ottawa, iii + 47 p.

23. FARQUHARSON, W.I. 1966. St. Lawrence Estuary Current Surveys. Bedford Institute of Oceanography, Rep. Ser. 66-6, 84pp.

24. FJELDSTAD, J.E. 1933 Internal Waves. Translation by Henry Stommel (Nov., 1945) of Interne Wellen, Geofysiske Publikasjoner, Vol. X, No. 6, Utgitt av det Norske Videnskaps-Akademie i Oslo.

25. FORRESTER, W.D. 1967 Currents and Geostrophic Currents in the St. Lawrence Estuary. B.I.O. Rep. No. 67-5, xiii + 175 p.

26. FORRESTER, W.D. 1972 Tidal Transports and Streams in the St. Lawrence River and Estuary. Int.Hyd.Rev.,XLIX, 1, pp. 95-108.

27. FORRESTER, W.D. 1974 Internal Tides in the St. Lawrence Estuary J. Marine Research, Vol.32, No.1, pp.55-56.

28. GODIN, G. 1971 Hydrodynamical Studies on the St. Lawrence River. Manuscript Report Series, No.18, EMR, Ottawa.

29. GODIN, G. 1972 The Analysis of Tides. University of Toronto Press.

30. GODIN, G. 1976 The Reduction of Current Observations with the Help of the Admittance Function. Technical Note 14 - Mar. Envir. Data. Serv. Dept. Fish. Envir. 13 pp.

31. GODIN, G. 1979 La Marée Dans le Golfe et l'Estuarire du Saint-Laurent. Le Naturaliste Canadien, 106(1), pp.105-121.

32. GREGG, M.C. and BRISCOE, M.G. 1979 Internal Waves, Fine Structure, Microstructure and Mixing in the Ocean. Reviews of Geophysics and Space Physics, Vol.17, No.7, pp.1524-1547.

33. INGRAM, R.G. 1976 Characteristics of a Tide Induced Estuarine Front. J.of Geophysical Research, Vol.81,No.12, pp.1951-59.

34. INGRAM, R.G. 1978 Internal Wave Observations off Isle Verte. J. Mar. Res., Vol.36, No.4, pp.715-724.

35. INGRAM, R.G. 1979 Water Mass Modification in the St. Lawrence Estuary. Le Naturaliste Canadien, 106(1), pp.45-54.

36. KAMPHUIS, J.W. 1968 Mathematical Model Study of the Propagation of Tides in the St. Lawrence River and Estuary. N.R.C. Mechanical Engineering Report, MH-105.

37. KOUTITONSKY, V.G. 1979 Transport de Masses d'Eau à l'Embouchure de l'Estuaire du Saint-Laurent. Le Naturaliste Canadien, 106(1), pp.75-88.

38. KRAUSSE, W. 1966 Methoden und Ergebnisse der Theoretischen Ozeanographie. 2: Interne Wellen, Borntraeger, Berlin, 248 pp.

39. LEBLOND, P.H. and MYSAK, L.A. 1978 Waves in the Ocean. Elsevier Scientific Publishing Co., Amsterdam.

40. LEBLOND, P.H. 1978 On Tidal Propagation In Shallow Rivers. J. Geophysical Res. 83, C9, pp.4717-4721.

41. LIGHTHILL, J. 1978 Waves in Fluids. Cambridge University Press.

42. LONGUET-HIGGINS, M.S. 1953 Mass Transport in Water Waves. Philos. Trans. Royal Soc., London, A245, pp.535-581.

43. MAGAARD, LORENZ V. 1962 Zur Berechnung Inter Wellen in Meeresräumen Mit Nicht-Ebenen Boden Bei Einer Speziellen Dichteverteilung. Kiel. Meeresforschungen, Vol.18, pp.161-183.

44. MALVESTUTO, V. 1979 Internal Wave Motion in a Periodic Stratification. Physics of Fluids, Vol.22(10), pp.1862-1867.

45. McDOWELL, D.M. and O'CONNOR, B.A. 1977 Hydraulic Behaviour of Estuaries. McMillan Press Ltd., Cambridge.

46. MORTIMER, C.H. 1973 Large Scale Oscillatory Motions and Seasonal Temperature Changes in Lake Michigan and Lake Ontario. Special Report 12, Centre for Great Lakes Studies, Milwaukee, Wisconsin.

47. MUIR, L.R. 1975 Unsteady Flow in Networks of Open Channels. Manuscript Report Series No.1, Ocean and Aquatic Sciences, Cent. Region, Dept. Fisheries and the Environment. 115 p.

48. MUIR, L.R. 1978 St. Lawrence Current Survey: 1975 Data Report. Ocean and Aquatic Sciences, Cent. Region, Dept. Fisheries and the Environment. 315 p.

49. MUIR, L.R. 1979a St. Lawrence River Oceanographic Survey: 1977 Data Report. Ocean and Aquatic Sciences, Cent. Region, Dept. Fisheries and the Environment. Tidal, Met. and Current Meter Data, Vol.1, 199 p., Profile Data, Vol.2, 278 p.

50. MUIR, L.R. 1979b, Internal Tides in the Middle Estuary of the St. Lawrence. Le Naturaliste Canadien, 106(1), pp.27-36.

51. MUIR, L.R. and BUDGELL, W.P. 1975 St. Lawrence River Current Survey: 1973 Data Report: Ocean and Aquatic Sciences, Cent. Region, Dept. Fisheries and the Environment, 172 p.

52. MUIR, L.R. and HAMBLIN, P.F. 1977 The Computation of Vertical Structure Associated with Internal Gravity Waves. Unpublished Report, Canada Centre for Inland Waters. 71 p.

53. MUNK, W. and CARTWRIGHT, D. 1966 Tidal Spectroscopy and Prediction. Phil. Trans. Royal Soc. London, Ser. A., 259, pp.533-581.

54. NEU, H.J.A. 1975 Runoff Regulation for Hydropower and its Effects on the Ocean Environment. Can. J. of Civil Engineering, Vol.2, pp.583-591.

55. OFFICER, C.B. 1976 Physical Oceanography of Estuaries. Wiley Interscience, N.Y.

56. OUELLET, M.Y. and CHEYLUS, M.J.F. 1971 Étude du Modèle Mathématique de La Propagation Des Marées dans le Fleuve St. Laurent. Report CRE-71-05, Laval University.

57. PHILLIPS, O.M. 1966 Dynamics of the Upper Ocean. Cambridge Univ. Press, London.

58. PINGREE, R.D. and GRIFFITHS, D.K. 1980 A Numerical Model of the M2 Tide in the Gulf of St. Lawrence. Oceanologica Acta, 3(2) pp.221-225.

59. PRANDLE, D. and CROOKSHANK, N. 1974 Numerical Model of the St. Lawrence Estuary. J. Hyd. Div. ASCE, Vol.100(HY), Proceedings Paper (10472), pp.517-529.

60. PRINSENBERG, S.J., WILMOT, W.L. and RATTRAY, M. Jr. 1974 Generation and Dissipation of Coastal Internal Tides. Deep-Sea Research, Vol.21, pp.263-281.

61. PRINSENBERG, S.J. and RATTRAY,M. Jr. 1975 Effects of Continental Slope and Variable Brunt-Vaisala Frequency on the Coastal Generation of Internal Tides. Deep-Sea Research, Vol.22, pp.251-263.

62. PROUDMAN, J. 1952 Dynamical Oceanography. Dover Publications, New York.

63. RABINOWITZ, P. 1970 Numerical Methods for Nonlinear Algebraic Equations. Gordon & Breach Science Publishers, London.

64. ROBERTS, J. 1975 Internal Gravity Waves in the Ocean. Marcel Dekker Inc., New York.

65. SANDSTROM, H. 1966 The Importance of Topography in Generation and Propagation of Internal Waves. Ph.D. Thesis, University of California.

66. SNEDECOR, G.W. and COCHRAN, W.G. 1967 Statistical Methods. 6th Ed. Iowa State Univ. Press, Ames, Iowa, U.S.A.

67. SOULSBY, R.L. 1978 The Use of Depth Averaged Current to Estimate Bed Shear Stress. Internal Document 26, IOS, Crossway, Taunton, Somerset.

68. STEVEN, D.M. 1974 Primary and Secondary Production in the Gulf of St. Lawrence. McGill University, Montreal, M.S. Report 19.

69. STOKES, G.G. 1847 On the Theory of Oscillatory Waves. Transactions of the Cambridge Philosophical Soc. Vol. VIII, p.441.

70. TURNER, J.S. 1973 Buoyancy Effects in Fluids. Cambridge Univ. Press.

71. VERMERSCH, J.A. Jr., and BEARDSLEY, R.E. 1976 A Note on the Theory of Low-Frequency Waves in a Rotating, Stratified Channel. Studies in Applied Mathematics, Vol.55, pp.281-291.

72. WATSON, E.R. 1904 Movements of the Waters of Loch Ness, as Indicated by Temperature Observations. Geographical Journal London, Vol. 24. pp.430-437.

73. WEBB, M.S. 1975 A Surface Water Temperature Climatology of the Laurentian Great Lakes. Climatological Studies No.27, Atmospheric Environment Service, Canada.

74. WUNSCH, C. 1968 On the Propagation of Internal Waves up a Slope. Deep-Sea Research, Vol.15, pp.251-258.

75. WUNSCH, C. 1969 Progressive Internal Waves on Slopes. J.F.M. Vol.35, Part I, pp.131-144.

76. WUNSCH, C. 1971 Internal Waves. EOS, Transactions of the American Geophysical Union, Vol.52, pp.233-235.